CREEP, SHRINKAGE AND ELASTIC MODULUS OF MALAYSIAN CONCRETE

FINAL REPORT

(PROJECT NO: LPIPM/CREAM/UPP 02-02-06-09-23)

JUNE 2008

SUMMARY

Inadequate provision for durability design may lead to premature deterioration, high repair and maintenance cost during the life-cycle of the structure. Poor quality of materials, poor attention to details and serviceability design as well as lack of attention to the construction procedures are some of the main causes of accelerated deterioration and decline in durability. Therefore knowledge on material properties and structural behaviour pertaining to serviceability performance is crucial to promote the shift to more efficient and sustainable concrete structures.

Creep and shrinkage are critical properties for the calculation of stresses, deflection, cracking, buckling and failure of structures under sustained loads. However due to the fact that the implications for under-prediction of creep and shrinkage are time-dependent, considerations and provisions on these parameters are often overlooked or even simply ignored. One of the examples of the effect of these time-dependent deformation on buildings is published in National Building Studies Research Paper No. 28. The publication recorded that the biggest change of strain in the steel beams of the Ministry of Defence Building in Whitehall, London was caused by the shrinkage of the concrete after the floors had been cast. The strain due to concrete shrinkage was even larger than the strain induced by the loading of the floors subsequently (Mainstone, 1960). Thus time-dependent deformation of concrete should not be overlooked and has to be properly considered in the design stage.

However, till date exact mechanism of this particular behaviour is not fully understood. The prediction of creep and shrinkage values for concrete structures is still subjected to considerable prediction errors (Oh and Yang, 2000). One of the reasons is because of the viscoelastic properties and the heterogeneous composition in the concrete material. In addition to that, various internal and external factors that affect the magnitude of creep and shrinkage also contribute greatly to the ambiguity. Prediction of this time-dependent deformation is crucial for prestressed members and concrete structures which are sensitive to material properties. According to Peterson (1968) the losses in prestressed concrete due to creep and shrinkage may reach up to about 45% for concrete prestressed at 60% of its compressive strength and cured in relative humidity of 50%. An accurate prediction for creep and shrinkage losses is important for structures such as high rise buildings, segmental box girders, long span

bridges and structural members with high length to depth ratio. In the construction of such massive structures, more often than not, usage of higher strength concrete is required.

The existing prediction models of creep and shrinkage for design reference are available in concrete standard codes such as the BS 8110, Eurocode 2, ACI-209, CEB-FIP Model Code 1990, AS 3600 and B3 Model. These models are however mostly developed for concrete in the temperate climate condition. Creep and shrinkage strain is highly influenced by the ambient temperature and humidity because the environmental condition affects the movement of moisture in the concrete members. Therefore, the time-dependent deformation in tropical climate condition, which is hot and humid, is deemed to be different from the deformation occurred in temperate countries. In addition to that, most models do not provide prediction of creep and shrinkage for HSC, such as BS 8110 that caters for concrete strength up to $40N/mm^2$. Undoubtedly, there was even less information on creep and shrinkage of HSC in the tropical environment (Kribanandan, 2002).

The research was carried out for a period of 3 years in which data collection was made from standard specimens as well as from structural members cast in the laboratory and also on site. This work was supported by the Institution of Engineers Malaysia (IEM) and the results were closely monitored by the IEM Technical Committee on Concrete Design Code. The data collected will be proposed to be included as alternative to the values provided in the foreign design code and can be the basis for the local Nationally Determined Parameters (NDP) which will accompany the Eurocode 2, the code that will replace BS 8110.

Two workshops were conducted during the period this research in which penal from industries were invited for their input. The details of workshops are provided in LAMPIRAN.

RESEARCH TEAM

Wahid Omar – Leader
Ahmad Mahir Makhtar
Tan Pui Lai
Roslina Omar
Ng Ming Kwong

ACKNOWLEDGEMENT

We would like to thanks the Construction Research Institute of Malaysia (CREAM) of CIDB for the funding provided for this project. The supports provided by various organisations such as the Institute of Engineers Malaysia (IEM), Cement and Concrete Association (C & CA) and many experts (listed as participants in research workshops in LAMPIRAN) are highly appreciated. Thanks are also due to technical staff of Structures and Materials Laboratory, Faculty of Civil Engineering for their technical supports in conducting the experiments. Last but not least our sincere thanks to Research Management Centre (RMC) for managing the research fund

ABSTRACT

It has been widely acknowledged that creep and shrinkage of conrete are greatly influenced by the surrounding ambient. In spite of various research carried out to investigate the phenomena, little were conducted on time-dependent deformation for concrete in tropical climate. Locally, most creep and shrinkage predictions are obtained by referring to foreign design codes developed in temperate climate countries, risking inaccurate predictions. Therefore this research is dedicated to determine the magnitude of time-dependent deformation of concrete in the tropical climate. The objectives are to systematically collect creep and shrinkage data under the influence of tropical climate and to empirically develop a set of modification factors based on the best prediction model. Time-dependent deformation tests were carried out on standard specimens and on reinforced concrete columns and prestressed concrete beams under laboratory-controlled environment with temperature and relative humidity (RH) of 27±2^{o}C and 50±4% respectively, and natural tropical ambient. On site monitoring of pre-camber of post-tensioned prestressed beams was also carried out. The experimental data were assessed against various existing creep and shrinkage models such as Eurocode 2, ACI 209, B3 Model, CEB-FIP 1990, and Australian Standard 3600 in order to determine the best prediction for tropical concrete. The results show that time-dependent deformation of HSC in the tropical climate is significantly lower than most of the prediction by foreign standard codes. Based on statistical analysis, Eurocode 2 is identified as the best model for tropical concrete and thus chosen as reference model for development of modification factors. Through empirical analysis, modification factors named as TROPCS which stands for '*Tropical Creep and Shrinkage*' is introduced. Statistically, the prediction with adoption of TROPCS to Eurocode 2 model results in better accuracy. The coefficient of variation for prediction with TROPCS is at an average of 10.0% for creep and at 21.1% for shrinkage. Validations on the accuracy of TROPCS on structural members were conducted through the results of structural deformation. The results prove that the prediction with TROPCS factors is better than the prediction by EC 2 with the average coefficient of variation for TROPCS predictions on structural members at 12.5%, as compared to the coefficient of variation by EC 2 at 14.8%. The TROPCS modification factors are proposed to be included in the National Annex of Malaysian version of Eurocode 2 as an optional reference.

TABLE OF CONTENTS

LIST OF TABLES

LIST OF FIGURES

LIST OF NOTATIONS

$\varepsilon_E(t)$	-	Elastic strain at time t (micron)
$\varepsilon_{cr}(t)$,	-	creep strain at time t (micron)
$\varepsilon_s(t)$	-	shrinkage strain at time t (micron)
$\varepsilon_T(t)$	-	thermal strain at time t (micron)
$\varepsilon_\sigma(t)$	-	stress-induced strain, comprising of instantaneous strain and creep strain (micron)
$\varepsilon^o(t)$	-	stress-independent inelastic strain, consisting of shrinkage strain and thermal strain (micron)
t	-	time
t_o	-	Initial time at the beginning of loading or drying
$\varepsilon_{total}(t)$	-	Total deformation at time t (micron)
$\varepsilon_\sigma(t)$		Stress induced strain
$\varepsilon^o(t)$		Stress independent inelastic strain
σ	-	Stress
$J(t,t_o)$	-	compliance function or creep function
$C(t,t_o)$	-	Creep compliance or specific creep
E	-	Modulus of elasticity
ϕ		Creep Coefficient
ε_{cr}		Creep Strain
ψ		In chapter 3??
$E_{cm,28}$		Concrete modulus of elasticity at the age 28 days
f_{cm}		Mean concrete strength
A		Cross section area
u		Section perimeter
β_H		Creep correction factor for ambient relative humidity
$\varepsilon_{cr\text{-}ult}$		Ultimate creep strain
ϕ_{cc}		Design creep factor by AS 3600

f'_c	Characteristic cylinder strength by AS 3600
f_{cm}	Mean cylinder strength
$Ø$	Specimen diameter
s_d	Standard deviation
ϕ_{ult}	Ultimate creep coefficient
Re	Residuals
V	Coefficient of variation
V_m	Coefficient of variation for model prediction
α_1	Creep reduction coefficient to capture the reduction in deformation due to the provision of steel reinforcement
ε_{col}	total time-dependent axial strain of columns

Greek Symbols

υ	-	inclination angle of concrete compression (deg)
α	-	angle between shear reinforcement and main longitudinal bar (deg)
β	-	shear enhancement factor
ϕ	-	shear strength reduction factor for ACI-318
σ_{cp}	-	average stress in concrete due to axial force (N/mm^2)
τ_{Rd}	-	basic design shear strength (N/mm^2)
ρ_w	-	ratio of tension reinforcement to cut section of beam considered

CHAPTER 1

INTRODUCTION

Creep and shrinkage are critical properties for the calculation of stresses, deflection, cracking, buckling and failure of structures under sustained loads. However due to the fact that the implications for under-prediction of creep and shrinkage are time-dependent, considerations and provisions on these parameters are often overlooked or even simply ignored. One of the examples of the effect of these time-dependent deformation on buildings is published in National Building Studies Research Paper No. 28. The publication recorded that the biggest change of strain in the steel beams of the Ministry of Defence Building in Whitehall, London was caused by the shrinkage of the concrete after the floors had been cast. The strain due to concrete shrinkage was even larger than the strain induced by the loading of the floors subsequently (Mainstone, 1960). Thus time-dependent deformation of concrete should not be overlooked and has to be properly considered in the design stage.

However, till date exact mechanism of this particular behaviour is not fully understood. The prediction of creep and shrinkage values for concrete structures is still subjected to considerable prediction errors (Oh and Yang, 2000). One of the reasons is because of the viscoelastic properties and the heterogeneous composition in the concrete material. In addition to that, various internal and external factors that affect the magnitude of creep and shrinkage also contribute greatly to the ambiguity. Prediction of this time-dependent deformation is crucial for prestressed members and concrete structures which are sensitive to material properties. According to Peterson (1968) the losses in prestressed concrete due to creep and shrinkage may reach up to about 45% for concrete prestressed at 60% of its compressive strength and cured in relative humidity of 50%. An accurate prediction for creep and shrinkage losses is important for structures such as high rise buildings, segmental box girders, long span bridges and structural members with high length to depth ratio. In the construction of

such massive structures, more often than not, usage of higher strength concrete is required.

In general, concrete with 28 day uniaxial compressive cylinder strength exceeding 41 N/mm^2 is categorised as high strength concrete (HSC) (French et al., 1998; ACI 363R, 1992). In the local construction industry, usage of HSC is on the rise. For example, the construction of Petronas Twin Towers required the use of concrete strength up to 130 N/mm^2 whereas the 77-storey Telekom headquarters in Bangsar required 70 N/mm^2 of concrete strength (Kribanandan, 2002). In the time to come, more construction work will specify the usage of HSC, such as for the construction of monorail tracks and long-span bridges that is on the rise in this country. As the strength of concrete becomes higher and with the addition of mineral and chemical admixtures, the properties of HSC differ from normal strength concrete (NSC). Extrapolation from NSC without proper experimental verification is an imprudent act. For that reason, good understanding on the engineering properties, especially the time dependent characteristics of HSC is important.

The existing prediction models of creep and shrinkage for design reference are available in concrete standard codes such as the BS 8110, Eurocode 2, ACI-209, CEB-FIP Model Code 1990, AS 3600 and B3 Model. These models are however mostly developed for concrete in the temperate climate condition. Creep and shrinkage strain is highly influenced by the ambient temperature and humidity because the environmental condition affects the movement of moisture in the concrete members. Therefore, the time-dependent deformation in tropical climate condition, which is hot and humid, is deemed to be different from the deformation occurred in temperate countries. In addition to that, most models do not provide prediction of creep and shrinkage for HSC, such as BS 8110 that caters for concrete strength up to 40N/mm^2. Undoubtedly, there was even less information on creep and shrinkage of HSC in the tropical environment (Kribanandan, 2002).

1.1 Background of research

The time-dependent properties of concrete have been researched since the early decades of the last century. This time dependent deformation was first discovered in 1907 by Hatt of Purdue University, USA who published the first data on creep of reinforced concrete (Neville et al., 1983). Ever since then much research has been devoted to this complex problem in both the material and structural performance. This area of research continues to be active for a number of reasons including the significant structural effects caused by shrinkage and creep in modern concrete structures and in particular, the rapid development of high performance concrete in recent years. However, despite major successes in the use of HSC, the phenomenon on creep and shrinkage is still far from being fully understood.

Research on the effect of factors such as age at loading, stress intensity, on creep and shrinkage have been very commonly carried out. Recent development in this subject focuses on the time-dependent deformation of high performance concrete, the effect of various additives and admixtures in the concrete mix, the influence of cyclic loading and cyclic ambient conditions, the development of creep and shrinkage prediction model with evaluation on structural members (Han and Walraven, 1995; Li and Yao, 2001; Brooks, 1989; Koh et al., 1997; Vandewalle, 2000; Bazant, 2001) Most creep and shrinkage studies have been carried out under controlled temperature and relative humidity (RH) that simulates the climate condition of temperate countries.

Reports on creep and shrinkage tested under the surrounding apart from temperate condition are very limited in the literature. It is even more difficult to find publications on the influence of surrounding ambient on time-dependent deformation of HSC. Only a few papers are published and the climatic influence is usually based on case study of a specific country or locations. One of the literatures published is authored by Saiidi et al. (1998), which focused on box-girder bridge prestressed losses, particularly on creep and shrinkage in the dry climate of northern Nevada. The study was initiated due to the concern over potential adverse effect of low RH on prestress losses. The box girder was constructed with concrete strength of 30 N/mm^2

at 28 days, whereas the average temperature recorded for the duration of the study of 24 months was 29^{o}C and RH within 16% to 55%. A comparison of the measured losses to some prediction models was conducted and it was concluded that ACI 209 (1971) and Naaman (1982) show the best correlation to the measured data.

Another paper on the influence of climatic condition is based on the research conducted in North of Iran. The research that was carried out by Barr et al. (2003) investigated the influence of natural environment on drying shrinkage of concrete, with and without steel fiber reinforcement. The specimens were kept in controlled-room with temperature of 23 ± 2^{o}C with RH of 60 ± 5% and also under two natural environments of 23 ± 7^{o}C with RH 77 ± 8% and 25 ± 7^{o}C with RH 71 ± 8%. The results show that higher RH reduces shrinkage. However limited effect on the drying shrinkage and autogenous shrinkage was observed. This is due to the fact that the average temperature over a period of a year was not significantly different from that maintained in the controlled-room and the variation in RH was also relatively low. As the results were compared to the prediction by ACI 209 model, it was concluded that the correlation between the experimental and predicted shrinkage strain was good for the lower strength concrete. It was recommended that further work is required to improve the current prediction models for the use of concrete beyond the strength of 45N/mm^{2}.

Locally, the research related to time-dependent deformation focuses more on the influence of specific concrete additives on creep and shrinkage. Toshiro (1999) conducted a study on creep and shrinkage of concrete containing palm oil fuel ash (POFA) in Universiti Teknologi Malaysia. The test was carried out in controlled environment of 23 ± 1.1 ^{o}C and RH 50 ± 4% as recommended in the ASTM C512-87 instead of tropical condition. This was because the main objective of the study was to determine the influence of POFA in concrete. Thus regularised test condition enabled comparable study to be conducted between the measured data and other studies to determine the actual influence of the variable, which was the inclusion of POFA. Another investigation involving the test of creep and shrinkage carried out locally was conducted by Noor (2001). The main objective of the study was to asses the performance of lightweight prestressed concrete beams made from palm oil clinker.

Thus, the effects of environmental condition on time-dependent deformation of local concrete were not examined.

Tan K. L. (1996) conducted a study on long term deformation of Portland blast furnace slag cement concrete with creep and shrinkage as one of the properties assessed. The test, conducted over a duration 3 months were monitored under the ambient temperature of 30^{o}C and RH of 80% which is tropical climate as it was conducted in Singapore. In this study, the influence of ambient condition on long term deformation of concrete however was not discussed as the main focus was the effect of Portland blast furnace slag cement on concrete properties in general.

Mustafa and Yusuf (1991) conducted a study on the environmental effects on concrete behaviour in Universiti Kebangsaan Malaysia. The investigation revealed some preliminary information on concrete properties such as compressive strength, modulus of rupture, splitting tensile strength, elastic modulus and drying shrinkage of plain concrete. The mean concrete strength tested was 35N/mm^2. It was concluded that outdoor specimens in hot and humid climate exhibit 35% lower shrinkage strain than in temperate climate condition. The occurrence, as explained is due to the prevailing conditions of warm and humid weather that ensure continuous supply of water into the pore structure of cement gel. This phenomenon caused the evaporation process to be negligible and counteract the drying effect due to hot weather. However no prediction recommendation was given in this research publication.

In spite of the various research carried out, little investigations were conducted for concrete in the local context, particularly the effect of tropical climate on time-dependent deformation. Recommendations of time-dependent prediction models for local concrete has not been researched or published. For that reason, prediction recommendation for time-dependent deformation of tropical climate concrete is not available and the suitability of currently available models for local concrete are never verified. It was also clear from the literature available that understanding on the behaviour of HSC has not been established till date.

1.2 Significance of research

A standard prediction model with satisfactory degree of accuracy for tropical concrete is important for the construction industry. Besides eliminating problems at later stage of construction and also at the service stage, a reliable prediction model will reduce the cost of construction when individual time-dependent behaviour testing can be omitted.

The current practice of evaluating creep and shrinkage deformation in Malaysian concrete is based on British Standards or any other standards available. BS 8110 offers a simplified prediction method based on a nomograph reading with ambient RH, structural member size and age of loading as the determining factors. The prediction by BS 8110 is developed to cater for normal weight concrete between 2000kg/m^3 to 2800kg/m^3, in temperate climate condition. BS 5400: Part 4: 1990, the Code of Practice for Design of Concrete Bridges also provides recommendation for creep and shrinkage. However, as it is stated in the code the information given is essentially found in CEP/FIP International Recommendations for the Design and Construction of Concrete Structures, 1970 as amended in May 1972. The data are valid only for Portland cement concretes of normal quality, hardening under normal conditions and subject to service stresses at the most equal to 40% of the ultimate strength. The data are no more than a working basis for design references.

The ACI-209 regulation also does not cover for high strength concrete whereas the Australian Standard 3600 provides for cylinder strength up to 65 N/mm^2. In the CEB-FIP Model Code 1990, the concrete characteristic cylinder strength is specified up to 80N/mm^2. However it is stated in the comments for Clause 2.1.1.1 that constitutive relations for concrete characteristic cylinder strength higher than 50N/mm^2 should be used with caution and appropriate judgement because available information on behaviour of concrete with characteristics cylinder strength higher than 50N/mm^2 is limited.

In the application for higher strength concrete, extrapolation of the empirical equations is unjustified. This is due to different mix composition and material structure in high strength concrete as compared to normal strength concrete. In order to further stress on this point, even the prediction for NSC is also not accurate for concrete in the tropical climate as reported by Mustafa and Yusuf (1991). Therefore local experimental data is important towards a proper formulation of time dependent deformation for HSC.

Temperature and RH are major factors on creep and shrinkage as these two parameters influence the moisture content in the concrete pore structure. In the codes, values recommended are based on test carried out in controlled temperature of 23^{o}C and RH of 50% (ASTM C512-87, 1992) with reference to the seasonal temperate climate. The local tropical climate however is hot and humid all year round. Based on the data of Malaysian Meteorological Department, mean daily temperature is 27^{o}C and mean monthly RH is within 70% to 90%. Considering the fact that the magnitude of creep and shrinkage are greatly influenced by the environment condition, it is essential to assess the actual time-dependent deformation in the local environment.

A specific creep and shrinkage testing was carried out locally for the construction of the Petronas Twin Tower to determine the actual magnitude of deformation in Malaysia. This is an example of many other independent time-dependent testing carried out for the construction of massive structures locally. It is neither practical nor economical for designers to carry out testing for each special structure because a standard model is not available for Malaysian concrete.

Therefore this research work is dedicated to systematically collect local HSC creep and shrinkage deformation data. It should be noted that the concrete characteristic strength in this thesis is categorized in concrete Class ensuing the Eurocodes, as opposed to the term concrete grade specified in the British Standards. Both cylinder and cube characteristic strength is specified, with the reference to cylinder strength preceding the concrete cube strength. The range of concrete

strength studied in this research is between C40/50 and C65/80. This range is determined based on the most common HSC currently utilized in Malaysia (Kribanandan, 2002).

Testing was carried out on standard size cylinders, reinforced concrete columns and prestressed beams, under laboratory controlled environment. Preliminary test to identify the specimen size effect on creep and shrinkage was also conducted. Monitoring of prestressed post-tensioned beams was carried out on actual structural members on site and the concrete was also sampled for laboratory testing for a more accurate analysis. These test results will contribute towards verifying the accuracy of recommendations in BS 8110 and other design codes to Malaysian concrete.

Comparison and correlation of experimental data to the values in Eurocode 2 (EC 2), the latest concrete design code published, which is to be implemented in Malaysia is also conducted. From the experimental data obtained, modification factors for creep and shrinkage for Malaysian HSC based on EC 2 model calculation can be developed. The correction factors can be adopted in the National Annex of EC 2 for time-dependent deformation of concrete in the tropical climate. The results that are easily accessible will benefit local design engineers in verifying their structural design. It is also possible for the results to be applicable for other tropical countries. Ultimately this research is directed towards identifying the best estimate for concrete behaviour in structural design.

1.3 Objectives

The main objective of this research is to determine the magnitude of concrete creep and shrinkage deformation of HSC under tropical climate condition. Based on the literature review, it is proven that little was done on this subject even though the advantages in acquiring the knowledge on this subject are significant. Thus, this research is directed to achieve the objectives highlighted below:

(i) To collect and analyse data on creep and shrinkage deformation for HSC in the tropical climate;

(ii) To verify the degree of accuracy of time-dependent values recommended in foreign codes to the HSC in tropical climate;

(iii) To propose modification factors for creep and shrinkage deformation of HSC as provided in EC 2 design code for the application of concrete in the tropical climate;

(iv) To verify the accuracy of the proposed modification factors through laboratory scaled and actual size structural member testing in the laboratory and on site.

1.4 Scope of Research

The scope of this concrete time-dependent deformation research consist of the following:

(i) Collection of creep and shrinkage data and analysing the behaviour of creep and shrinkage in HSC under tropical climate in Malaysia;

(ii) The main variables studied are the effect of temperature and RH, concrete strength (C40/50, C50/60 and C65/80) and age at loading (7 and 28 days) on creep and shrinkage of HSC;

(iii) The specimens were tested in controlled room of 27±2^{o}C and RH of 50±4% and also in ambient condition of approximately 28.6±3^{o}C and RH of 65.9±15%.

(iv) Creep and shrinkage testing were conducted on both standard size specimens and structural elements. Creep test on standard size specimens was carried out on 100mmØx300mm cylinders according to ASTM C512-87 and shrinkage testing on 100x100x500 mm prism according to ASTM C157-91. The standard size specimens were all tested in the laboratory;

(v) The time-dependent deformation models assessed in this study are from Eurocode 2 (EC 2), ACI-209, Australian Standard 3600 (AS 3600), CEB-FIP 1990 Model Code and B3 Model (B3).

CHAPTER 2

LITERATURE REVIEW

The basic concept and knowledge on the subject of creep and shrinkage on concrete, the achievements and progress of previous researches must be understood before developing a prediction model for concrete in the tropical climate. In this chapter, the types of creep and shrinkage, its mechanism and the influencing factors that have been established from various previous researches is presented. As this study is focused on the prediction of time-dependent deformation on HSC in tropical climate, special attention is paid to the behaviour of time-dependent deformation on HSC. The influence of environment condition as well as other factors on creep and shrinkage are also discussed.

2.1 Time-dependent Deformation in Concrete

The deformation and deflection of concrete elements is a phenomenon reliant to the stress-strain behaviour of material that is directly controlled by the material constituent. Deformation that takes place consist of shrinkage strain that occurs when the specimen is exposed to drying, initial elastic strain that occurs when load is first applied and creep strain that occurs when the load is sustained over time.

Creep, as it is widely known is an increase in strain of materials under sustained load over time. The initial deformation due to load is the elastic strain, while the additional strain or time-dependent deformation due to the same sustained load is the creep strain. Creep cannot be observed directly and can only be determined by deducting elastic strain and shrinkage strain from the total deformation. Although creep and shrinkage are not independent phenomena, superposition of strain has been recognized as a valid principle by researchers and is widely adopted by prediction models (Bazant, 1988; Acker and Ulm, 2001). The principle of superposition states that the response to a sum of stresses or strain is the

total of the response each of them taken separately is valid. The principle of superposition for time-dependent deformation is as shown in Equation (2.1).

$$\text{Total strain, } \varepsilon_t = \text{Elastic strain, } \varepsilon_e + \text{Creep, } \varepsilon_{cr} + \text{Shrinkage, } \varepsilon_{sh} \quad (2.1)$$

Shrinkage is also another time-dependent shortening of concrete associated with loss of moisture that occurs at different stages of concrete age, independent to loading. Shrinkage is thought to be primarily related to the loss of adsorbed water in the cement gel. However if the concrete is continuously cured in saturated atmosphere after casting, it undergoes expansion, known as swelling. This expansion is due to the adsorption of water by the cement gel.

The initial modulus of elasticity is defined as the ratio of stress to corresponding strain under the proportional limit. Stress-strain curve of concrete is non-linear mainly due to the existence of creep, even at the initial stage of loading. Thus the demarcation between the immediate elastic strain and early creep strain is difficult. For practical purposes, arbitrary distinction is made with initial deformation resulting from application of design stress considered as elastic strain and creep is regarded as the subsequent strain under the sustained loading (Neville, 1990). The modulus of elasticity is related to the type of aggregate and the strength of concrete.

Figure 2.1, adopted from Neville (1981) illustrates the profile of different deformation, plotted with strain against time after loading. The horizontal line, labeled as (a) represents the nominal elastic strain while the first curve, (b) above the horizontal line represents shrinkage strain. Basic creep and drying creep are represented by the curves labeled (c) and (d) respectively. The total deformation is shown by the highest curve in the graph. The definition of basic and drying creep is stated Sub-Chapter 2.4. It is observed that creep and shrinkage strain continue to increase with time but the rate of the deformation decreases with time. The magnitude of these strain is influenced by numerous factors governed by the material composition and environmental condition and is discussed in Sub-Chapter 2.6.

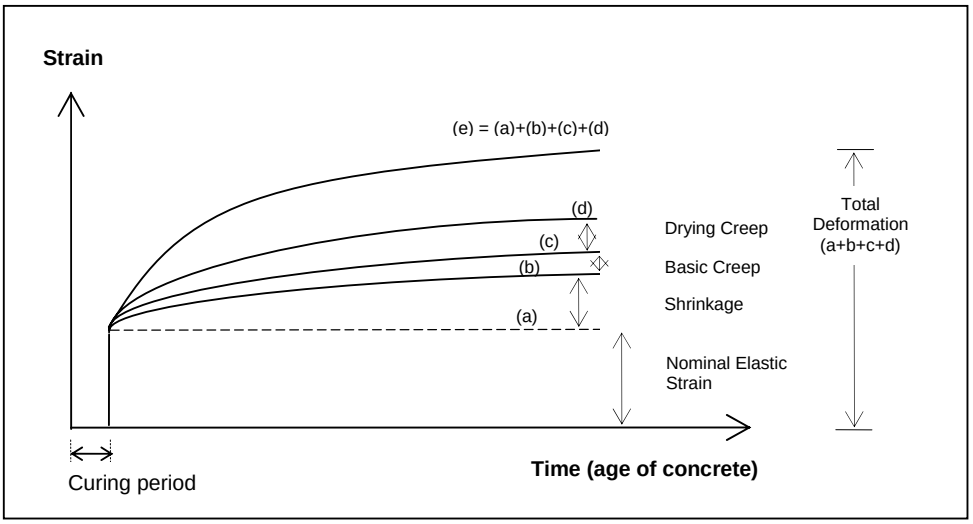

Figure 2.1:Time-dependent deformation in concrete

2.2 Modulus of Elasticity in Concrete

The modulus of elasticity of concrete is one of the most important mechanical properties of concrete. It represents a relation between stress and corresponding strain or between force and deformations of concrete (Neville and Brooks, 1990; Rashid, 2002). The modulus of elasticity is used to predict moments, stresses and deflection in the analysis of reinforced concrete structure. This property is required by designers for stiffness and deflection evaluations. Prediction of elastic modulus is also important in reinforced and prestressed concrete for shrinkage and creep evaluations as well as crack control, that is directly related to the durability of concrete structures (Nassif et al., 2005)

It is a well known fact that concrete does not exhibit linear elastic behaviour after removal of load, even at low stresses because permanent deformation due to creep exists after removal of load. The pattern of this behaviour can be described as non-linear and non-elastic, as illustrated in the stress-strain curve in Figure 2.2. While establishing the modulus of elasticity in concrete, the basis should be clearly defined. Generally three types of static modulus of elasticity are usually referred and the few common types are explained here.

Initial tangent modulus: The tangent to the curve at the origin is the initial tangent modulus. With reference to Figure 2.2, adapted from Neville (1981), the initial tangent modulus is the line starting from point O. The determination of the initial tangent modulus is not easy but an approximate value can be obtained – the secant of the stress-strain curve on unloading is often parallel to the initial tangent modulus. This initial tangent modulus is approximately equal to the dynamic modulus (Neville and Brooks, 1990).

Tangent modulus: Tangent modulus is represented by the slope of a line drawn tangent at any point to the stress strain curve. This applies only to very small changes in load above or below the stress at which the tangent modulus is considered (Neville and Brooks, 1990). As for an example, it is the line drawn tangent to the point A in Figure 2.2.

Secant modulus: Secant modulus is represented by the slope of a line drawn form the origin to any point B on the curve. There is no standard method in determining the secant modulus but usually point B is at the strain corresponding to one-third of the ultimate load. Secant modulus is a more practical measure of the modulus of elasticity and is mostly taken as the static modulus of elasticity.

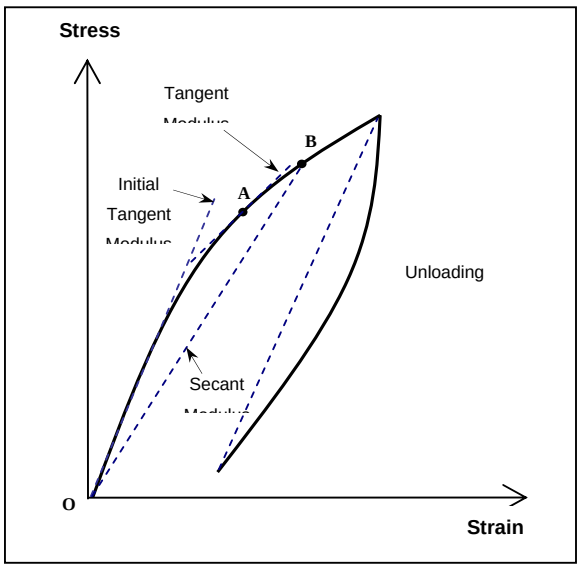

Figure 2.2: Typical stress-strain curve for concrete

2.2.1 Factors Affecting Modulus of Elasticity

Modulus of elasticity increases with increase of compressive strength but there is no agreement on precise form of relationship. The actual values range between 500 and 1600 times the compressive strength (Reynolds, 1988). The magnitude of elastic modulus of concrete depends on a variety of factors. These include the properties of mortar, properties and proportions of coarse aggregates, size and shape of specimens, degree of wetness of concrete at the time of testing, rate of loading, as well as the testing method to obtain the modulus of elasticity (Iravani, 1996; Mokhtarzadeh and French, 2000).

Under the circumstances when the test condition is the same, the type of coarse aggregate can be singled out to be the most significant parameter that affects the modulus of elasticity. Various researches conducted concluded that concrete with the same compressive strength may have different modulus of elasticity if different types of aggregates are used (Mansur et al., 1994; Iravani, 1996; Mokhtarzadeh and French, 2000). For a particular concrete strength, sandstone gives the smallest elastic modulus, followed by gravel whereas dolomite provides the largest value. Limestone, granite, quartzite, traprock and diabase on the other hand are found to give comparable elastic modulus values (Rashid et al., 2002).

2.3 Shrinkage in Concrete

Shrinkage strain in concrete may be divided into different types according to its influencing factors with chemical, hygral and thermal changes in the medium as the main origin components (Acker and Ulm, 2001). Besides causing shrinkage, these three components will also result in swelling of concrete under the condition of ingress of moisture into the concrete. Under the influence of the three basic origins, shrinkage can be further divided and classified into drying, capillary, autogenous, carbonation and thermal shrinkage (Acker and Ulm, 2001; Neville and Brooks, 1990). These five types of shrinkage are commonly known due to the significant dimensional strain it causes to the concrete. The primary type of shrinkage is drying

shrinkage. Unless specifically designated, shrinkage is generally taken to mean drying shrinkage.

Drying Shrinkage : Drying shrinkage occurs due to the loss of a layer of adsorbed water from the surface of the gel particles. This layer is roughly one water molecule thick or about 1% of the size of the gel particles (MacGregor, 1997).

Capillary Shrinkage : Capillary or plastic shrinkage is the result of capillary pressure produced by surface tension of water in fresh concrete during the early hours of drying, when concrete is still in the plastic state (Ojdrovic and Zarghamee, 1996). It is attributed to the development of capillary stress as water menisci develop due to loss of water by evaporation from the surface of concrete. According to Neville and Brooks (1990), the magnitude of this volumetric contraction is of the order of 1% of the absolute volume of dry cement.

Autogenous Shrinkage : Autogenous shrinkage is a phenomenon that occurs as water is removed internally by chemical combination during hydration in a moisture-sealed state (Bazant, 1988). The macroscopic volume reduction is due to self desiccation whereby cementatious materials shrink without any change in weight (Tazawa and Miyazawa, 1995). It occurs at a constant temperature without the influence of external load, moisture movement or carbonation. Autogenous shrinkage is significant for high strength and high performance concrete, when the water-cement ratio is less than 0.4. It is reported by Tazawa and Miyazawa (1995) in their research paper that for w/c of 0.3 and 0.17, autogenous shrinkage may reach up to 1100×10^{-6} and 4000×10^{-6} micron, respectively at the age of 14 days. The magnitudes reported are fairly large. The strain increases dramatically when the water-cement ratio is reduced.

Chemical Shrinkage : Chemical shrinkage is a term used to cover a number of distinct shrinkage or swelling mechanisms such as hydration shrinkage, thermal shrinkage, dehydration shrinkage, crystallization swelling, carbonation shrinkage and conversion shrinkage (Ojdrovic and Zarghamee, 1996). All these volume change are caused by chemical reactions (Bazant and Wittmann, 1982).

Carbonation Shrinkage : Carbonation shrinkage is a part of chemical shrinkage caused by reaction of CO_2 with the hydrated cement when concrete is carbonated in a low relative humidity environment (Neville and Brooks, 1990). In the presence of CO_2, the maximum shrinkage occurs at about RH of 50%. The amount of carbonation shrinkage can equal the drying shrinkage, effectively doubling the total amount of shrinkage (MacGregor, 1997).

Thermal Shrinkage : Thermal shrinkage refers to thermal actions of temperature variations applied at the surface of material due to climatic influence as well as industrial origin such as thermal treatment to accelerate concrete hardening. In addition to that, thermal shrinkage also occurs due to the heat produced in the mass of the concrete by the hydration of the cement. This particularly happens to structural elements of greater thickness when the rate at which hydration heat released is larger than the rate of diffusion through conduction (Acker and Ulm, 2001). As a consequence to the heat flow, a gradient of temperature potential is generated and strains that result from the thermal shrinkage are then not uniform, engendering structural effects and stresses.

2.3.1 Swelling in Concrete

When concrete is re-saturated, swelling occurs but the swelling is insufficient to completely compensate for the shrinkage that occurred in drying, unless shrinkage compensating expansive cement is used (Bazant, 1988). This shows that a part of the shrinkage is irreversible and it should be distinguished from the reversible moisture movement caused by alternating storage under wet and dry conditions.

Swelling occurs when there is a continuous supply of water to the concrete during hydration, causing it to expand due to absorption of water by the cement gel (Neville and Brooks, 1990). The water molecule acts against the cohesive forces and tend to force the gel particles further apart, with a resultant swelling pressure. In addition, the ingress of water decreases the surface tension of the gel and a further small expansion takes place (Neville, 1981). Figure 2.3, adapted from Neville and

Brooks (1990) shows the moisture movement in concrete with reversible and irreversible shrinkage deformation as well as concrete swelling.

The swelling of concrete is considerably small, approximately 100 x 10^{-6} – 150 x 10^{-6} for a mix with cement content of 300 kg/m^3. This value is reached 6 – 12 months after casting, and only a very small further swelling takes place. The swelling is accompanied by an increase in weight of the order of 1%. The increase in weight is thus considerably greater than the increase in volume; as water enters in occupy the space created by the decrease in volume on hydration of the system cement plus water (Neville, 1981).

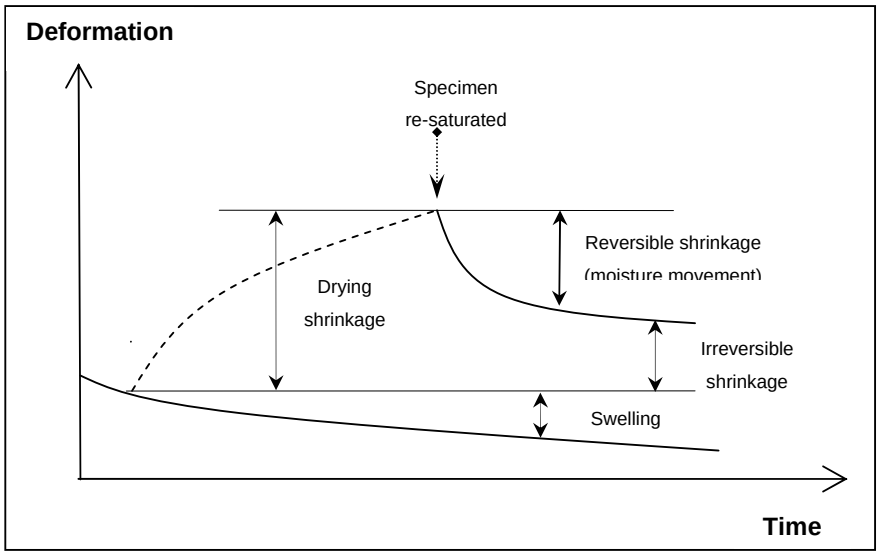

Figure 2.3: Moisture movements in concrete when it has dried from age t_o and re-saturated at age t

2.4 Creep in Concrete

Creep may be defined as the slow deformation of a material over an extended period of time while under sustained load. The strain which is produced in the course of a creep test at the end of loading may be three or four times the initial elastic strain (Acker and Ulm, 2001). Therefore creep is of considerable importance in structural mechanics. Besides that, creep may also be viewed from another standpoint, to be known as a form of relaxation of material. This occurs when the restraints are such

that a stressed concrete specimen is subjected to a constant strain; creep will manifest itself as a progressive decrease in stress with time (Neville, 1981). However in most cases, the detrimental effect of creep prevails.

The occurrence of creep is based on the viscous component in the concrete as well as hygrometric and hydrometric condition of the material. Creep strain can be defined into several different components with basic creep and drying creep being the two most recognized forms. In addition to that, the classification also comprises of transitional creep strains that causes a magnification of creep rate (Hauggaard et al., 1999). These transient phenomena can be considered as the result of local reductions in rigidity at the site of phase changes occurring in the cement paste due to interaction with the environment (Parrott, 1978). The details of the different types of creep strain are discussed here.

Basic Creep : Basic creep is creep deformation that occurs under a constant compression at hygrometric equilibrium, without the event of moisture exchange between the ambient and the medium (Acker and Ulm, 2001).

Drying Creep : Drying creep, also known as the Pickett effect is the additional creep strain in excess of basic creep when the same concrete is allowed to dry under load, in response to the changes in its environment (Metha, 1986). The magnitude of creep obtained is mainly due to drying creep as water movement in concrete induced higher stress. The strain is expressed in millimeters per millimeter, resulting in a dimensionless pure number. If the moisture content increases, wetting creep will result. Both wetting and drying creep are considered as transitional hygral creep strains (Bazant, 1988).

Transitional Thermal Creep : The term transitional thermal creep is used to describe the additional strain that occurs when the temperature of concrete changes while under load (Bazant et al., 2004). The temperature changes can be due to the influence of the surrounding ambient or due to the heat development of cement paste hydration.

Transitional Chemical Creep : Transitional chemical creep might be applied to the extra strain observed when the concrete undergoes significant chemical reactions while under load. A few examples of significant chemical reactions are such as hydration, carbonation and sulphate attack. Transitional chemical creep due to hydration may account for the relatively high creep strains observed for concrete loaded at early ages (Bazant, 1988).

2.4.1 Creep Recovery

When the sustained load is removed, the strain decreases immediately by an amount equal to the elastic strain at the given age, generally lower than the elastic strain on loading. This instantaneous recovery is followed by a gradual decrease in strain, called creep recovery. The shape of the creep recovery curve is rather like that of the creep curve. However the recovery approaches its maximum value much more rapidly. Creep is not a simply reversible phenomenon. Therefore the reversal of creep will not be complete, resulting in residual deformation after sustained application of load. Figure 2.4, taken from Neville (1981) shows the creep recovery curve and the residual deformation when specimen is unloaded.

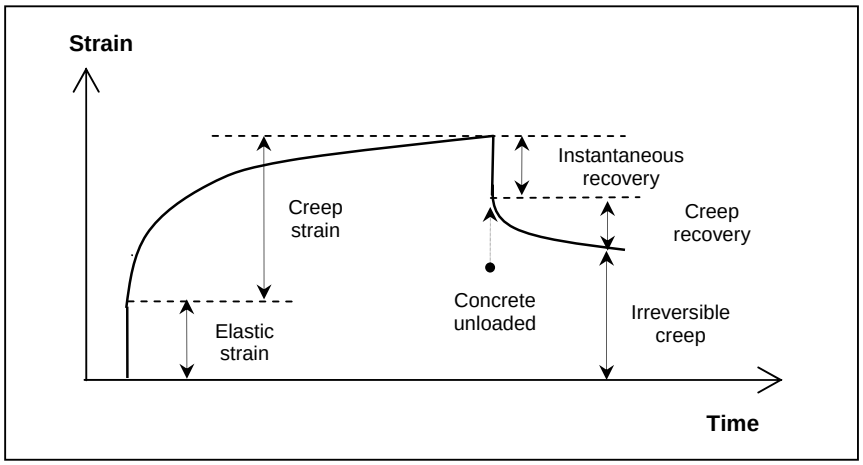

Figure 2.4: Creep recovery curve of concrete when load is removed

2.4.2 Terms and Definitions

The presentation of creep data in different ways to facilitate the strain calculation and prediction has formed a few terminologies in defining creep strain. Different terms are used under different conditions depending on the suitability. Definition of a few of the common terms used is explained in this section.

The ultimate creep, ε_{ult} is the maximum magnitude of creep predicted attainable by the structure according to the prediction models. According to BS 8110, this final value is made referring to 30 years of duration after load. The 30 year duration is determined from the findings that creep of concrete after 30 years under load is negligible (Neville, 1990).

Creep coefficient, ϕ expresses the creep strain as a fraction of the elastic strain. Typically the creep coefficient falls in the range 2.0 – 6.0 for ultimate creep. Most of the standard codes specify prediction of creep in the term of creep coefficient as the influence of concrete elastic property is eliminated. This allows flexibility for application.

$$\phi = \frac{\varepsilon_{cr}}{\varepsilon_E} \tag{2.2}$$

where

ε_{cr} = creep strain (micron)

ε_E = elastic strain (micron)

The creep strain can also be given in terms of strain per unit stress. Such value is called specific creep or creep compliance, C and is given in millimeters per millimeter per unit stress. It is used in order to compare the creep potential of concrete loaded at different levels of stress.

$$C = \frac{\varepsilon_{cr}}{\sigma} \tag{2.3}$$

Creep function, $J(t,t_o)$ or also known as compliance function is often expressed as a sum of the elastic compliance $1/E(t_o)$ and the creep compliance, $C(t,t_o)$. It represents the strain at time t produced by a unit constant stress, σ that has been acting since time t_o.

$$J(t,t_o) = 1/E(t_o) + C(t,t_o)$$

$$= \frac{1+\phi(t,t_o)}{E(t_o)} \tag{2.4}$$

2.5 Mechanism of Creep and Shrinkage

The intricate phenomenon of creep and shrinkage have been studied and explained based on two opposite mechanisms in the past. The first is the material science approach based on direct investigation of the physical properties of water near the solid surfaces with details of the microstructure in hardened cement paste. Second is the practical technical approach based on macroscopic measurements of creep and shrinkage deformation carried out on large concrete specimens (Bazant and Wittmann, 1982).

The behaviour of composite material cannot be linked to the mechanism of microstructure alone as the effects of pores, inclusions and cracks also have to be taken into consideration. Bazant and Wittmann (1982) in their study explained that the actual behaviour of creep and shrinkage depends on both real and apparent mechanisms. Real mechanisms can be considered as the microstructural material properties determined by the physical and chemical make-up of the hydrated cement paste (Bazant, 1988). The apparent mechanisms are caused by factors which modify the anticipated strain such as crack formation, moisture gradient and internally created localised stress.

The subdivision of processes involved in creep and shrinkage of concrete in real and apparent mechanisms are presented in Table 2.1. The main reason apparent mechanisms are introduced is because these time-dependent deformation incurred cannot be directly linked to the real creep or shrinkage mechanisms. A number of apparent mechanisms are always involved in modifying the behaviour. In most cases,

the deformation of concrete material occurs under simultaneous creep and shrinkage. The mechanism under this condition will also be discussed in this section. It should be noted however that the mechanisms discussed here have yet to be proven to be the only processes involved in the creep and shrinkage mechanism as interpretation of the behaviour of time-dependent deformation is still a matter of major controversy.

Table 2.1: Summary of creep and shrinkage mechanism

Concrete Deformation	Real Mechanism	Apparent Mechanism
Creep (no exchange of moisture)	Short-time creep, Particle displacement	Internal stress distribution
Shrinkage (no external load)	Capillary shrinkage, Chemical shrinkage, Drying shrinkage	Hygral gradient, Crack formation
Simultaneous Creep and Shrinkage		Hygral gradient, Crack formation, Drying creep, Load induced shrinkage

2.5.1 Creep Real Mechanism

2.5.1.1 Short-term Creep

The short-term creep mechanism was first suggested by Ruetz (1966) and further pursued by Wittmann (1982). This mechanism is known to be caused by a development of capillary stress due to redistribution of capillary water towards the largest diameter pores within the structure of hardened cement paste. It may be attributed to a change of the hygral equilibrium in the gas filled space which generates strain and stresses and eventually microcracking which results in the short-term component of creep (Acker and Ulm, 2001).

2.5.1.2 Long-term Creep of Particle Displacement

Long-term creep in hardened cement paste occurs under the displacement of gel particles. When load is applied on concrete, most of the resulting compression

across the micropores is carried by the solid particles. The effect of high enough transverse pressure will push some of the bonded particles above their activation energy barriers. This causes the particles to migrate to locations of lower stress, reducing the transverse pressure and forming new bonds that inhibit further movements and retard local deformation for a while. The movement of migration of solid particles contributes to the deformation due to a loss of mass and thickness in the adsorbed layers (Bazant and Wittmann, 1982).

2.5.2 Apparent Creep Mechanism

2.5.2.1 Shrinkage Induced Creep or Drying Creep

The most obvious and probably the most important apparent creep mechanism is drying creep. The drying creep effect, which is also known as the stress-induced shrinkage or Pickett effect is a transient effect consisting in the fact that the apparent creep during drying is much larger than the sum of basic creep and drying shrinkage. The physical source of drying creep is known to involve two different mechanisms. One of it may be due to the fact that as water is diffusing out of the loaded gel micropores it creates disorder. This facilitates in the migrations of solid particles. Another possible mechanism is of an apparent additional creep due to microcraking (Bazant and Wittmann, 1982) or also known as strain-softening damage (Bazant and Xi, 1994) produced by drying in the specimen as a whole.

2.5.2.2 Thermal Transient Creep

The transitional thermal creep represents a transient increase of creep after a temperature change of either heating or cooling. In the case of cooling, the transient increase is of the opposite sign than the final change in creep rate after a steady state lower temperature has been regained. Similar to the drying creep effect, a change in temperature has two analogous mechanisms, firstly involving a thermal gradient and then followed by a hygral gradient (Bazant et al., 2004). The thermal gradient will result in microcracking whereas a change of chemical potential of nanopore water

will change the level of microprestress. All these will lead to internal stress distribution that changes the creep rate.

2.5.2.3 Heterogeneous Structure of Hardened Cement Paste

In the composite material of concrete, the aggregate and the hardened cement paste react in different ways when subjected to loading. The aggregate react in a linear elastic way while the hardened cement paste can be considered viscoelastic. Aggregates are generally dimensionally stable and will elastically restrain the potential deformation of the paste. Therefore, when creep deformation in the binding matrix takes place, stresses will be set up at the paste-aggregate interface and may cause microcracking and modify the internal stress distribution.

2.5.3 Shrinkage Real Mechanism

2.5.3.1 Capillary Shrinkage

As explained in Sub-Chapter 2.3, capillary shrinkage is associated to induce surface tension by loss of water due to evaporation from the surface of concrete. The loss of free water first occurs when drying begins the hygral actions induce internal relative humidity gradients within the cement paste structure. With time, water molecules are transferred from the large surface area of the calcium silicate hydrates into the empty capillaries and then out of the concrete. As the larger pores are emptied, the capillary tension increases, causing compression of the solid skeleton that resulted in contraction of cement paste. If the process is not excessive until cracks are formed, this mechanism leads to a beneficial compaction of fresh concrete. However if the drying continues, homogenous water phase disintegrates and the second stage of capillary shrinkage occurs due to entrapment of water in the narrow spaces between neighbouring particles (Bazant and Wittmann, 1982). The irreversible part of shrinkage is associated with the formation of additional physical and chemical bonds in the cement gel when adsorbed water has been removed.

2.5.3.2 Chemical Shrinkage

The chemical reactions involved in causing shrinkage strain in cement paste are hydration of cement and also secondary reactions, such as formation of enttringite, thermal changes, dehydration, crystallization swelling, carbonation and conversion shrinkage (P. Lura et al., 2003). These chemical processes in the medium resulted in volume change, hygral difference and formation of new products that create internal pressure and additional strain. The hydration of cement leads to volume and dimensional changes in concrete that is usually proportional to the degree of hydration. If the main constituent of Portland cement react with water, a characteristic volume change and a gross volume decrease of about 7% is observed (Bazant and Wittmann, 1982).

Similar to hygral actions, thermal actions are resulted from variations of ambient conditions which generate heat flows, and as a consequence causes a gradient of temperature potential. In addition to that, when Portland cement reacts with water, a degree of heat is liberated. The specific heat of hydration depends on the chemical composition of the cement. Some of the heat is liberated while the concrete is still young and easily deformable. As the rate of hydration slows down, the temperature decreases and as a consequence a concrete specimen undergoes thermal shrinkage, which can cause serious cracking (Acker and Ulm, 2001).

The chemical reaction of carbonation on the other hand occurs when the carbon dioxide in the air diffuses into the permeable concrete and react with $Ca(OH)_2$ compound of the hydrated cement. This reaction produces $CaCO_3$ and H_2O. The liberated water evaporates and this resulted in a decrease in volume. In additional to that, decomposition of the calcium compounds in the hydrated matrix combined with alternating wetting and drying in air containing CO_2 leads to an increase in the magnitude of irreversible shrinkage (Nawy, 2001).

2.5.3.3 Drying Shrinkage

Under the condition of hygral difference between the medium and ambient, withdrawal of water from hardened concrete causes drying shrinkage. A part of this

movement is irreversible and should be distinguished from the reversible moisture movement caused by alternating storage under wet and dry conditions. The irreversible part of shrinkage is associated to the formation of additional physical and chemical bonds in the cement gel when adsorbed water has been removed. As drying continues, adsorbed water is removed and the change in the volume of unrestrained cement paste at that stage is approximately equal to the loss of water layer one molecule thick from the surface of all gel particles (Neville, 1981)

2.5.4 Shrinkage Apparent Mechanism

2.5.4.1 Influence of Cracking

Cracks are formed under drying condition as the tensile stresses in the drying outer zones of concrete overcome the tensile strength of the material. These cracks may be either continuous and visible, or discontinuous and so fine and densely spaced that they are described in a smeared, continuous manner as strain softening (Bazant, 1988). Strain softening is the occurrence of microcracking in concrete. Shrinkage takes place in the porous matrix only and the hygral length change of most aggregates can be neglected. The differential stresses between the paste and aggregate cause additional cracking in the structure of concrete. Real shrinkage mechanisms only govern the strains of the porous matrix. Therefore crack formation in the heterogeneous matrix is an apparent shrinkage mechanism. Cracks inevitably change the time-dependence as well as the final value of shrinkage and the proportion of reversible and irreversible shrinkage (Bazant and Wittmann, 1982).

2.5.4.2 Influence of Geometry

Hygral gradient starts to build up in a specimen immediately after the drying process begins. Depending on the geometry and the diffusion coefficient, the hygral gradient can exist in concrete for many years. Hygral gradient occur in a drying specimen as the shrinkage of the outer layer is hindered by the still saturated inner part. The measured length change under these conditions is the consequences of the

resulting internal stress distribution. This change of internal stress results in a modified geometry-dependent shrinkage (Bazant and Wittmann, 1982). In addition to that, irreversible changes in specimens such as microcraking, continued hydration or time-dependent changes in microstructural properties will give rise to the effect of size (Bazant, 1988). Thus the influence of size is an important parameter in the prediction of shrinkage strain.

2.6 Factors Influencing Creep and Shrinkage

The factors for creep and shrinkage are commonly classified as internal and external factors. The internal factors are those material characteristics which are fixed once and for all when the concrete is cast. Some of the examples are the mix composition, materials properties and quality. The external influence on the other hand refers to the factors which can vary after casting such as the influence of environment condition on concrete structures (Bazant, 1988). The effects of a few main factors on time-dependent deformation are discussed here and the influencing factors for both creep and shrinkage are summarized in Table 2.2.

Table 2.2: Influencing factors of creep and shrinkage strain

Category	**Influencing Factors**	
	Creep	**Shrinkage**
Internal Factors	Aggregate – volume and mechanical properties	Aggregate – volume and mechanical properties
	Cement types and content	Cement types and content
	Water-cement ratio	Water-cement ratio
	Concrete strength	Concrete strength
	Member size	Member size
External Factors	Curing condition	Curing condition
	Temperature and humidity	Temperature and humidity
	Age at loading	Age when drying begins
	Stress intensity	-

2.6.1 Internal Factors

2.6.1.1 Aggregate

The effect of aggregate quantity and properties in concrete is highly considerable for time-dependent deformation because the aggregate acts as a restraint to the deformation when creep and shrinkage occurs only on cement paste. For a constant paste volume content, an increase in the aggregate volume decreases creep. As for an example, an increase from 65% to 75% lowered creep by 10% (Neville, 1981) and this behaviour is the same regardless of whether the coarse aggregate is natural stone or lightweight artificial aggregate. When the aggregate used is of higher modulus of elasticity, creep and shrinkage strain is reduced.

2.6.1.2 Cement

Cement plays a vital role in influencing creep and shrinkage because the time-dependent deformation occurs chiefly in the hydrated cement paste that surrounds the aggregate. The type of cement affects creep in terms of its strength gain potential and its strength at the time of load application. It was reported that rapid-hardening cements such as Type III cement tend to creep less because it is able to harden faster. This increases the stiffness of the concrete matrix when the load is applied and thus, the concrete is more resistant to creep (Neville, 1970).

2.6.1.3 Silica Fume

Besides the influence on types of cement, mineral admixtures such as silica fume is known to play a vital role in influencing creep and shrinkage in concrete. Generally, the inclusion and increase in the proportion of silica fume decreases creep and drying shrinkage strain. This pattern of behaviour is observed in the result of study conducted by Mazloom et al. (2003) and Khatri and Sirivivatnanon (1995). The decrease in creep and drying shrinkage can be attributed to the additional pozzolanic reaction resulting in stronger concrete pore structure and higher resistance to deformation caused by applied force (Li and Yao, 2001; Haque, 1996). However, an increase in the proportion of silica fume increases autogenous shrinkage of HSC

(Mazloom et al., 2003; Jensen and Hansen, 2001; Tazawa and Miyazawa, 1995; Zhang et al., 2003). The investigation by Mazloom at al. (2003) reported that inclusion of 10% and 15% of silica fume increases autogenous shrinkage by 33% and 50%, respectively. The significant increment in autogenous shrinkage is due to the refinement of pore size distribution that leads to a further increase in capillary tension and more contraction of cement paste.

2.6.1.4 Ground Granulated Blast Furnace Slag

In many concrete mixtures, Portland cement is partially replaced with ground granulated blast furnace slag (GGBS). The study on creep and shrinkage of high strength concrete conducted by Li and Yao (2001) reported a reduction in the strain for concrete with 30% replacement of GGBS. The inclusion of GGBS helps to promote hydration of cement and increases the density of hardened cement paste. This strengthens the pore structure of concrete, thus producing concrete that is more resistant to deformation. The findings by Tan K. L (1996) also agree that the inclusion of GGBS reduces creep of concrete. In addition to that, Tan K. L. (1996) observed that slag replacement of 55% resulted in lower creep than at replacement of 22%. This is probably because the pores of the concrete were more effectively filled up by the hydration product at higher slag content.

The adverse effect however is observed when slag is use at high replacement level. This is proven in the result of Khatri and Sirivivatnanon (1995) as concrete with 65% slag replacement exhibit approximately 10% higher in specific creep as compared to the control concrete. Chern and Chan (1989) who performed creep and shrinkage tests on specimens with varying amounts of GGBS reported that an increase in slag contents actually increases creep and shrinkage of concrete. It is believed that the increased shrinkage may be due to the greater volume of paste in the concrete when GGBS is substituted on an equal mass basis because slag has lower specific gravity than Portland cement (ACI Committee 226, 1994).

2.6.1.5 Fly Ash

The effect of fly ash on creep of concrete are limited primarily to the extent to which fly ash influences the ultimate strength and the rate of strength gain. Concrete with given volume of cement plus fly ash loaded at age of 28 days or less will normally exhibit higher creep strain than concrete having an equal volume of cement only, due to the lower strength of fly ash concrete at time of loading (Lane and Best, 1982). However both Lane and Best (1982) and Ghosh and Timusk (1981) showed that the concrete with fly ash proportioned to have the same strength at the age of loading as concrete without fly ash produced less creep strain at all subsequent ages. This is due to the greater rate of late age strength gain common to most fly ash concrete (ACI 226, 1994).

Tangtermsirikul, 1995 conducted test on 15 x 40 x 160 mm prism specimens to measure length change of concrete containing Class C and Class F fly ash. The drying shrinkage tests were conducted in a controlled environment of 25^{o}C and 60% relative humidity. The class C fly ash is reported to exhibit lower drying shrinkage than the ordinary cement paste mixtures. The application of the fly ash reduced the water requirement of the mixtures, thus reducing the shrinkage. The Class C fly ash also reduced the autogenous shrinkage due to chemical expansion of the concrete mixture.

2.6.1.6 Water-Cement Ratio

The magnitude of time-dependent deformation is also influenced by the water-cement (w/c) ratio that is directly related to the concrete strength. The water content of a mixture greatly impacts the paste rigidity. Lower water content results in higher strength and fewer pores in the mature cement, which increases the rigidity of the solid matrix and decreases deformation (Smadi et al., 1987). At higher w/c ratio, more excess water remains in the concrete after hydration. More excess water means a potential for higher drying creep and shrinkage. Therefore with a constant cement content, creep and shrinkage increases with increasing w/c ratio. Generally, within a wide range of mixes, creep is inversely proportional to the strength of concrete at a specific age of loading (Neville, 1990).

2.6.1.7 Chemical Admixutres

With the progressive development of concrete technology, the inclusion of chemical admixtures to improve the concrete performance is becoming a common practice. Superplasticiser has been invariably added into concrete mixes to reduce mixing water content and at the same time produce concrete with good workability. Alexander et al. (1980) conducted a study on the effect of sulphonated melamine formaldehyde superplasticiser on creep and shrinkage in concrete. The w/c ratio for both superplasticised and control concrete was 0.3 and the superplasticiser added was 1% of the weight of cement. Based on the results, it was reported that creep of superplastised concrete was 10% higher than the control concrete. Higher drying shrinkage was also observed for superplasticised concrete within the range from 10% at early and late ages, to about 25% at intermediate ages was observed. This result is in agreement with Brooks (1989) finding that reported approximately 30% lower in shrinkage strain for ordinary concrete compared to concrete with plasticizing admixtures.

Addition of superplasticizer to concrete modifies the forces between grains of cement, resulting in breaking down of large agglomerates into smaller ones; releasing free water. Dispersion of cement, the release of free water and low external humidity will contribute to speeding up cement grain hydration. Therefore addition of superplasticizer results in accelerated hydration and thus increases shrinkage (Jasiczak and Szymanski, 2004).

2.6.1.8 Size and Shape of Specimen

The practical significance of the size of concrete members usually lies in making a transition from the results of creep tests on laboratory specimens to the behaviour of full-size members. Several investigations have indicated that creep and shrinkage strain decreases with an increase in the size of specimen (Almudaiheem and Hansen, 1987; Omar et al., 2004, Bryant and Vadhanavikkit, 1987; Mazloom and Brooks). The work of Hansen and Mattock (1966) indicates that both creep and shrinkage of concrete are functions of the volume surface ratio of the member. Thus

the size of members is an indirect effect and is mainly controlled by the surface area of specimens. It was concluded that when a free surface is sealed, creep is unaffected by the size of the members. Therefore the prediction of creep and shrinkage models allows for the size effects in terms of volume to surface ratio or effective thickness. The latter is defined as the ratio of twice the cross section area to the exposed perimeter.

The mechanism of creep and shrinkage is highly related to mobility of moisture in the member. Therefore creep and shrinkage of concrete are greatly influenced by the size of the parts because larger specimens with deeper sections have thicker average drying paths that slow down the diffusion of adsorbed moisture from the specimen (Acker and Ulm, 2001). However, it should be noted that Bissonnette at al. (1999) disagree that larger specimen exhibit lower shrinkage. His report indicated that that the ultimate shrinkage does not differ much from one specimen size to the other and believe that only the rate of drying is affected by the size of specimen.

On the influence of shape of concrete members, Hansen and Mattock (1966) reported that the effect is very small when tested on specimens with equal volume-surface ratio. The shape of specimen affects the moisture distribution within it. For the same volume-surface ratio, prism specimens tend to exhibit lower shrinkage and drying creep than for cylinders. This is due to the fact that the variation in relative humidity along a diagonal is different than along a normal to the surface. On the whole, the shape factor is of very lesser importance than the size factor and for most practical purposes can be neglected (Neville at al., 1983).

2.6.2 External Factors

2.6.2.1 Curing Method

The curing method can substantially impact the creep and shrinkage behavior of concrete. The curing becomes even more important if the concrete contains supplementary cementing materials such as fly ash, ground granulated blast furnace

slag or silica fume. It is reported by ACI Committee 517 (1963) that low pressure steam curing reduces creep. Steam curing at 63^{o}C for 13 hours reduced creep by 30% to 50% due to accelerated hydration of the cement and the moisture loss that occurs when the specimens are transferred to a drier, cooler environment (ACI Committee 517, 1963). Mokhtarzadeh and French (1990) reported that higher curing temperature resulted in more creep as higher temperature increases the porosity and internal cracking, which contribute to creep.

2.6.2.2 Ambient Temperature

Many research that has been carried out in the past concluded that higher temperature leads to higher creep. However it is not a monotonic function of temperature. It passes a maximum in the vicinity of 71^{o}C and thereafter decreases with further rise in temperature (Nasser and Marzouk, 1981). Nasser and Neville (1965) have suggested that in the range of 71^{o}C to 82^{o}C, some of the adsorbed water starts to evaporate off. Thereafter, the gel becomes the sole deformable phase which explains the reason for the decrease in creep rate beyond 82^{o}C. Ratio of creep strain at 71^{o}C to creep strain at 21^{o}C is about 2.4 in the case where specimens are permanently stored, and as much as 4.0 when temperature is raised a week before loading (Nasser and Neville, 1967).

2.6.2.3 Relative Humidity

On the effect of relative humidity (RH), creep may be 2 to 3 times lower at RH of 100% than at RH of 50% (Troxell, 1958). Shrinkage is also lower at higher RH and the result from research conducted by Barr et al. (2003) confirms on this influence. At lower RH, drying creep or drying shrinkage is expected to occur and one of the reasons for the additional strain is the diffusion of moisture from the medium to the ambient. Another example on the influence of RH on shrinkage is the result of research conducted by Bissonnette et al. (1999). In his study, drying shrinkage is reported to be approximately inversely proportional to the RH of the surrounding atmosphere within the range of RH 48% to 100%.

2.6.2.4 Age at Loading

Another factor that affects creep is the age at loading. At a later age of loading, magnitude of creep decrease due to the strength development and quality of gel improvement in concrete (Neville, 1990). Similar behaviour is observed for shrinkage as the deformation is lower at later age of drying due to longer moisture curing time and better concrete strength development. The effect of this factor is well established through various researches in the past as well as recent ones (Song et al., 2002).

2.6.2.5 Stress Intensity

Creep is a deformation induced by constant sustained stress. Therefore the stress intensity on the concrete affects the magnitude of creep deformation. Numerous tests have indicated that creep deformation is proportional to the applied stress but this proportionality is valid only for low stress levels (Marzouk, 1991). The upper limit of the relationship cannot be determined accurately but can vary between 0.2 to 0.5 of the ultimate strength. This range in the limit of the proportionality is expected due to the large extent of microcracks that exist at about 40% of the ultimate load. The strain is recoverable up to 30 – 50% of the ultimate strain when the sustained stress is removed (Nawy, 2001).

2.7 Structural Issues Related to Creep and Shrinkage

In general, the effects of creep should be taken into account only for the serviceability limit states. However, creep can sometimes occur and have an influence on behaviour at the ultimate limit state. This applies to second-order effects where creep increases the initial eccentricity, and also for structures where the time dependent deformations are large in relations to the deformability of some of their elements such as differential shortening for high rise buildings (MacGregor, 1997).

In most cases, the deformation due to temperature, creep and shrinkage shall be checked in design of structures to ensure the safety at the serviceability limit state such as durability and performance of the structures. As in shrinkage, creep increases the deformation of columns, deflection of beams and slabs, and causes loss of prestress force. In addition to that, the initial eccentricity of a reinforced concrete column increases with time due to creep, resulting in the transfer of the compressive load from the concrete to the steel in the section (Nawy, 2001). In the construction of cantilever box girder bridges, accurate prediction of creep and shrinkage is important to ensure matching vertical and horizontal alignment during stitching of decks. In order to show an example of the seriousness of those deformations in the design of concrete structures, three related research studies are highlighted here.

In the high rise buildings, vertical members are subjected to a large axial shortening due to elastic, creep and shrinkage deformations. Creep and shrinkage may be more important for floor levelness and exterior wall movement. In the study conducted by Park (2003), it is estimated that the maximum vertical shortening of an exterior column of a 70-storey concrete building is approximately 91.4 mm, whereas the maximum differential shortening between the exterior column and the interior wall is approximately 25.4 mm. These phenomenon are shown in Figure 2.5 (Park, 2003). The differential shortening is large and may cause excessive cracking. Thus, to avoid unexpected damage, the elastic and inelastic shortening of vertical members should be accurately predicted and properly compensated for.

Creep and shrinkage are of primary importance in the design of prestressed concrete members as they reduce the compressive stress induced by the prestressing force. Such reduction may affect the formation of cracks in members (Neville, 1970). The losses may reach up to about 45% for concrete prestressed at 60% of its compressive strength and cured in relative humidity of 50% (Peterson, 1968). It is therefore essential to be able to predict the magnitude of creep and shrinkage effects to an acceptable accuracy.

Another significant influence of creep and shrinkage in reinforced and prestressed concrete design is the deflection of the structural members. The magnitude of deflection changes with time due to the effect of creep and shrinkage

and also the way elastic modulus of concrete is predicted. Deflection may affect the serviceability and also the aesthetic value of the structures. Inaccurate prediction of deflection such as excessive pre-camber in prestressed concrete beam may incur additional cost to the construction.

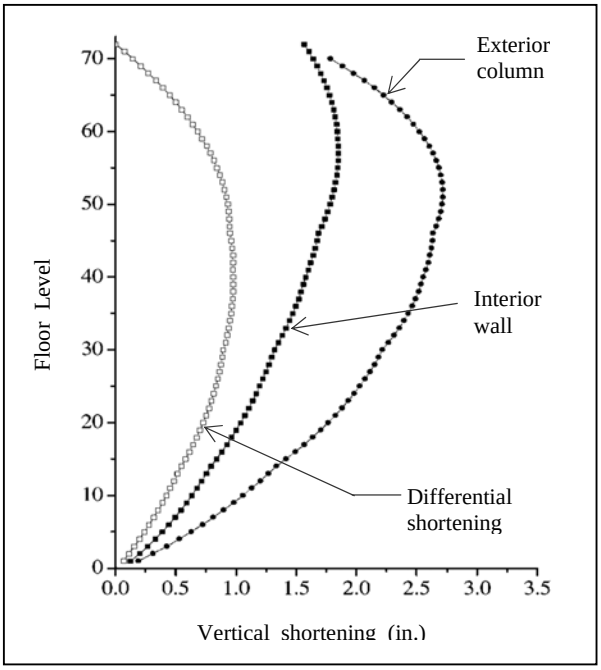

Figure 2.5: Differential shortening between the exterior column and the interior wall after slab casting for a 70-storey building

2.8 High Strength Concrete

The definition of high strength concrete (HSC) varies with time and geographical location, depending mainly on the availability of raw materials and technical knowledge as well as the demand from the construction industry in a particular region or country. In the North American practice, concrete with 28 day cylinder compressive strength more than 41N/mm^2 is considered as HSC (ACI 363R, 1992). On the other hand, the CEB-FIP (1990) state-of-the-art report on HSC defines it as concrete with a minimum 28 day compressive strength of 60N/mm^2. As for this research, definition of HSC is in line with the definition by ACI, which is approximately equivalent to compressive cube strength of 50N/mm^2.

Over the last several decades, in order to improve the performance and strength of concrete, research has focused on altering the mix design to reduce the porosity matrix phase. As a result, changes in mixture proportioning have been advocated to reduce the water-to-cement ratio. Concrete of Grade 50 to 70 that used to be hard to achieve is no longer foreign to the construction industry today owing to the inclusion of chemical admixtures and cement replacement materials. Admixtures such as superplasticizers and cement replacement materials such as fly ashes and silica fumes improve the dispersion of cement in the mix, producing workable concrete with low water-cement ratios. The resulting concrete has lower void ratio and is stronger than usual concrete (MacGregor, 1997).

In Malaysia, concrete with high compressive strength has been successfully produced commercially for use in high-rise buildings as well as other special structures. The most recognizable building with HSC is the Petronas Twin Towers Kuala Lumpur which required the use of concrete strength up to 130N/mm^2. Another example of HSC usage in Malaysia is the 77-storey Telekom headquarters in Bangsar that required the supply of 70N/mm^2 concrete (Kribanandan, 2002).

With the rapid increase in the use of new additives, there is a need to accurately predict properties of the concrete, especially the modulus of elasticity, shrinkage, creep, permeability and durability (Bazant and Baweja, 2000; Nassif et al., 2004). On top of that, Mansur et al., (1994) also concluded in his study that as the strength of the material gets higher, some of the characteristics and engineering properties of HSC become different from those of NSC. Thus, for an effective and safe application of HSC, especially in our own country, there is a need to verify on the behaviour of the material and its performance in the tropical climate.

2.8.1 Chemical and Mineral Admixtures of High Strength Concrete

The use of mineral admixtures in the industry is becoming increasingly popular, especially for high strength and low permeable concrete. Addition of silica fume (SF) and fly ash (FA) or ground granulated blast furnace slag (GGBS) together with chemical admixtures such as retarder and superplasticiser has become an

integral part of HSC production. Besides producing good quality concrete, the use of mineral admixtures carries additional benefit; utilization of waste product as these materials are actually produced as by-products of industry. The properties and performance of the materials used in this study; silica fume, ground-granulated blast furnace slag and superplasticiser are elaborated here.

2.8.1.1 Silica Fume

Silica fume is a by-product of the smelting process in the production of silicon metal and ferrosilicon alloys. In general, the silica fume used in concrete are those with composition of silicon ranging from 85% to 96%. The mean particle sizes of silica fume are in the range of 0.1 to 0.2 μm. Its specific gravity is about 2.20 but the bulk density is only at 200 to 300 kg/m^3 (Hollands, 2005). Besides Norwegian Standard NS 3050:1976, there is currently no British or American standard for silica fume.

The benefits from adding silica fume are the result of changes from two different but equally important processes to the microstructure of the concrete. The first is the physical aspect of silica fume and the second is its chemical contribution. In terms of the physical aspect, addition of silica fume beings millions of very fine particles into the concrete mixture, filling the spaces between cement grains. This phenomenon is frequently referred to as particle packing or micro-filling.

Silica fume has very high amorphous silicon dioxide content that makes it a very reactive pozzolanic material in concrete. As the Portland cement in concrete begins to react chemically, it releases calcium hydroxide ($Ca(OH)_2$). The silica fume reacts with this $Ca(OH)_2$ to form additional binder material called calcium silicate hydrate (C-S-H), which is very similar to the C-S-H formed from the Portland cement. This chemical reaction leads to a reduction in permeability and enhancement of mechanical properties, thus producing more durable concrete (Hollands, 2005).

2.8.1.2 Ground-Granulated Blast Furnace Slag

Ground-granulated blast furnace slag (GGBS) is a by-product of the iron production process. The mechanism of hydration differs from that of pozzolanic materials like PFA or silica fume and it occurs in two stages. First, blastfurnace slag containing sufficiently high calcium oxide (CaO) content reacts with water to produce some calcium silicate hydrates ($C_3S_2H_3$); a reaction that does not happen in pozzolanic materials. In the second stage, pozzolanic reaction takes place. Calcium hydroxide ($Ca(OH)_2$) released from the hydration of cement and slag will further react with blastfurnace slag to form more calcium silicate hydrates ($C_3S_2H_3$). This phenomenon helps to decrease permeability and improves the strength of the paste.

The use of GGBS provides a wide range of advantages. GGBS is an ideal material for high strength concrete where the use of cement replacement materials is required to control the danger of shrinkage cracks as well as thermal cracks. There is also an increase in durability of concrete containing GGBS due to finer pore structure and reduced permeability when hydration products replace calcium hydroxide. The resistance to sulphate attack and to salts in sea water is also improved as the diffusion coefficient of aggressive ions is reduced due to lower permeability.

2.8.1.3 Superplasticiser

Currently, a third generation of water reducers based on polycarboxylate polymers with long, comb-type side chains (PCE) has been developed. The dispersing and fluidifying property of PCE works through a double action of electrical repulsions and steric hindrance effects (Abdelrazig, 2006). When carboxylic acid adsorbed on the surface of cement particles, it become negatively charged and thus mutually repulsive. This inhibits the natural agglomeration of cement particles and enhances dispersion of cement, hence reduces water requirement in concrete. At the same time, bleeding is reduced due to the improved cohesion in the mix.

As compared to the traditional superplasticisers, this new generation comb-type polycarboxylate polymers are more effective in water reducing capability, controlled workability through longer slump retention and are ideal formulation to keep concrete cohesive and homogeneous.

2.8.2 Creep of High Strength Concrete

It is a well established fact that the creep coefficient value are less in HSC than in normal strength concrete. Table 2.3 presents the creep coefficient value for normal and high strength Portland cement concrete, obtained from a study by Nilson (1985). It is seen from the data that the ratio of creep coefficient in HSC to NSC can be as low as half of the coefficient for normal strength concrete. On the other hand, based on a study by Marzouk (1991), creep strain of HSC is reported to be 15% – 20% higher than normal strength concrete, depending on time after loading.

The explanation of this phenomena is given by Smadi (1987). HSC has low water-cement ratio in the mix design that resulted in fewer pores in the mature cement. This increases the rigidity of the solid matrix, thus creep and shrinkage deformation decreases, as it has been discussed in Sub-Chapter 2.8.1.

Swamy (1985) has also demonstrated that both the specific creep and the creep coefficients for HSC are sufficiently lower than those of NSC to give distinctive performance benefit to HSC. Due to the low creep strain for HSC, volumetric change throughout the loading history of concrete element is lower than NSC. This volumetric stability contributes significantly to the high performance characteristics of HSC. The usage of cementitious replacement material further lower the creep strain as compared to values obtained for Portland cement concrete. The effect of replacement materials were discussed in Sub-Chapter 2.6 and 2.8.

Table 2.3: Creep coefficient comparison for normal strength and high strength Portland cement concrete

Type of concrete	Concrete strength, $f_{c,28}$ [N/mm^2 (psi)]	Creep coefficient, C_u	$C_{u,HSC}/\ C_{u,NSC}$
Normal strength concrete	20.7 (3000)	3.1	1.0
	27.6 (4000)	2.9	0.94
High strength concrete	41.4 (6000)	2.4	0.77
	55.2 (8000)	2.0	0.65
	69 (10000)	1.6	0.52

2.8.3 Shrinkage of High Strength Concrete

Shrinkage is known to occur in the cement paste matrix with the aggregate functioning as restraining element. As it has been discussed earlier, shrinkage strain is highly influenced and approximately proportional to the percentage of water by volume in the concrete (MacGregor, 1998). Therefore, although HSC contain high cement content, the magnitude of shrinkage is known to be either lower due to the low water-cement ratio or about the same as of normal concrete because of higher degree of autogenous shrinkage.

Within the last decade autogenous deformation has received appreciable attention due to the rise in the usage of HSC in the construction industry. This is due to the fact that autogenous shrinkage is significant for HSC with water-binder (w/b) ratio less than 0.4. It was proven that the magnitude of autogenous shrinkage of HSC could be almost the same as drying of normal strength concrete (Tazawa and Miyazawa, 1995).

The destructive effects of autogenous deformation are microcracking which may increase the tensile strain capacity and also development of internal stresses. Microcracks due to restrained autogenous shrinkage may connect into a continuous

crack pattern and form macrocracks that constitute to serious problem with regards to strength, durability and aesthetics (Jensen and Hansen, 2001).

2.9 Summary of Literature Review

1. Concrete time-dependent deformation related research have been carried out for over a century with research interest ranging from the fundamental mechanism of the deformation to the effect of various influencing factors and also on structural issues related to the deformation.

2. Based on the literature study conducted, it is observed that although much progress and success have been achieved, only a few had expressed interest on the subject of concrete tested under different climatic conditions, and there hasn't been any research directly addressing on effect in tropical climate. As the influence of ambient RH is relatively significant on creep and shrinkage, it is important to understand the magnitude of deformation for concrete in the tropical condition.

3. Despite of extensive research work carried out, especially in the subject of parametric influence, the complex behaviour and heterogenous properties of concrete and the influence of various parameters proves to be a challenge to fully determine the mechanism of creep and shrinkage.

4. With reference to the various research carried out, the creep and shrinkage mechanism may be addressed in two forms - apparent and real mechanism. Real mechanism is the deformation that occurred at the microstructural level, influenced by the physical and chemical make-up of the hydrated cement paste and the apparent mechanism which is caused by factors which modify the anticipated strain such as crack formation.

5. Until the complex creep and shrinkage mechanism in the concrete microstructure have been established and fully understood, the macroscopic behaviour of concrete structural members is also recognized to be equally

important. The concrete macroscopic behaviour provides a direct structural response under various influencing parameters which can be adopted as empirical correction.

6. Creep and shrinkage effects are most important for various advanced modern designs with daring structures of large span, height or slenderness, innovative structural forms, usage of high strength concrete and structures exposed to severe environments or those carrying high permanent loads. For such structures, the effectiveness of the updating of the prediction model based on limited short-time tests of the given concrete is the paramount criterion. Such updating offers the only way to achieve reliable long-time predictions.

7. In order to be at par with the global construction industry growth, the local construction industry has to move forward towards constructing sustainable structures with nominal defects. One of the effective steps is to incorporate reliable prediction of creep and shrinkage into the design consideration and in order to achieve that, reliable creep and shrinkage prediction model with better accuracy has to be established.

CHAPTER 3

TIME-DEPENDENT DEFORMATION MODELS

Six existing prediction models from Eurocode 2 (EC 2), British Standards 8110 (BS 8110), CEB-FIP Model Code 1990 (CEB 1990), American Concrete Institute 209 Standard (ACI-209), Australian Standards 3600 (AS 3600) and Model B3 (B3) developed by Z. P. Bazant and S. Baweja are reviewed and evaluated. It also presents and compares the prediction capabilities of these six methods.

3.1 Criteria for Development of Creep and Shrinkage Model

As the actual mechanism and concrete model for time-dependent deformation is too complex and is still unclear till date, the prediction formula is still dependent on experimental derivations. Thus, development of creep and shrinkage functions is based on both mathematical expressions for time-dependency form and fitting of empirical coefficients (Bazant and Baweja, 2000). A few main criteria to observe in the formulation of the time-dependent deformation models are as listed:

(i) The mathematical form of the model should conform to the mechanical analysis and studies of the physical mechanisms (Bazant, 2001);

(ii) The model shall be able to predict the time-dependent deformation for any concrete under any conditions (Neville et al., 1983);

(iii) The required input parameters should preferably be of values readily known to the engineer at the design stage, namely; the characteristic concrete strength, age of concrete at beginning of drying or loading, duration of drying or loading, element size and ambient humidity (Bazant, 2000);

(iv) The model should allow extrapolation in both time and size of measured shrinkage and creep compliance (Bazant, 2000);

(v) Ultimately, the equation should be easy to use with an acceptable range of coefficient of variation from experimental data (Bazant and Baweja, 2000).

3.2 Development of Creep Model

For prediction and analysis purpose, the total strain of a uniaxially loaded concrete specimen at time t after the casting of concrete is obtained based on the principle of superposition. The total deformation at any time, $\varepsilon_{total}\ (t)$ comprises of the summation of elastic strain, $\varepsilon_E\ (t)$, creep strain, $\varepsilon_C\ (t)$, shrinkage strain, $\varepsilon_S\ (t)$ and thermal strain, $\varepsilon_T\ (t)$. The total strain can also be subdivided into two components as in Equation (3.1), which is the stress-induced strain, $\varepsilon_\sigma(t)$ comprising of instantaneous strain and creep strain, and the stress-independent inelastic strain $\varepsilon^o(t)$ that consists of shrinkage strain and thermal strain (Bazant and Wittmann, 1982).

$$\begin{aligned}\varepsilon_{total}\ (t) &= \varepsilon_E(t) + \varepsilon_{cr}(t) + \varepsilon_s(t) + \varepsilon_T(t) \\ &= \varepsilon_\sigma(t) + \varepsilon^o(t)\end{aligned} \tag{3.1}$$

The influence of stress on creep strain may be shown graphically by creep isochrones in Figure 3.1. The lines indicate the values of creep strain produced by various constant stresses for the same time period, at different age of loading. It is observed from Figure 3.1 that for stresses within the service range, or up to approximately 50% of the strength, creep is seen to be proportional to stress for all the different age at loading. Due to the proportionality property, Equation (3.1) can be rewritten as Equation (3.2) where the applied stress act is a constant function.

$$\varepsilon_{total}\ (t) = \sigma\, J(t,t_o) + \varepsilon^o\ (t) \tag{3.2}$$

where

ε_{total} = total strain

σ = stress applied

t = time considered during the loading duration

t_o = time at the beginning of loading

$J(t,t_o)$ = compliance function or creep function representing the strain at time t due to a unit constant stress, σ that has been acting since t_o

As given in Equation (3.3), compliance function is the sum of instantaneous elastic deformation per unit stress, $\frac{1}{E(t_o)}$ and creep deformation per unit stress, $C(t,t_o)$ known as creep compliance or specific creep. When Equation (3.3) is simplified by having $E(t_o)$ as the denominator, creep coefficient, $\phi(t,t_o)$ which is normally recommended in standard codes for the prediction of creep is formed. The creep coefficient represents the creep strain as a fraction of elastic strain at time of loading, t_o. The typical shape of the compliance function is sketched in Figure 3.2.

$$J(t,t_o) = \frac{1}{E(t_o)} + C(t,t_o)$$
$$= \frac{1+\phi(t,t_o)}{E(t_o)} \qquad (3.3)$$

where

$E(t_o)$ = modulus of elasticity of concrete at time t_o

$C(t,t_o)$ = creep compliance or specific creep

$\phi(t,t_o)$ = creep coefficient at time t

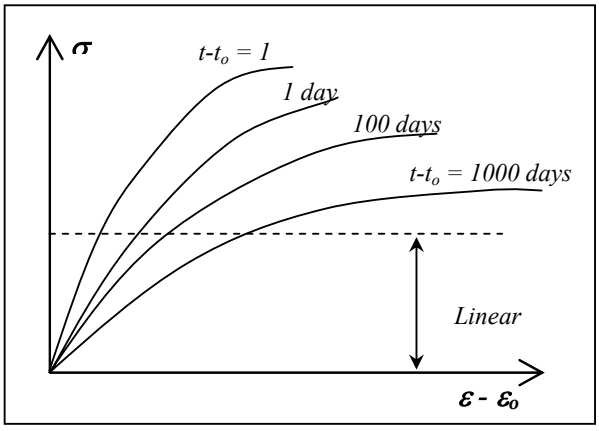

Figure 3.1: Creep isochrones

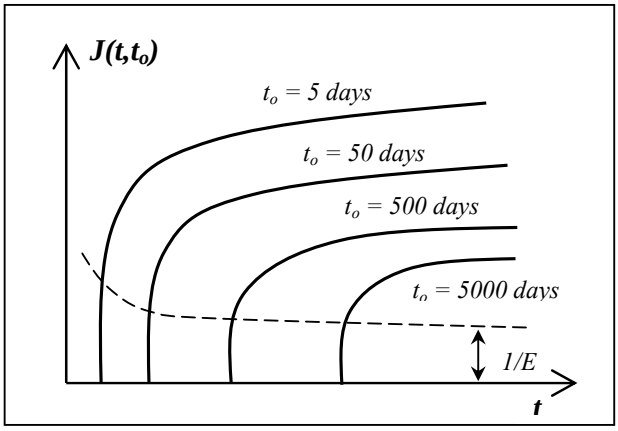

Figure 3.2: Creep compliance function

3.2.1 Formulation of Creep Coefficient

Various attempts have been made to express the relation of creep with time in the form of an equation so that values of creep may be predicted without having to perform long-term test. As the progress of creep with time under load follows a definite pattern, the basic creep of concrete which occur at constant moisture and thermal state may be described by a few mathematical expressions. The common mathematical expressions for the development of basic creep with time are the power function, hyperbolic function, exponential, double power law and also triple power law (Neville et al., 1983). These expressions are discussed in this section.

3.2.1.1 Hyperbolic Expression

The introduction for the use of hyperbolic expression to represent relations between creep and time were first proposed by Ross (1937) and Lorman (1940). The expression proposed is as follows:

$$\varepsilon_{cr}(t, t_o) = \frac{(t - t_o)}{A + B(t - t_o)} \tag{3.4}$$

where

$\varepsilon_{cr}(t, t_o)$ = creep strain at time t

A, B = empirical constants obtained through linear function

t-t_o = duration of loading

This expression is convenient for fitting of test data but unfortunately it does not apply to long creep duration as it greatly underestimates the long-time value. In addition to that, hyperbolic expressions tend to underestimate creep at early ages and overestimate the strain value at time after loading between 20 to 100 days. Therefore this expression has to be used with inclusion of other expressions. Till date, hyperbolic expression is the basis of creep-time function for most prediction models with incorporation of other expressions to overcome the inaccuracy.

3.2.1.2 Power Expression

Straub was the first person to suggest that creep can be expressed as a power function in 1930 (Neville et al., 1983). The general form of the power law of load duration is given in Equation (3.5).

$$\varepsilon_{cr}(t, t_o) = A(t - t_o)^B \tag{3.5}$$

where

$\varepsilon_{cr}(t, t_o)$ = creep strain at time t

A, B = empirical constants

Formulation of this equation empirically is simple, however the results are deemed to be applicable for relatively short period of time; 3-100 days after load (Bazant, 1988). In long-term creep, power expression overestimates the strain value.

3.2.1.3 Logarithmic Expression

The US Bureau of Reclamation developed a creep expression with the assumption that the rate of specific creep is inversely proportional to time, as given by Equation (3.6). The general solution for the initial condition of $\varepsilon_{cr}(t,t_o) = 0$ when $t = 0$, if $A \neq 0$ is given in Equation (3.7) (Neville et al., 1983).

$$\frac{d\varepsilon_{cr}(t,t_o)}{d(t-t_o)} = \frac{F(t_o)}{(t-t_o)+A} \tag{3.6}$$

$$\varepsilon_{cr}(t,t_o) = F(t_o)\log\left[\frac{(t-t_o)}{A}+1\right] \tag{3.7}$$

where

$\varepsilon_{cr}(t, t_o)$ = creep strain at time t

$F(t_o)$ = the rate of creep with logarithm of time obtained experimentally

A = a constant

The time shift is determined by the initial condition and becomes unity regardless of the value of A. Since no further distortion of the time element is desired, A can be assumed to be unity and Equation (3.8) is derived. Thus specific creep is a linear function of the logarithm of the time under load.

$$\varepsilon_{cr}(t,t_o) = F(t_o)\log[(t-t_o)+1] \tag{3.8}$$

Good agreement with one-year experimental data has been obtained, at least for mass concrete used on the US Bureau of Reclamation projects, but creep values for short period under load depart from the straight line, similar to the behaviour of the hyperbolic curve. The value of $F(t_o)$ must be obtained from experimental data for each type of concrete and age at application of load.

3.2.1.4 Exponential Expression

Probably the first exponential expression developed for creep was derived by Thomas from considerations of the rate of creep. Later, McHenry assumed that for a given concrete, application of load creates a certain creep potential. The rate of creep at any time is proportional to the amount of potential creep still to appear, of which a characteristic of visco-elastic flow is and may be expressed as Equation (3.9). Integration of Equation (3.9) with the boundary condition of $c_{cr} = 0$ when $(t-t_o) = 0$ yields Equation (3.10) (Neville et al., 1983).

$$\frac{d\varepsilon_{cr}(t,t_o)}{d(t-t_o)} = A[\varepsilon_{cr-\infty} - \varepsilon_{cr}(t,t_o)] \quad (3.9)$$

$$\varepsilon_{cr}(t,t_o) = \varepsilon_{cr-\infty}\left[1 - e^{-A(t-t_o)}\right] \quad (3.10)$$

where

$\varepsilon_{cr-\infty}$ = the ultimate creep strain

$\varepsilon_{cr}(t,t_o)$ = the creep strain at time t

A = empirical constant

For a particular concrete and given conditions, the constants $\varepsilon_{cr-\infty}$ and A can be determined from a plot of creep strain against the rate of creep. However, creep prediction based on Equation (3.10) has not shown good agreement with experimental data.

3.2.1.5 Double Power Law

Another approach in the formulation of basic creep is the double power law. The basic creep may be well described by power curves of load durations $(t-t_o)$, and by inverse power curves of age at loading, t_o which lead to the double power law which was proposed by Bazant and Osman (1979).

$$\varepsilon_{cr}(t,t_o) = A(t_o^{-m} + B)(t-t_o)^n \quad (3.11)$$

where

$\varepsilon_{cr}(t,t_o)$ = the creep strain at time t

A, B, m, n = empirical constants

The double power law acquires a rather broad range of applicability. It agrees reasonably well with the known data for creep up to 30 years of duration and at the same time describes quite well the test data for load durations under 1 day. The power curves however keeps on increasing with time and do not have a bounded final value.

3.2.1.6 Triple Power Law

Careful examination shows that the double power law exhibits certain deviations from experimental data which seem to be systematic rather than random. In particular, for a short age at loading and very long load duration, the final slope of the creep curve obtained from the power law is too high. An improvement can be obtained by triple power law (Bazant, 1988), which specifies the unit creep rate, the time derivative of the compliance function as shown in Equation (3.12).

$$\frac{\partial J(t,t_o)}{\partial t} = \hat{J}(t,t_o) = \frac{\psi}{E_o}\frac{t_o^{-m} + A}{(t-t_o)^{1-n}(t/t_o)^n} \tag{3.12}$$

where

$J(t,t_o)$ = creep compliance function

ψ =

E_o = modulus of elasticity of concrete

A, m, n = empirical constants

This formula contains one more constant than the double power law, which is the age coefficient, ψ. For short load durations of $t\text{-}t_o \ll t_o$, t/t_o may be substituted to be 1, upon which Equation (3.12) becomes identical to the derivative of the double power law.

3.3 Formulation of Shrinkage Strain

It is generally accepted that shrinkage has a limiting value. Therefore the shrinkage-time expressions are more straightforward. The basic shrinkage expressions with time are of exponential or hyperbolic power, as given in Equation (3.13) and (3.14), respectively (Neville et al., 1983).

$$\varepsilon_{sh}(t,t_{sh,o}) = \varepsilon_{sh,\infty}\left[1 - e^{A'(t-t_{sh,o})}\right] \tag{3.13}$$

$$\varepsilon_{sh}(t,t_{sh,o}) = \left[\frac{(t-t_{sh,o})}{A'+B'(t-t_{sh,o})}\right]^m \tag{3.14}$$

where

$\varepsilon_{sh}(t,t_{sh,o})$ = shrinkage at time t measured from the start of drying, $t_{sh,o}$

$\varepsilon_{sh,\infty}$ = ultimate shrinkage

A', B' and m = empirical constants

3.4 Provision for Modulus of Elasticity

In the prediction calculation of creep, modulus of elasticity of concrete has to be properly determined. Separation of the stress-produced strain into the instantaneous or elastic strain and creep strain is ambiguous because significant creep exists even for extremely short load durations (Bazant, 1988). Practically, there would be no problem if the analysis is based on creep function, $J(t,t_o)$ because the subdivision of the total stress-induced deformation into elastic and creep parts is artificial. On top of that, only the total value matters for structural analysis. However, there is no objection in characterizing creep by creep coefficient, $\phi(t,t_o)$ provided that the creep coefficient and elastic modulus must both be determined from the same compliance function, using the same load duration for the initial elastic deformation.

It is observed that most creep models provide creep prediction in terms of creep coefficient, $\phi(t,t_o)$. This creep coefficient prediction is formulated based on compliance function and corresponding elastic strain. Thus application of compatible modulus of elasticity is important in the calculation to determine creep strain. In general, the application of modulus of elasticity should be with reference to the values recommended by each prediction model or through experimental results. Careful consideration needs to be taken into account when the modulus of elasticity applied is obtained from other prediction or references.

3.4.1 Modulus of Elasticity Prediction by EC 2

The proposed static modulus of elasticity by Eurocode 2 (EC 2) is found in Clause 3.1.3 of the code. With reference to the clause, the proposed modulus of elasticity calculation formula for general application is given as Equation (3.15) here. The recommended values are provided for normal-weight concretes with quartzite aggregates. As stated in the code, under the case when limestone or sandstone aggregates are used, the modulus of elasticity for concrete shall be reduced by 10% and 30%, respectively. As for concrete containing basalt aggregates, the value should be increased by 20%.

$$E_{cm,28} = 22\left(\frac{f_{cm}}{10}\right)^{0.3} \tag{3.15}$$

where

$E_{cm,28}$ = modulus of elasticity of concrete at age 28 days

f_{cm} = mean concrete strength at age 28 days

3.4.2 Modulus of Elasticity Prediction by BS 8110

British Standards 8110 (BS 8110) provides a range of possible values as well as the mean value for 28-day static modulus of elasticity of normal-weight concrete in Part 2: Section 7.2 of the code. With reference to Section 7.2, the proposed mean values for modulus of elasticity by BS 8110 is reproduced here as Table 3.1 for easy reference and for discussion purposes. The mean values for normal weight concrete given in Table 3.1 are derived from Equation 3.16.

$$E_{cm,28} = K_o + 0.2f_{cu,28} \tag{3.16}$$

where

$E_{cm,28}$ = modulus of elasticity of concrete at age 28 days

$f_{cu,28}$ = mean concrete compressive cube strength at 28 days (N/mm^2)

K_o = constant closely related to the modulus of elasticity of the aggregate that is taken as 20 kN/mm^2 for normal weight concrete

Table 3.1: Typical range for the static modulus of elasticity at 28 days for normal weight concrete (Table 7.2, BS 8110: Part 2: 1997)

Concrete characteristic cube strength at 28 days, $f_{cu,28}$ (N/mm^2)	Modulus of Elasticity, $E_{cm,28}$ (kN/mm^2)	
	Mean Value	Typical Range
20	24	18 - 30
25	25	19 – 31
30	26	20 – 32
40	28	22 – 34
50	30	24 – 36
60	32	26 – 38

3.4.3 Modulus of Elasticity Prediction by CEB-FIP 1990

The CEB-FIP Model Code 1990 (CEB-FIP 1990) estimates 28-day modulus of elasticity from Equation (3.17). CEB 1990 considers the aggregate type in the modulus of elasticity expression and Equation (3.17) applies for concrete made of quartzitic aggregates. Under the circumstances when other aggregates is used, the modulus of elasticity may be calculated by multiplying $E_{cm,i}$ with the coefficients α_E given in Table 3.2. It is observed that the basis of prediction of modulus of elasticity by EC 2 and CEB 1990 are the same with similar prediction equations.

$$E_{cm,28} = 21.5\left(\frac{f_{cm}}{10}\right)^{1/3} \tag{3.17}$$

where

$E_{cm,28}$ = modulus of elasticity at 28 days (kN/mm^2)

f_{cm} = mean concrete compressive cylinder strength at 28 days (N/mm^2)

Table 3.2: Effect of type of aggregate on modulus of elasticity

(Table 2.1.5, CEB-FIP Model Code 1990)

Aggregate Type	Coefficient, α_E
Basalt, dense limestone aggregates	1.2
Quartzitic aggregates	1.0
Limestone aggregates	0.9
Sandstone aggregates	0.7

3.4.4 Modulus of Elasticity Prediction by ACI-318

The American Concrete Institute 318 (AC1-318) method and B3 mode1 adopt the same equations to calculate the modulus of elasticity. According to ACI-318, the modulus of elasticity of concrete can be calculated using Equation (3.18). This equation was derived from short-time test on concretes with densities ranging from 1442 kg/m^3 to 2482 kg/m^3 and corresponds to the secant modulus of elasticity at approximately $0.50f_{cm,t}$. For concrete with normal density of 2323 kg/m^3, Equation (3.18) is simplified to the following as given by Equation (3.19). The scatter of data for modulus of elastic prediction is very wide for this prediction because the equation ignores the type of aggregate used in the concrete (MacGregor, 1997).

$$E_{cm,t} = 0.043\rho^{1.5}\sqrt{f_{cm,t}} \tag{3.18}$$

$$E_{cm,t} = 4733\sqrt{f_{cm,t}} \tag{3.19}$$

where

ρ = density of concrete (kg/m^3)

$f_{cm,t}$ = mean compressive cylinder strength of concrete at age t (N/mm^2)

3.4.5 Modulus of Elasticity Prediction by AS 3600

The modulus of elasticity of concrete as recommended by Australian Standards (AS 3600) is found in Clause 6.1.2 of the standard. As proposed by AS 3600, the values may be obtained either through calculation using Equation (3.20) shown here or determined by test in accordance with AS 1012.17.

$$E_{cm,t} = 0.043\rho^{1.5}\sqrt{f_{cm,t}} \tag{3.20}$$

where

ρ = density of concrete (kg/m^3)

$f_{cm,t}$ = mean compressive cylinder strength of concrete at age t (N/mm^2)

It is observed that Equation (3.20) is the same as provided by ACI 318. However, the general density for normal weight concrete is defined differently by both codes. According to AS 3600, the density for normal weight concrete is taken to be not less than 2400 kg/m^3. Therefore with inclusion of concrete density at 2400kg/m^3, Equation (3.20) is simplified to as shown by Equation (3.21). It should be noted that the AS 3600 stated that the recommended modulus of elasticity has an error range of ±20%.

$$E_{cm,t} = 5050\sqrt{f_{cm,t}} \tag{3.21}$$

where

$f_{cm,t}$ = mean compressive cylinder strength of concrete at age t (N/mm^2)

3.5 Standard Code Provision for Creep and Shrinkage

In most standard codes, creep strain is characterized by the creep coefficient obtained either through tables of values or defined by a formula based on experimental data of the concrete properties. The providence of formula provides better and more a more defined value as compared to graphs and tables. Six prediction models on creep and shrinkage reviewed in this section are EC 2 (2004), BS 8110 (1997), CEB 1990 (1993), ACI-209 (1992), AS 3600 (1988) and Model B3 (2000). With the exception of the Model B3 (2000), the models considered are obtained from structural design codes of practice.

These empirically based models are subjected to different levels of accuracy with different parameters accounted for in the calculation. The parameters accounted for creep and shrinkage strain for each prediction models studied is summarised in Table 3.3. With reference to the table, the main factors considered by all the codes to predict creep and shrinkage are the effective section thickness and RH of ambient. In addition to that, consideration of age at loading is also another essential factor for creep prediction. It is observed that B3 offers a more comprehensive model in predicting the strain value than the other five methods with more parameters accounted for in the calculations.

Table 3.3: Variables considered in predicting creep and shrinkage for standard codes

Variables	Standard Codes											
	EC 2		BS 8110		CEB-FIP		ACI 209		AS 3600		B3	
	Cr	Sh	Cr	Sh	Cr	Sh	Cr	Sh	Cr	Sh	Cr	Sh
1. Compressive strength	●	●			●	●			●		●	●
2. Cement content							●	●			●	
3. Water-cement ratio											●	
4. Slump							●	●				
5. Aggregate-cement ratio											●	
4. Fine aggregate percentage							●	●				
5. Water content												●
6. Cement type	●	●				●	●	●				●
7. Air content							●	●				
8. Effective section thickness	●	●	●	●	●	●	●	●	●	●	●	●
9. Shape of specimen											●	●
9. RH of ambient	●	●	●	●	●	●	●	●	●	●	●	●
10. Temperature of ambient	●								●	●		
11. Age at loading	●		●		●		●		●		●	
12. Age when drying begins		●				●	●	●				●
13. Curing conditions							●	●				●

Note: Cr = creep, Sh = shrinkage

3.5.1 Eurocode 2

In the recommendation of creep and shrinkage by EC 2, two alternative approaches are provided; a simplified method introduced in Clause 3.1.4 of EC 2 and comprehensive calculation equations presented in Annex B of the code. The comprehensive calculation involves a set of extensive formulae to calculate the development of the time-dependent deformation with time when more accurate value is required. The simplified approach presents the values of creep coefficient and shrinkage strain with reference to graphs and tables. The simplified approach is also derived from comprehensive calculation in Annex B, only presented in a simplified manner to assist user for easy reference.

3.5.1.1 Creep Prediction by EC 2

Equation (3.22) summarises the comprehensive formula provided in Annex B of EC 2, for calculation of creep coefficient, $\phi(t,t_o)$. The equation is determined with consideration of ambient relative humidity, notional size of specimens, concrete strength, age at loading, duration of loading and type of cement. The effect of type of cement and ambient temperature are taken into account by modifying the age of loading and age of concrete, respectively. The comprehensive formulation is given in Appendix A1.

As stated in EC 2, the prediction formula is valid for concrete subjected to stress no greater than 45% of the ultimate compressive strength of concrete at the time of loading. The concrete strength catered for is between concrete class C16/20 and C90/105. The strength classification for EC 2 is categorized as concrete Class with both 28-day cylinder and cube characteristic strength specified. Reference to cylinder characteristic strength precedes the cube strength. As stated in the code, the mean coefficient of variation of the predicted creep data, deduced from a computerised data bank of laboratory test results, is of the order of 20%.

$$\phi(t, t_o) = \left[\frac{(t-t_o)}{(\beta_H + t - t_o)}\right]^{0.3} \cdot \frac{1}{0.1 + t_o^{0.2}} \cdot \frac{16.8}{\sqrt{f_{cm}}} \cdot 1 + \frac{1 - RH/100}{0.1 \cdot \sqrt[3]{h_o}} \qquad (3.22)$$

where

β_H = correction factor for ambient relative humidity

$= \quad 1.5 * \left[1 + (0.012 * RH)^{18}\right](h_o) + 250 \cdot \alpha_3$; with $\alpha_3 = \left(\frac{35}{f_{cm}}\right)^{0.5}$

t = age of concrete at the time considered (days)

t_o = age of concrete at loading (days)

f_{cm} = mean concrete cylinder strength (N/mm^2)

RH = ambient relative humidity (%)

h_o = specimen notional size (mm)

$= 2A/u$

In cases where when accuracy is not the main concern and only a rough estimate of creep is required, ultimate creep coefficient for RH 50% (indoor condition) and 80% (outdoor condition) is provided in a nomograph form. Concrete strength, specimen size, types of cement and age at loading are the factors considered. The values given in this section caters for concrete exposed to the ambient temperature within the range of -40^{o}C to 40^{o}C and a mean relative humidity within 40% to 100%. The creep coefficient for this simplified method is also derived from the comprehensive calculation equations, with simplifications through grouping the results into a few common cases. The result obtained from this simplified method is valid for concrete under compressive stress lower than 45% of the ultimate compressive strength of concrete at the time of loading. The nomograph and the method to determine the creep coefficient is given as Figure A1.1 in Appendix A1.

The basic formulation for creep in EC 2 is adopted from CEB-FIP 1990 Model, having the same parameters considered. The product form of the creep coefficient adopts the double power law by having power curve of load duration and inverse power curve of the age at loading. The influence of concrete strength, ambient RH and size are multiplicative functions that act as correction factors. In general, the proposed calculation method by EC 2 is easy to use and caters for a wide range of different concrete conditions. Reference to the simplified prediction for quick assumption is of satisfactory for most design cases. The comprehensive calculation is adopted for cases of special structures that require better accuracy. It is

noted that this model does not separate the creep coefficient into basic and drying creep.

3.5.1.2 Shrinkage Prediction by EC 2

As for the prediction of shrinkage, the total shrinkage strain is divided into two components; drying and autogenous shrinkage strain. In this investigation, only the drying shrinkage strain, ε_{cd} is studied as the procedures for autogenous shrinkage measurement is complex and the instruments are unavailable in the laboratory. Thus, the autogenous shrinkage is not evaluated here. The development of drying shrinkage strain with time by EC 2 is given as Equation (3.23) and (3.24). The complete formulation for shrinkage by EC 2 is presented in Appendix A1.

It is observed through Equation (3.23) and (3.24) that the parameters considered in EC 2 to determine drying shrinkage strain are duration of drying, specimen size, concrete strength, ambient RH and the type of cement. It is also noted that the drying shrinkage-time dependence equation is developed based on hyperbolic expression. In addition to that, drying is a process governed by diffusion theory and this theory is complied here through the size dependence function with the drying times proportional to square size of structural members (Acker and Ulm, 2001).

$$\varepsilon_{cd}(t) = \frac{(t - t_s)}{(t - t_s) + 0.04\sqrt{h_o^3}} \cdot k_h \cdot \varepsilon_{cdo} \tag{3.23}$$

$$\varepsilon_{cdo} = 0.85\left[\left(220 + 110 \cdot \alpha_{ds1}\right) \cdot \exp\left(-\alpha_{ds2} \cdot \frac{f_{cm}}{f_{cmo}}\right)\right] - 1.55\left[1 - \left(\frac{RH}{RH_o}\right)^3\right] \cdot 10^6 \tag{3.24}$$

where

k_h = coefficient depending on notional size as provided in Table A1.1 in Appendix A1.

t = age of concrete at the time considered (days)

t_s = age of concrete when drying begins (days)

ε_{cdo} = nominal unrestrained shrinkage strain

α_{ds1} = coefficient which depends on the type of cement

α_{ds2} = coefficient which depends on the type of cement

f_{cmo} = 10 N/mm^2

RH_o = 100%

Under the case when exact accuracy is not a stringent requirement, the simplified method for shrinkage is available. The simplified method provides the final value of nominal shrinkage strain, ε_{cdo} in a table for concrete with cement Class N and the strength class within the range of C20/25 to C90/105. The ambient RH provided is between 20% and 100%. This tabulation of values is given as Table A1.2 in Appendix A1. The coefficient of variation from this simplified model method is of about 30%.

3.5.2 British Standards 8110

The creep and shrinkage prediction model recommended by BS 8110 is by far the simplest model discussed in this study. The method provided is straightforward and easy to use as the ultimate creep coefficient can be directly obtained through the nomograph. However, with the simplification through the provision in the form of graphs, the accuracy of the prediction is compromised. The range of applicability of the model is also limited and adjustment of the parameters with inclusion of short-time test data to suit specific concrete is not feasible. In addition to that, BS 8110 does not state the range of concrete strength applicable for this prediction, but only specify that it is applicable for normal weight concrete, which is normally taken between 25N/mm^2 to 40N/mm^2.

3.5.2.1 Creep Prediction by BS 8110

The development of this model is with reference to the work of Parrott J. L. (1979). In this prediction, the magnitude of creep provided is the ultimate creep coefficient, ϕ_{ult} which is a deformation of concrete under load after 30 years. The

values are directly provided in the form of a nomograph, as shown in Figure A2.1 in Appendix A2. The parameters taken into account in determining the magnitude of creep coefficient are ambient RH, age at loading and notional thickness of member. At a constant RH, BS 8110 suggests that approximately 40%, 60% and 80% of the final creep develops during the first month, 6 months and 30 months under load, respectively. This approximation may lead to a big range of inaccuracy.

In spite of the convenience in reading the creep values through the graph, it is more practical to define the creep coefficient by a formula. Provision in equations has the beneficial effect of smoothing the results and is able to prevent error through interpretation of the graph. The code specified that the prediction caters for normal weight concrete but fails to state the concrete strength limit. The concrete strength is also not included as one of the determining parameters and the effect of different concrete strength is only indirectly considered through the modulus of elasticity during the calculation of creep strain. In addition to that, this method is also too simplified that it only provide the ultimate creep coefficient and does not provide for the development of creep with time.

3.5.2.2 Shrinkage Prediction by BS 8110

Shrinkage strain is provided for 30 years and 6 months period in the form of a graph, as shown in Figure A2.2 in Appendix A2. The parameters required to determine the values of shrinkage strain are the notional size and relative humidity. The values given are applicable for plain, normal-weight concrete within the range of 2000 kg/m^3 to 2800 kg/m^3 with normal workability. The concrete shall not contain water reducing admixture with original water content about 190 L/m^3. With different water content, shrinkage is assumed as directly proportional to water content within the range of 150 L/m^3 to 230 L/m^3.

Similar to the prediction of creep, the shrinkage prediction method is too simple and the presentation in the graph form limits the range of applicability. It is interesting to note that BS 8110 predicts the same value of shrinkage for concrete with different strengths, provided that the concrete is categorised as normal weight

concrete. In the definition of normal weight concrete, no specific strength range is given in the standard code but would normally be taken between 25N/mm^2 to 40N/mm^2, which does not cover for high strength concrete. Besides that, the recommendation of shrinkage by BS 8110 is no longer valid with the inclusion of water reducing admixtures. Considering the increase in the use of admixtures in the concrete industry, the application of this code is rather limited.

3.5.3 CEB-FIP Model Code 1990

The CEB-FIP Model Code 1990 is produced by the Euro-International Concrete Committee and International Federation for Prestressing. The CEB 1990 is a prediction model developed by Müller and Hilsdorf (1990) to predict the mean time-dependent deformation for normal weight, plane structural concrete. The prediction of creep and shrinkage of concrete by the CEB 1990 is restricted to ordinary structural concretes, having 28 days mean cylinder compressive strength varying from 12 to 80 MPa, mean RH 40 to 100% and mean temperature 5 to 30^{o}C.

3.5.3.1 Creep Prediction by CEB-FIP 1990

The expression for creep coefficient is provided as Equation (3.25).

$$\phi(t,t_o) = \left[\frac{(t-t_o)}{\beta_H + (t-t_o)}\right]^{0.3} \cdot \frac{1}{0.1+t_o^{0.2}} \cdot \frac{5.3}{\sqrt{f_{cm}/10}} \cdot 1 + \frac{1-RH/100}{0.46\sqrt{h_o/101.6}} \qquad (3.25)$$

where

t = age of concrete at the time considered (days)

t_o = age of concrete at loading (days)

β_H = correction factor for ambient relative humidity

f_{cm} = mean concrete cylinder strength (N/mm^2)

RH = ambient relative humidity (%)

h_o = specimen notional size (mm)

When the equation is observed closely, it is noted that the basic formulation of creep coefficient is similar to EC 2, with similar pattern and parameters considered. Similar to many other prediction models, the CEB-FIP 1990 model calculates a creep coefficient to predict the creep. However, instead of basing the creep coefficient on the modulus of elasticity at the age of loading, it is based on the modulus at 28 days. This model does not consider the effects of curing (duration or method) for the calculation of compliance. This model has a coefficient of variation of 20.4% for creep compliance. The full prediction equations are presented in Appendix A3.

3.5.3.2 Shrinkage Prediction by CEB-FIP 1990

The equations by CEB-FIP 1990 are only applicable for the longitudinal shrinkage deformation of plain or lightly reinforced normal weight concrete elements. The axial shrinkage strains, ε_{cs} occurring between time t_s at the start of shrinkage and t in plain concrete can be predicted using the following formula

$$\varepsilon_{cs}(t,t_s) = \varepsilon_{cso}\left[\frac{(t-t_s)/t_1}{350(h_e/h_o)^2 + (t-t_s)/t_1}\right]^{0.5} \tag{3.26}$$

$$\varepsilon_{cso}(t,t_s) = -1.55\left[1-\left(\frac{RH}{RH_o}\right)^3\right] \cdot [160 + \beta_{sc}(9\text{-}f_{cm}/f_{cmo})] \times 10^{-6} \tag{3.27}$$

where

ε_{cso} = basic shrinkage strain for a particular concrete and RH

h_e = is the effective thickness of specimen to account for volume surface ratio given by $2A_c/u$

h_o = 100mm

RH = ambient relative humidity (%)

RH_o = 100%

β_{sc} = is a coefficient to describe the development of shrinkage between time t_s and t as a function of the effective thickness of member

f_{cm} = mean compressive cylinder strength at 28 days (N/mm^2)

f_{cmo} =10N/mm^2

t_1 =1 day

It is observed that the basic shrinkage strain is in negative for RH between 40% and 99%, implying that the concrete shortens due to shrinkage. Under the atmospheric condition with RH greater than 99%, the basic shrinkage strain is in positive, indicating swelling. The coefficient of variation is at 32.9%, which is a very large spread. If shrinkage has a critical effect on a given structure, shrinkage test is recommended to be carried out using the concrete in question. The full prediction equations are presented in Appendix A3.

3.5.4 American Concrete Institute 209R-92

3.5.4.1 Creep Prediction by ACI 209R-92

The model recommended by ACI Committee 209 was developed by Branson and Christianson (1971), with minor modifications introduced in ACI 209R-82. This model was initially developed for the precast-prestressing industry (Branson and Ozell, 1961). However it has since been used in the design of structures for many years. The recommended approach provides a simplified expression of creep coefficient that represents an average value for concrete under a set of standard conditions and correction factors for conditions other than the standard. This procedure is applicable to normal weight and light weight concretes, Types I and III cement and concrete cured through either moist curing or steam curing.

The standard conditions are summarized in Table A4.1 in Appendix A4. Under the standard condition, the creep coefficient, ϕ is a product of time-ratio and ultimate creep coefficient, v_u as given in Equation (3.28). The average value for v_u is taken as 2.35. Other than the standard conditions specified in ACI, the correction factors, F_C are proposed, as given in Equation (3.28). The calculation equations for the correction factors are shown in Appendix A4.

$$\phi = \frac{(t - t_o)^{0.6}}{10 + (t - t_o)^{0.6}} v_u \cdot F_{CT} \cdot F_{Ch} \cdot F_{Ct} \cdot F_{Cs} \cdot F_{Cc} \cdot F_{Cf} \cdot F_{Ca} \quad (3.28)$$

where

t_o = age at loading (days)

t = current age (days)

v_u = ultimate creep coefficient defined as ratio of creep strain to initial strain, with recommended average value at 2.35

F_{CT} = ambient relative humidity correction factor

F_{Ch} = minimum thickness of member correction factor

F_{Ct} = age at loading correction factor

F_{Cs} = slump correction factor

F_{Cc} = cement content correction factor

F_{Cf} = percent fines correction factor

F_{Ca} = percentage of air content correction factor

3.5.4.2 Shrinkage Prediction by ACI 209R-92

The shrinkage strain, $\varepsilon_s(t,t_s)$ is formulated based on the ultimate shrinkage strain multiplied by a hyperbolic time function and corrections factors, as given in Equation (3.29). The provision for shrinkage is applicable to concretes cured under moist and steam curing; and Types I and III cement. $\varepsilon_{sh,u}$ is the ultimate shrinkage strain after infinite time, recommended to be 780 x 10^{-6} for concrete under the standard conditions. As for conditions other than the standard set, correction factors are introduced to $\varepsilon_{sh,u}$. A function of seven correction factors consisting of environmental humidity, age at drying, minimum thickness of structural member, slump, cement content, fine aggregate percentage and air content as given in Equation (3.29) are considered.

$$\varepsilon_s(t,t_o) = \varepsilon_{sh,u} \frac{t - t_o}{k + (t - t_o)} \cdot F_{ST} \cdot F_{Sh} \cdot F_{Ss} \cdot F_{Sc} \cdot F_{Sf} \cdot F_{Sa} \quad (3.29)$$

where

t_s = age at the end of curing (days)

t = current age (days)

$\varepsilon_{sh,u}$ = ultimate shrinkage strain after infinite time, for standard condition, the value is recommended to be 780×10^{-6}

F_{ST} = ambient relative humidity correction factor

F_{Sh} = minimum thickness of member correction factor

F_{Ss} = slump correction factor

F_{Sc} = cement content correction factor

F_{Sf} = percent fines correction factor

F_{Sa} = percentage of air content correction factor

For both creep and shrinkage prediction for ACI, it is observed that the standard conditions do not include the concrete strength but the concrete composition e.g. slump of 70mm, air-content up to 6%, fine aggregates 50%, cement between 279 to 446 kg/m^3 and curing humidity more than 95%. The reference to slump is no longer an accurate gauge of concrete strength ever since the introduction of water reducing admixtures such as superplasticiser into the concrete composition. Therefore the user has to be aware of the application of each correction parameters proposed to determine the applicability. The full prediction formulae for creep and shrinkage, including the correction equations are presented in Appendix A4.

The advantages of this model include its simple form to use and that it is relatively easy to adjust to match short-term test data simply by modifying ultimate shrinkage or creep to produce the best fit of data. However the limitations in providing a good accuracy and also in the method of accommodating member size for the standard condition calculation are the main setback to the application of this model. In the study on accuracy of creep and shrinkage prediction models to the RILEM data bank, Bazant and Baweja (2000) concluded that the coefficient of variation for ACI is the highest among all other models studied, indicating the lowest level of accuracy. It is reported that the coefficient of variation for ACI is at 45% for creep with drying and at 55% for shrinkage. Fanourakis and Ballim (2003) also confirmed on this finding in their research when comparing the results from different investigations.

3.5.5 Australian Standard 3600

3.5.5.1 Creep Prediction by AS 3600

In the recommendation of Australian Standard 3600, the design creep factor, ϕ_{cc} which is an equivalent to creep coefficient, is provided as in Equation (3.30). ϕ_{cc} takes into consideration the effect of loading duration, age at loading, size of specimens and environmental condition through three functions, $\phi_{cc.b}$, k_2 and k_3..

$$\phi_{cc} = k_2 \, k_3 \, \phi_{cc.b} \tag{3.30}$$

where

$\phi_{cc.b}$ = basic creep factor provided based on concrete characteristic strength as given by Table A5.1 in Appendix A5

k_2 = coefficient for duration of loading, specimen size and environment conditions

k_3 = strength ratio of age at loading to 28 day-strength.

The prediction of creep by AS 3600 is summarized in Appendix A5. basic creep factor, $\phi_{cc.b}$ is,. k_2 and k_3 are creep factor coefficient which are provided in the form of graphs as shown in Figure A5.1 and Figure A5.2, respectively in Appendix A5.

3.5.5.2 Shrinkage Prediction by AS 3600

The design shrinkage strain, ε_{cs} by AS 3600 is determined based on the basic shrinkage strain, $\varepsilon_{cs.b}$ and shrinkage strain coefficient, k_1, as given in Equation (3.31).

$$\varepsilon_{cs} = k_1 \, \varepsilon_{cs.b} \tag{3.31}$$

where

k_1 = shrinkage strain coefficient that is dependent on environment condition, effective thickness and the duration of drying.

$\varepsilon_{cs.b}$ = basic shrinkage strain, taken equal to 850 x 10^{-6} for normal class concrete, or determined from measurements on similar local concrete.

k_1 is provided in the form of graphs as shown in Figure A5.3 in Appendix A5. For the case of special class concrete, AS 1012.13 recommended for the basic shrinkage strain, $\varepsilon_{cs.b}$ to be determined through measurement on similar concrete tested after 8 weeks of drying.

It is interesting to note that the concrete are categorised into four exposure condition in the AS 3600, namely arid, interior environments, temperate inland and tropical and near coastal. The climate categorisation replaces the ambient RH parameter. Consideration shall be given to the fact that ϕ_{cc} and ε_{cs} have a range coefficient of variation at the range of ±30% and ±40%, respectively as reported in the standard.

3.5.6 B3 Model

The Model B3 is the third major refinement in a series of models developed at Northwestern University by Z.P. Bazant and S. Baweja. This improved version of the earlier models namely BP Model and BP-KX Model is simpler, agrees better with the experimental data and is better theoretically justified than the previous models (Bazant and Baweja, 2000). The simplification of formulae is achieved through sensitivity analysis, incorporation of theoretically derived rather than empirical expression for the drying creep, and calibration of the model by an enlarged data set. However when this model is compared to the other models reviewed in this thesis, the calculation equations are more complex and requires more input parameters.

The prediction of material parameters of B3 model is restricted to Portland cement concretes, having 28 days mean cylinder compressive strength varying from 17 to 70 N/mm^2, water-cement ratio of 0.30 to 0.85, aggregate-cement ratio of 2.5 to

13.5 and cement content of 160 to 720 kg/m^3. The service stress for creep is restricted up to about 0.45$f_{cm,28.}$ The formulae are valid for concretes cured for at least one day. It is reported that the prediction of concrete outside the limitations stated can be performed using B3 model if the parameters are calibrated with tests (Bazant and Baweja, 2000).

3.5.6.1 Creep Prediction by B3 Model

Model B3 expresses creep strain as the product of the elastic deformation of concrete at the time of loading and creep strain, known as the creep compliance function. The compliance function is given as Equation (3.32).

$$J(t,t_o) = q_1 + C_o(t,t_o) + C_d(t,t_o,t_{sh,o}) \quad (3.32)$$

where

q_1 = instantaneous strain due to unit stress

$C_o(t,t_o)$ = compliance function for basic creep, as given in Equation (3.33)

$C_d(t,t_o,t_{sh,o})$ = compliance function that predicts additional creep that occur under the influence of drying, given as Equation (3.34)

$$C_o(t,t_o) = q_2 Q(t,t_o) + q_3 \ln\left[1 + (t - t_o)^n\right] + q_4 \ln(t/t_o) \quad (3.33)$$

$$C_d(t,t_o,t_{sh,o}) = q_5 \left[\exp\{-8H(t)\} - \exp\{-8H(t'_{sh,o})\}\right]^{1/2} \quad (3.34)$$

where

q_2, q_3, q_4, q_5 = empirical material constitutive parameters given by formulae based on concrete strength and composition, provided in Appendix A6.

$Q(t,t_o)$ = function of age at loading and duration of loading that can be calculated from the formula given in Appendix A6

$H(t), H(t_o)$ = expression that accounts for average of pore RH within the cross section, $0 \le H \le 1$

$t'_{sh,o}$ = the time at which drying and loading first act simultaneously (days)

An important advantage of this model is that all the free parameters for creep with elastic deformation, which are q_1, q_2, q_3, q_4 *and* $q5$ are contained in the formulae linearly. Therefore modification of the coefficients for a particular concrete can be conducted with experimental results. However one disadvantage to this model is that the requirements for input data are not generally available during the time of design, such as specific concrete proportions and mean compressive strength of concrete. Therefore assumptions on the concrete properties need to be made during design stage. The coefficient of variation for creep prediction of B3 Model is reported to be at 23% (Bazant and Baweja, 2000)

3.5.6.2 Shrinkage Prediction by B3 Model

The shrinkage strain is predicted with consideration of age of drying, cement type, concrete mean compressive strength at 28 days, curing condition, modulus of elasticity of concrete at 28 days, ambient RH, shape of specimen, specimen volume to surface ratio and water content in the concrete. All the parameters are taken into account through the shrinkage formula provided and the comprehensive calculation equations are presented in Appendix A6.

$$\varepsilon_{sh}(t,t') = -\alpha_1\alpha_2[1.9\times10^{-2}\,w^{2.1}f_c^{-0.28}+270]\times10^{-6}\cdot k_h\cdot\tanh\sqrt{\frac{t-t'}{\tau_{sh}}} \quad (3.35)$$

where

α_1 = coefficient for type of cement

α_2 = coefficient for curing condition

w = water content in concrete mix

k_h = humidity correction factor for final shrinkage

τ_{sh} = shrinkage half-time (days)

Bazant and Baweja (2000) reported that the coefficient of variation of the errors of the prediction of shrinkage is at 34%.

3.6 Summary on Existing Models Review

1. Creep and shrinkage deformation is too complex to be represented by a single mathematical expression. It has to be a combination of a few, and formulation based on pure mathematical functions is almost impossible. Thus incorporation of empirical coefficients is required in the development of prediction models for better accuracy.

2. As for the prediction of concrete modulus of elasticity, European methods refers to concrete strength as reference parameter while the American formulation is with reference to concrete weight.

3. Based on the six prediction methods discussed, it is observed that both intrinsic and extrinsic parameters are equally important in influencing the magnitude of creep and shrinkage strain in concrete. The main parameters considered are concrete mechanical properties, effective section thickness and ambient RH.

4. It is observed that there are two different approaches to the prediction of creep and shrinkage by the current models; first is through calculation from a set of equations while the other is determined through graph reading. Even though the calculations through equations are tedious, it tends to allow more flexibility in the application and provide for a better accuracy. The graph reading though convenient, a good accuracy is difficult to obtain and interpolation of data is only limited to linear relationship.

5. For most prediction equations, it can be summarised that the hyperbolic power function is adopted as the basis for most models because the function best reflect the pattern of creep and shrinkage deformation over time. In addition to that, most prediction models propose correction factors to widen the range of concrete applicable.

6. Generally, the coefficient of variation reported by the models are within the range of 20-30% for creep and 30-40% for shrinkage, except for ACI 209 model which is reported to have a coefficient of variation at 45% for creep with drying and 55% for shrinkage.

CHAPTER 4

EXPERIMENTAL WORK

4.1 Experiment Framework

The experiment framework is divided into three stages as shown in Figure 4.1. Stage 1 was the preliminary testing involving short term creep test and trial mix of HSC. The short term creep test was conducted to assess the effect of specimen sizes on time-dependent deformation. The trial mixes were carried out to determine the most effective mix in achieving the desired high concrete strength. These preliminary tests were important in determining suitable testing parameters for this study.

At Stage 2, creep and shrinkage test were conducted on standard size specimens - 100mm Ø x 300 mm cylinders and 100x100x500 mm prism, according to the basic methodology in ASTM C512-87 and ASTM C157-92, respectively. Concrete casting and curing ware conducted in compliance with ASTM C192–90(a). In maintaining test consistency, the concrete material properties testing consisting of compressive strength, modulus of elasticity and Poisson's ratio were also carried out according to ASTM method. The compressive strength test was conducted in compliance to ASTM C39-86 whereas the elastic modulus and Poisson's ratio were tested based on ASTM C469-87(a). Due to the limitation of apparatus, the concrete porosity test was conducted according to on vacuum saturation method as specified in RILEM CP 113 (1984). As the results of porosity content is intended for relative comparison between the concrete batches, reference to testing method besides ASTM is justified.

At Stage 3, the experiment work consists of laboratory test of time-dependent deformation of structural members; reinforced concrete columns and pretensioned prestressed beams. While the laboratory standard size

specimens are able to produce the material response, a close prediction of deformation for structural members cannot be expected. With the presence of longitudinal and shear reinforcement in actual structures, creep strain is said to be smaller than in plain concrete due to the distribution of stress onto the steel. Thus the structural members testing verify the applicability and reliability of laboratory specimen results for the application of structural design.

HSC columns were cast and tested for time-dependent shortening under load. Columns are main supporting elements in a structure that function to transfer the load of a structure to the foundation system. Therefore columns are subjected to sustained dead loads and live loads throughout the entire design live. The continual sustained load causes creep and deflections, subsequently increases the moment induced by the additional eccentricity, weakening the column. At the same time, columns also undergo shrinkage, increasing the deformation of the element. Therefore assessment of creep in concrete columns is an important area of studies.

Prestressed concrete beams were tested to investigate the structural performance and prestress losses under the effects creep and shrinkage. The beams were tested for precamber, time-dependent deflection and prestress losses, mainly on concrete creep and shrinkage. This step is to obtain a good correlation of time dependent deformation between laboratory standard size specimen and structural members for verification of proposed prediction model.

For an actual understanding of actual structural behaviour, field data is also gathered through monitoring of structural members behaviour on site. Therefore field testing was carried out on post-tensioned prestressed beams to check on the initial pre-camber after prestressing. The results obtained from field testing provide the actual deformation that occurs on site under tropical climate condition to verify the time-dependent deformation prediction proposed in this study.

In addition to that, the concrete used in casting the post-tensioned prestressed beams on site were sampled to conduct creep and shrinkage testing. The use of the ready-mixed concrete from site for creep and shrinkage test provided a more credible and conclusive results in addition to the laboratory batched concrete tested. Besides that, the actual concrete properties of the prestressed beams were also directly tested.

Strain measurement and data collection commenced with the completion of specimen preparation and setting up of loading apparatus. As the main subject of study is on time-dependent deformation, the duration of strain measurement continued for a duration between 6 months and 12 months, as indicated for each testing. The whole series of test conducted as explained in this chapter offered a comprehensive set of test to gather reliable and conclusive time-dependent deformation behaviour of HSC in the tropical climate.

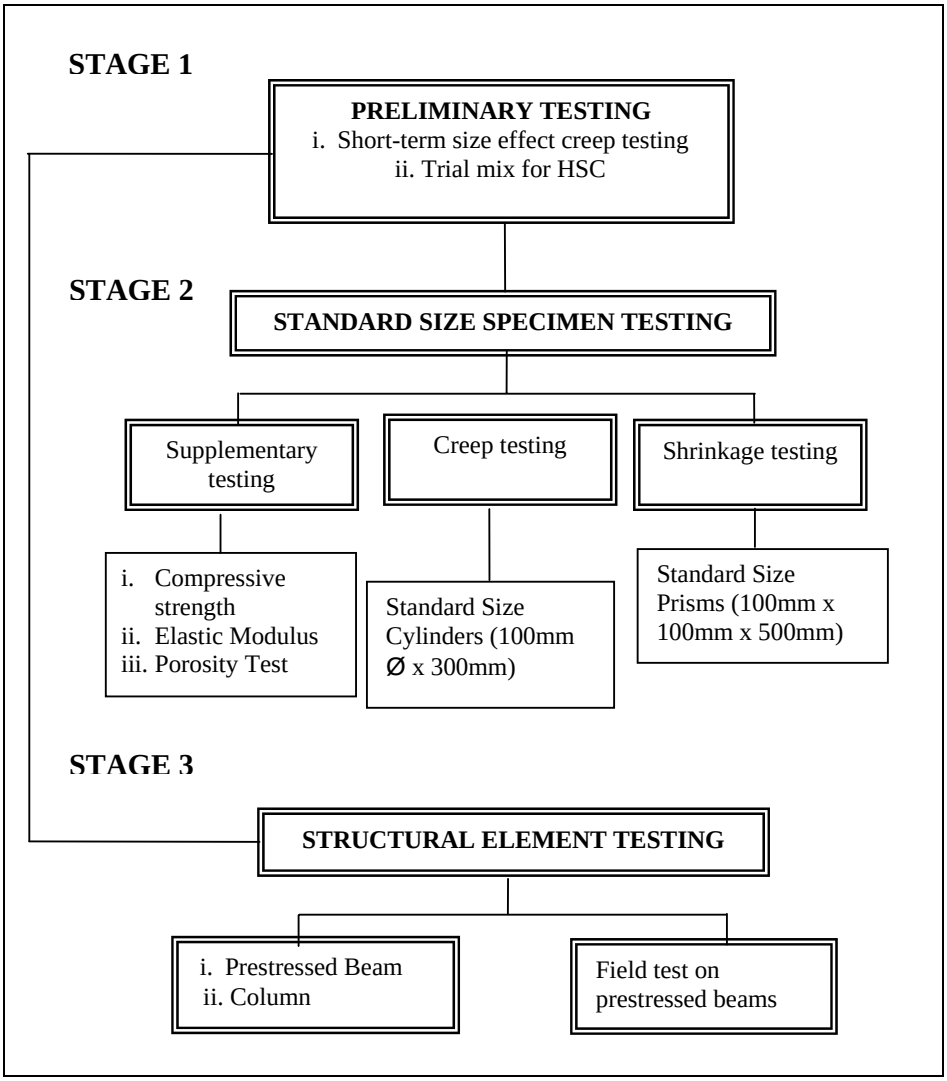

Figure 4.1: Laboratory experiment layout

4.2 Creep and Shrinkage Testing Parameters

The development of prediction model for local HSC requires the analysis on a comprehensive set of data with evaluation of key parameters of time-dependent deformation besides the effect of the ambient environment. Therefore Table 4.1 and Table 4.2 present the variables of this research on standard size specimens and structural members respectively for time-

dependent deformation. The variables assessed consist of concrete strength, age at loading or drying and surrounding ambient of test condition.

Three different strength classes of HSC tested are C40/50, C50/60 and C70/80. The strength classification in this thesis is with reference to the Eurocode system. The characteristic strength is categorized as concrete Class with both 28-day cylinder and cube characteristic strength specified. Reference to cylinder strength precedes cube strength. This range of concrete strength is determined based on the common usage of HSC in the current market. Structures constructed using concrete within the range of C40/50 – C50/60 has become a common practice these days. A few of the renowned construction projects in the country that utilize concrete strength within that range are the SMART Tunnel, the KL monorail tracks and the Petronas Twin Towers. The application of concrete of higher strength will be more common in the years to come considering the advancement in concrete technology and the rapid growth in the construction industry. The wide range of strength variation provides a stronger establishment for hypothesis and allows for a wider application of results.

Structural members testing were conducted only on two concrete classes C40/50 and C65/80 as structural verification on all the concrete classes is time consuming and inefficient. C40/50 was chosen due to the extensive usage in practice while C65/80 was tested to allocate for the highest strength tested in this research, also as a reference for higher strength concrete. These two concrete classes tested will enable a better coverage of the strength range. With reference to Table 4.2, two numbers of concrete columns were tested on C40/50 concrete in controlled condition for statistical verification. Two more columns with C65/80 concrete were each tested under controlled room and ambient condition. The C65/80 columns were tested under ambient condition in order to be comparable to the standard size specimens of C65/80 tested under the same condition. The laboratory prestressed beams, which were tested under ambient condition were also tested on C65/80 concrete. The post-tensioned beams tested on site are concrete C40/50, based on the strength specification for the bridge structure.

The age of specimen testing for standard size specimens are set at 7 days and 28 days. The age of 7 days was chosen to simulate the condition of concrete of actual structures at the end of curing and removal of formwork on site. In addition to that, 7 days is also the minimal curing period for slag-cement that has slightly slower strength gain as compared to OPC. Testing of specimens at the age of 28 days was carried out to determine the material behaviour when the HSC has achieved its desired strength. As for testing on structural specimens, the tested loading age is set at 7 days to simulate the standard construction site practice.

The specimens were tested under controlled environment with ambient temperature of 27 ± 2^{o}C to simulate tropical condition and RH of 50% to simulate the ambient of indoor condition in order to obtain maximum deformation. The average testing temperature of 27^{o}C is based on the standard recommendation for tropical climate. The level of tolerance of ± 2^{o}C and RH ± 4% for the control environment is based on the requirements in ASTM C512. In addition to that, a few sets of specimens were kept under natural condition with RH varying between 60% and 85% with the temperature between 22^{o}C and 32^{o}C. These specimens were kept exposed to the outdoor change of weather under the laboratory shelter. It was not directly exposed to outdoor, under the effect of weathering in order to shelter and secures the loading apparatus.

For each set of testing, a total of 15 numbers of specimens were prepared for creep, control, compressive strength and elastic modulus testing. As for shrinkage testing, three specimens were cast in 100x100x500 mm prism for each batch of concrete. Three numbers of specimens were tested for each set of creep and shrinkage testing to verify on the consistency and accuracy of the test results for statistical analysis. The creep specimens were loaded at 40% of the ultimate strength at the age of loading. The percentage of load application is determined based on the fact that creep strain is approximately proportional to stress when applied compressive stress is less than 50% of the ultimate compressive strength of concrete.

In the ASTM C512, recommended size for creep specimen is 150mm Ø x 300 mm cylinder. However as stated in ASTM C192, a reduction in specimen size is allowed under the condition that the diameter of cylinder be at least three times the nominal maximum size of the coarse aggregate in the concrete with a minimum specimen size of 50mm Ø x 100 mm. The creep test by Neville in University of Leeds was conducted on cylinder of 76mm x 267mm with an aspect ratio of 3.5. In the research conducted by Vandewalle (2000), the specimen size of 120mm Ø x 300 mm cylinder was tested. Considering the fact that the nominal maximum size of aggregate used throughout this research is 20mm, creep was tested on 100mm Ø x 300 mm cylinder concrete.

A reduction in the specimen size has proven to be beneficial in terms of cost and easier handling during testing. The reduction of specimen size allows a reduction in material usage up to more than 50%. Most of all, the capacity of testing instruments such as the compression machine and creep rigs have also been significantly reduced with the use of 100mm Ø specimens. The effect of specimen size on creep for 100mm Ø x 300 mm and 150mm Ø x 300 mm cylinders were checked through a short-term creep test. The experimental investigation was carried out to determine the difference and also to validate on the suitability of the specimen size. Details of the short-term experiment are elaborated in Sub-Chapter 4.6 and the results are presented and discussed in Chapter 5.

Table 4.1: Creep and shrinkage test parameters on standard size specimens

Curing and Test Condition	Test	Age of Testing (days)	Concrete Class	Specimen Size	No. of Specimens Tested
1. Moist cured and tested in controlled condition (27±2°C and RH 50±4%)	Creep	7	C40/50	100mm Ø x 300mm cylinders	6
			C50/60		6
			C65/80		6
		28	C40/50		6
			C50/60		6
			C65/80		6
	Shrinkage	7	C40/50	100x100x 500mm prism	3
			C50/60		3
			C65/80		3
		28	C40/50		3
			C50/60		3
			C65/80		3
2. Moist cured and tested in natural ambient	Creep	7	C65/80	100mm Ø x 300mm cylinders	6
	Shrinkage	7	C65/80	100x100x 500mm prism	3

Table 4.2: Creep and shrinkage test parameters on structural members

Curing and Test Condition	Test	Age of Testing (days)	Type of Specimen	Concrete Class	No. of Specimens Tested
1. Moist cured and tested under 27 ±2°C and RH 50 ±4%	Creep and Shrinkage	7	Column	C40/50	2
				C65/80	1
2. Moist cured and tested under actual room condition	Creep	7	Column	C65/80	1
	Pre-camber, Time-dependent deflection	7	Pre-tensioned Prestressed Beam	C65/80	2
3. Tested under site condition	Pre-camber	28	Post-tensioned Prestressed Beam	C40/50	4

4.3 Concrete Materials

The production of HSC that has to consistently meets the requirements of workability and strength development places stringent requirements on material selection. Quality materials are required although the design of the materials proportion is the major factor in achieving desired strength. Based on the trial mixes carried out in the preliminary testing, suitable materials for the production of high strength concrete were determined. The properties of the reinforcement bars for columns and prestressing tendons for the prestressed beams are also discussed here.

4.3.1 Cement

The HSC mixes for this research were batched using slagcement; Portland cement containing 30% interground granulated blast furnace slag, unless otherwise stated. The slagcement was supplied by YTL Cement Sdn. Bhd. The physical properties and chemical composition of the slagcement, as provided by the supplier are presented in Table 4.3. Slagcement was used in favour of Ordinary Portland Cement because replacement of slag contributes towards improving concrete workability. At high concrete strength, inclusion of slag replacing the high cement content required helps to control the danger of shrinkage cracks as well as thermal cracks. Besides, in the design for HSC, cement replacement materials are always incorporated in the industry for cost-effective measures. Thus the usage of slagcement is in-line with the industrial practice.

Table 4.3: Chemical and physical properties of slagcement

Items		**Slagcement**
Silicon dioxide (SiO_2)	% (m/m)	34.3
Calcium Oxide (CaO)	% (m/m)	42.8
Magnesium Oxide (MgO)	% (m/m)	5.7
Manganese Oxide (Mn_2O_3)	% (m/m)	0.3
Chloride (CI^-)	% (m/m)	0.01
Insoluble Residue	% (m/m)	0.3
Sulphide Sulphur (S^2)	% (m/m)	0.2
Sulphur Trioxide (SO_3)	% (m/m)	0.3
Loss on Ignition	% (m/m)	0.4
Specific surface	(m^2/kg)	400
Setting Time		
Initial	(min.)	184
Final	(hr.)	3.9
Soundness	(mm)	0.3
Chloride Content	% (m/m)	0.01

4.3.2 Coarse Aggregate

The coarse aggregate used was crushed granite with maximum nominal size of 20mm, produced from Gunung Raya quarry in Johor, Malaysia. Based on the supplier's specification, the coarse aggregate is in compliance to MS 29 (1995). Sieve analysis for the aggregate was conducted according to ASTM C136-84a and specific gravity test was also conducted in compliance to ASTM C127-84. During the concrete mix design stage, the aggregate was assumed to be under saturated surface dry condition. The aggregate moisture content was tested and determined a day before every concrete batching to obtain a better assessment on the moisture content in the concrete mix.

4.3.3 Fine Aggregate

River sand with maximum nominal size of 5mm were used as fine aggregate. The fine aggregate used was categorized as Zone 2. Sieve analysis of the fine aggregate was conducted in compliance to ASTM C136-84a. One day prior to each concrete batching, the moisture content of the fine aggregate were carried out to determine the amount of moisture in the concrete mix.

4.3.4 Superplasticiser

In order to achieve the desired high strength with low water cement ratio yet good workability, polycarboxylic ether polymers superplasticiser under the commercial name of Glenium ACE 32 from Degussa Construction Chemicals Malaysia Sdn. Bhd was added to the concrete mix. The molecular configuration of Glenium ACE 32 accelerates the cement hydration and effectively reduces water, giving better performance compared to other superplasticisers. Thus, it is more suitable and preferred to other superplasticiser for the HSC mix in this study. Glenium ACE 32 complies to the specification of ASTM C494 Type A and F. The properties of Glenium ACE 32, as provided by the supplier are presented in Table 4.4.

Table 4.4: Properties of superplasticiser, Glenium ACE 32

Items	Glenium ACE 32
Specific Gravity	1.050
pH	7.00
Alkali (%)	≤ 0.50
Chloride (%)	≤ 0.10
Chlorine (%)	≤ 0.10

4.3.5 Silica Fumes

In order to achieve the desired high strength and control the cement content in the mix, silica fume was added into the mix composition. Silica fume was also introduced into the mix to simulate the industrial HSC mix for prestressed members and high rise columns, when creep and shrinkage are most critical. The densified silica fume used was obtained from Degussa Construction Chemicals Malaysia Sdn. Bhd. The chemical composition of the silica fume is presented in Table 4.5.

Table 4.5: Chemical Properties of Silica Fume

Items		**Silica Fume**
Silicon dioxide (SiO_2)	% (m/m)	92.3
Aluminium Oxide (Al_2O_3)	% (m/m)	2.7
Ferric Oxide (Fe_2O_3)	% (m/m)	1.4
Calcium Oxide (CaO)	% (m/m)	0.5
Magnesium Oxide (MgO)	% (m/m)	0.3
Sulfur Oxide (SO_3)	% (m/m)	0.1
Sodium Oxide (NaO_2)	% (m/m)	0.1
Potassium Oxide (K_2O)	% (m/m)	0.1
Loss on Ignition	% (m/m)	1.8

4.3.6 Steel Reinforcement Bars and Stirrups

High yield hot rolled deformed bar with nominal diameter of 10mm was used as the reinforcement bars for concrete columns and the nominal reinforcement at the top of the prestressed concrete beams. The stirrups for both columns and prestressed beams was 6mm diameter mild steel bars.

4.3.7 Prestressing Tendons

The strands used in this study were from Grade 270 with nominal diameter of 9.53mm. The strands were manufactured to meet the requirements of ASTM A416-96. The prestressing strand is classified as low relaxation strand. Before the strand was used for the concrete casting, some of the tendon properties such as the maximum loading, maximum strain and the value of modulus of elasticity were tested. The test was carried out according to ASTM A370-92 using Dartec Universal Testing Machine with 250kN capacity. The stress-strain curve was recorded using the computer program attached to the testing machine. Direct tensile tests were performed on five samples measuring 600mm to obtain the specified properties. During the test, direct tensile force was applied until the specimens failed.

4.4 High Strength Concrete Mix Design and Batching Procedures

4.4.1 Trial Mix and Concrete Mix Design

The selection of mix proportions involves a balance between economy and specific concrete casting requirements such as workability, strength, durability and density. The required characteristics of the mix are governed by the function of the concrete member and also the exposure conditions expected to be encountered. Seven sets of trial mixes were conducted prior to the main creep and shrinkage testing. A total number of six 150mm cubes and six 100mmØ x 300mm cylinders were prepared for each batch of trial mix for compressive strength test. The trial mix results helped to determine the mix composition and suitable materials used for the high strength concrete mix.

The concrete mix proportions were designed based on ACI 221 (1993) ‘Proportion for HSC with Ordinary Portland Cement and Ground Granulated Blast Furnace Slag’. Reference was also made to specifications given by the blended cement supplier, YTL Cement Sdn. Bhd. Optimum mix design to achieve the specific strength were obtained after some adjustment to

the mix proportion subsequent to trial mix testing. The optimum mix designs for three strength classes of HSC, C40/50, C50/60 and C70/80 investigated in this study are given in Table 4.6.

With reference to Table 4.6, concrete batches A1, A2 and A3 refers to concrete class C40/50, C50/60 and C65/80, respectively that were batched and tested for creep and shrinkage on standard size specimens. Concrete batches B1 and B2 refer to concrete C40/50 and C65/80, respectively that was batched for column testing. The B3 batch was used to cast pre-tensioned prestressed beam for deflection test and it is of concrete strength class C65/80. Generally, the mix composition of concrete for all batches A and B concrete were the same for the same strength. In addition to that, the mix design for the concrete batched on site for post-tensioned prestressed beam testing is also presented in Table 4.6. The mix composition and materials used for batch D1 is different from batch A and B because it was produced by ready-mixed concrete plant for actual structures on site for a particular construction project. The strength class for batch D1 is at C40/50.

Table 4.6: High strength concrete mix design for C40/50, C50/65 and C65/80

Concrete Batch No.	**A1**	**A2**	**A3**	**B1**	**B2**	**B3**	**D1**
Strength class	**C40/ 50**	**C50/ 60**	**C70/ 80**	**C40/ 50**	**C70/ 80**	**C70/ 80**	**C40/ 50**
Slagcement (kg/m^3)	426	441	493	426	441	493	-
Mascrete (kg/m^3)	-	-	-	-	-	-	450
Silica Fume (kg/m^3)	20	30	40	20	30	40	-
Coarse Aggregate (kg/m^3)	1021	1032	1036	1021	1032	1036	1000
Fine Aggregate (kg/m^3)	779	768	710	779	768	710	746
Water (kg/m^3)	165	160	160	165	160	160	153
Glenium ACE 32 (L/m^3)	1.7	3.4	6.6	1.7	3.4	6.6	-
Daracem (L/m^3)	-	-	-	-	-	-	5.85
Daratard (L/m^3)	-	-	-	-	-	-	1.35
w/c ratio	0.37	0.34	0.30	0.37	0.34	0.30	0.34

Note: *A1, A2, A3 are composition for creep and shrinkage on standard size specimens testing*

B1, B2 are composition for column testing

B3 is the composition for prestressed beams tested in the laboratory

D1 is for post-tensioned prestressed concrete tested on site

4.4.2 Concrete Batching and Casting Procedures

The mixing procedure for concrete batch A and B was carried out according to the method of mixing silica fume concrete, as provided by The Silica Fume Association. The recommended procedure in ASTM C192-90(a) is found unsuitable as it does not cater for the inclusion of silica fume into the mix. Thus the mixing time is not long enough to break down the agglomerations and to disperse the densified silica fume.

All materials were stored in ambient condition in the laboratory 24 hours before bathing to prevent direct influence of weather condition such as extreme drying or wetting on the materials. A tilting drum mixer of 0.3m^3 capacity was used for all concrete batching throughout the research. The mixing procedure started with placing 75% of water into the mixer, followed by the coarse aggregate. Subsequently, silica fume was added into the revolving mixer before superplasticiser was slowly poured in. These materials were then mixed for approximately 1½ minutes. Next, the cement was added into the mixer and the materials were mixed for another 1½ minutes. Thereafter the fine aggregate was added and the remaining water was used to wash in all the ingredients. With all the materials placed according to its order into the mixer, the concrete was mixed for approximately 5 minutes, followed by a 3 minutes rest and thereafter another 5 minutes of mixing. Workability test adopted in this study was the slump test, carried out in accordance to ASTM C143

The concrete was then cast into steel or plank moulds according to the type of test to be conducted. Moist gunny sacks were used to cover the surface of specimens to avoid water evaporation. For the standard size specimens, it was demoulded at 24 hours after casting and immediately placed under curing. The casting of concrete columns and pre-tensioned prestressed beams is detailed in the next sub-chapter.

4.4.3 Specimen Curing

According to ASTM C512, creep specimens should neither be cured by immersion in water nor cured under streams of running water. Therefore after demoulded, all the creep and shrinkage specimens were immediately covered with a layer of wet gunny sacks followed by plastic sheets at normal room temperature to prevent loss of water. The specimens were kept moist throughout the duration of either 7 or 28 days of curing.

4.5 Concrete Properties Testing

4.5.1 Compressive Strength Test

Compressive strength is an important property of concrete as it is the main feature in identifying the general characteristics and quality of concrete. It is used as the main parameter for structural design in codes of practice and standards. The British Standards define compressive strength based on 150mm concrete cubes whereas the American and European codes specify the strength in terms of cylinder strength. Considering the current stage of transition from British Standards to the European codes, the compressive strength test in this research was conducted in both cubes and cylinder.

4.5.1.1 Sample Preparation and Test Procedures

The 150mm cubes were tested in compliance to British Standards BS 1881: Part 116: 1983 whereas the cylinders were tested according to ASTM C39-86 procedures. The cylinder specimens were prepared in two sizes; 150mmØ x 300mm and 100mmØ x 300mm. The former size is for reference to the EC 2 whereas the latter is to determine the capacity and load intensity of the creep specimens. Concrete specimens for batches A and B were cast and tested in the laboratory. Batch D however were cast on site and tested for compressive strength in the laboratory.

Prior to loading, each specimen was weight to determine the concrete density. The testing compression machine used was ‘Tonipact 3000’ crusher with the capacity of 3000kN. The specimens were placed on the lower bearing block and aligned to the center of thrust of the spherically seated block. The rate of loading was kept at 7.0kN/s for 150mm cubes, 5.0kN/s for 150mmØ cylinder and 3.0kN/s for the 100mmØ cylinder. The load was then applied until the specimen fails. For every set of test, three numbers of specimens were tested and the compressive strength is obtained based on the average of the three.

4.5.2 Modulus of Elasticity and Poisson's Ratio Test

The elastic modulus and Poisson's ratio testing was conducted on 100mmØ x 300mm cylinder specimens. The elastic modulus is of relevance to determine the initial strain of the concrete specimens for each creep test. This property also represents a relation between stress and corresponding strain or between force and deformations of concrete (Rashid, 2002). The Poisson's ratio on the other hand shows the degree of axial contraction and lateral extension of concrete under compression. The tests conducted in compliance to ASTM C469-87a, provided the result of secant modulus and Poisson's ratio.

4.5.2.1 Sample Preparation and Test Procedures

Three cylindrical specimens were prepared and cured in the same way as to the creep specimens. After the curing process, electrical strain gauges of 60mm in length (TML PL-60) were vertically attached on the four circumferential positions of the specimens. In order to determine the Poisson's ratio, the strain gauges of one of the specimens were prepared differently. Two gauges were attached vertically at two diametrically opposite points of the specimens whereas another two strain gauges were attached horizontally at two directly opposite points.

After compressive strength test of companion specimens, the elastic modulus specimens were placed on the lower platen of the 'Tonipact 3000' compression machine. The axis of the specimens was carefully aligned to the centre of thrust of the spherically seated upper bearing block. The specimens were then loaded for four cycles at 40% of its ultimate compressive strength, at the rate of 1kN/s. During the first loading, data was not recorded to observe the performance of the gauges and to ensure a uniform loading onto the cylinder. The deformation was measured and recorded with a data logger at the three subsequent loading. The transverse strain was also recorded from

one of the specimens to determine the Poisson's ratio. Figure B1 in Appendix B shows the photo of the elastic modulus testing.

4.5.3 Porosity Test

The performance of concrete under a particular environment cannot be solely related to its strength alone but it is a function of its pore structure and permeability. The total porosity of a material is defined as a function of the bulk volume of the material occupied by voids. The presence of a large number of small pores, in which some of these pores are bottle neck has made the need to choose the method for determining the total porosity of mortar and concrete closest to the actual value as vital. The method adopted to determine total porosity of concrete for this research is the vacuum saturation method. This method was used as it is simple and cost effective.

4.5.3.1 Sample Preparation and Test Method

Cylindrical specimens of 100mmØ x 50mm thickness were used as porosity test samples throughout this investigation. The specimens were tested on each concrete batch A1, A2 and A3 at both 7 days and 28 days. The apparatus used in this investigation was developed by Cabrera and Lynsdale (1988), as illustrated in Figure 4.2.

Six numbers of 50mm samples for each set of testing were first placed in the vacuum saturator chamber, set to a pressure of -760 mm for 3 hours. During this period, desiccants were present to absorb all excess moisture in the chamber. Thereafter, distilled water was added into the chamber until the specimens were submerged and negative pressure was again applied for additional 3 hours. After the end of this period, the vacuum valve was switched off and the pressure resumed to atmospheric pressure with the specimens still submerged in water. It was then left to be submerged in the water for 24 hours to ensure full saturation. After the period of full saturation,

the specimens were weighed in water and in air, then kept in the oven at 105°C for 24 hours and dry weight was then obtained.

Based on the vacuum saturation method, total porosity of concrete, P is calculated using Equation 4.1. The result shows a total porosity value and does not distinguish between the entrapped air voids, entrained air voids or the water voids.

$$P = \frac{W_{ssd} - W_d}{W_{ssd} - W_{ssw}} \quad x \quad 100 \tag{4.1}$$

where

W_{ssd} = weight of saturated surface dry specimen in air (kg)

W_d = weight of oven dried specimen in air (kg)

W_{ssw} = weight of saturated specimen in water (kg)

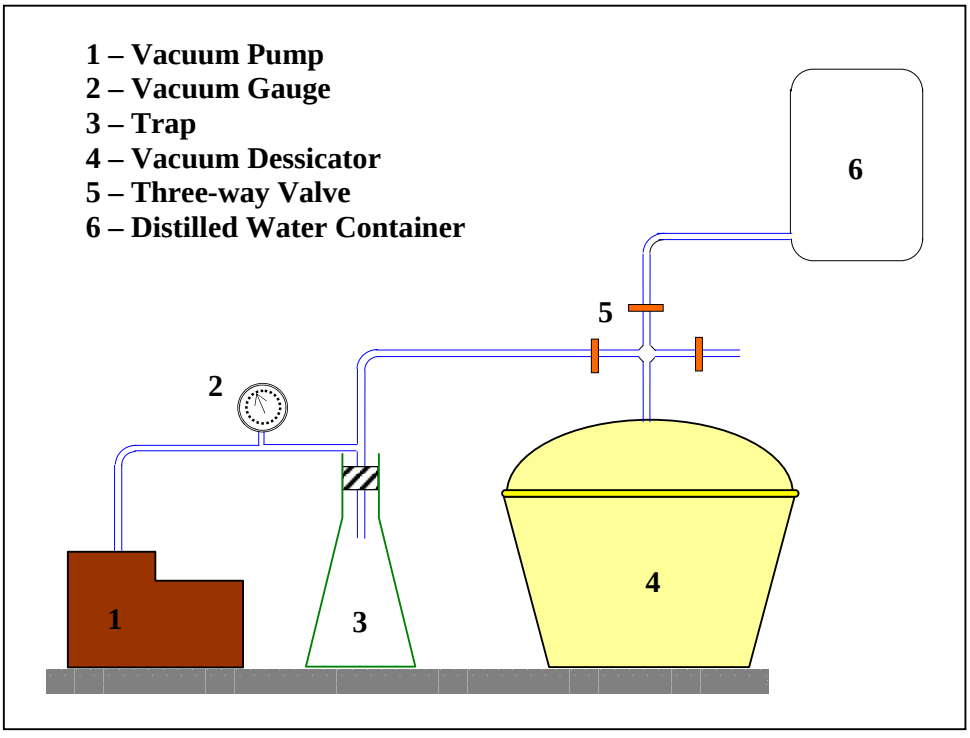

Figure 4.2: Schematic diagram for vacuum saturation apparatus for determining total porosity

4.6 Short-term Creep Test on Different Specimen Sizes

In the initial stage of the research work, short-term creep test was conducted on two specimen sizes - 150mmØ x 300mm cylinder to 100mmØ x 300mm cylinder. The main objective of the test was to investigate the feasibility of reducing the creep specimen size from the ASTM 512-87 recommendation of 150mmØ cylinder to 100mmØ cylinder. The effect of specimen sizes on creep strain and the correlation of results between the two sizes is also determined from this experiment.

In this experiment program, a total number of 15 cylinders of each size and 6 cubes were cast with concrete C32/40. Details of the testing parameters are presented in Table 4.7. The concrete mix design, labelled as P1 is presented in Table 4.8. As the main variable for this short term test is the specimen sizes, the concrete mix does not contain additional additives or admixtures and only Ordinary Portland Cement is used to eliminate unnecessary influence from other parameters. This explains the lower concrete strength as compared to the main set of creep and shrinkage testing.

The specimens were moist cured for 7 days before concrete properties testing commenced. The test consists of creep test, monitoring of companion specimen for skin shrinkage, modulus of elasticity and compressive strength test. The creep test was carried out at the concrete age of 7 days, according to the ASTM C512-87 method under the ambient condition of 27±4^{o}C and RH of 70±10%. The procedures for modulus of elasticity and compressive strength test were as explained in Sub-Chapter 4.5 and the procedure for creep testing is elaborated in Sub-Chapter 4.8. The strain reading for creep and shrinkage was only taken up to 60 days due to constrain in the utilisation of equipment. However, a good conclusion of the size effect and correlation between the two specimen sizes was obtained.

Table 4.7: Details of short-term creep test

Curing and Test Conditions	Concrete Class	Age of Testing (days)	Type of Specimens	Test	Total Specimens Tested
1. Moist cured and tested under 27 ±4°C and RH 70 ±10%)	C32/40	7	100mm Ø x 300mm cylinders	Creep	3
				Drying shrinkage	3
			150mm Ø x 300mm cylinders	Creep	3
				Drying shrinkage	3

Table 4.8: Mix design for concrete P1

Materials/Details	P1 Concrete
Ordinary Portland Cement (kg/m^3)	347
Coarse Aggregate (kg/m^3)	1248.8
Fine Aggregate (kg/m^3)	693.8
Water Content (kg/m^3)	170
w/c ratio	0.49

4.7 Experiment Test Controlled Room

A temperature and humidity controlled room was set up in the Civil and Structures Laboratory in Universiti Teknologi Malaysia for this research. The room which was designed to maintain a temperature of 27±2°C and RH of 50±4% is closed and screened from the natural ambient with a polythene curtain and a wooden door. The controlled room was equipped with two sets of air-conditioners and four sets of Wood's MDE 25 dehumidifier to achieve the specified ambient. The dehumidifier, as shown in Appendix B, Figure B2 has the capacity of removing approximately 11800mL of water per 24 hours. The surrounding ambient of this room was recorded by a unit of hygrothermograph whereas a unit of digital hygrotherm functioned as a monitoring device that detects immediate change in the surrounding ambient. Figure B3 in Appendix B shows the picture of both the hygrothermograph

and hygrotherm. Figure B4 in Appendix B shows the condition of the controlled room.

4.8 Creep Test on Standard Size Specimens

With the objective to determine time-dependent deformation data for Malaysian concrete, creep testing was carried out in control room of 27±2^{o}C and RH of 50±4% as well as under natural ambient for a better simulation of tropical condition. The test was conducted in compliance to ASTM C512-87.

4.8.1 Creep Samples Preparation

The concrete creep cylinder specimens were cast in steel moulds, vertically in four layers, consolidated with 25 strokes at each layer using tamper rod. The higher number of layers was to achieve better compaction due to due to the higher aspect ratio of the specimen size. No poker vibrator was used for casting as to the recommendation in C192-90(a). Concrete was demoulded at 24 hours after casting and immediately placed under curing.

A total of fifteen (15) cylinder specimens were cast for each set of testing with three for creep and another three remained unloaded as control for shrinkage measurement. Four specimens were tested for compression, three for elastic modulus testing and one for porosity test. Another one specimen was then cut into 150mm thickness to be used as dummy specimen. The dummy specimens were required at both ends of creep specimens in the loading rig to ensure better distribution of stresses onto the specimens.

After the required curing period, mechanical grinding was performed on specimens with uneven surface and the planeness of the tested face was checked. A flat surface is critical for creep testing to obtain equal distribution of load on all the stacked specimens and to avoid eccentricity in loading. This helped in preventing local failure due to excessive deformation at a particular point and to avoid premature failure due to the high brittleness of HSC.

Gauge studs with effective distance of 200mm were then fixed on four circumferential positions of the specimens with rapid setting epoxy under the brand name of Araldite. One of the three creep specimens for each set of testing were fixed with two 60mm strain gauges (TML PL-60), attached at opposite faces for electrical strain monitoring. Before fixing of the studs and strain gauges, the surface of the specimens was first smoothened by abrasive paper and cleaned with acetone.

4.8.2 Creep Test Apparatus

Based on ASTM C512-87, a coil spring loading system was selected as the loading frames in this study. The function of spring in this uniaxial compression loading system is to sustain the magnitude of load applied due to the change in length of specimens caused by creep, maintaining a constant stress (Neville, 1970). Without springs, the applied stress of creep specimens compressed between two plates held by metal rods will sequentially be reduced.

Figure 4.3 shows the schematic representation of the creep testing set-up with the loading frame and data logging system. A load cell, Kyowa with 50 ton capacity, as shown in Figure B5 in Appendix B was loaded together with the specimens to register the stress applied. The stress was then displayed and recorded on a 30 channel data logger, Tokyo Sokki Kenkyujo (TDS 303) as shown in Figure B6 in Appendix B. The measurement of creep as well as the control specimens was performed using a mechanical Demec gauge of 200mm gauge length as shown in Figure B7 in Appendix B.

4.8.3 Creep Test Procedures

Creep test was carried out on 7 days and 28 days. Before the start of the test, ultimate compressive strength was conducted on four 100mm Ø cylinders to determine the magnitude of stress to be applied on the specimens.

The value of stress applied was taken at 40% of the average ultimate compressive strength.

The creep specimens were stacked up to three layers with the dummy specimens mounted at the top of upper specimen and the bottom of the bottom specimens. The test set up is as shown in Figure 4.3 and a picture of the set-up of the creep rig is shown in Figure B8 in Appendix B. The load was applied through a hydraulic jack with hand pump with the rate of approximately 1kN/s and monitored from the data logger through the load cell. Precaution was exercised to ensure that the loading was directly axial and uniform to avoid eccentric loading. This was practiced by applying small preload not exceeding 1.38 N/mm^2 and strain reading was then recorded to check on strain variation around each specimen. After this step, the load was removed and specimens were realigned for greater strain uniformity. Figure B9 and B10 in Appendix B show the set up of creep specimens tested in the controlled room and ambient condition, respectively.

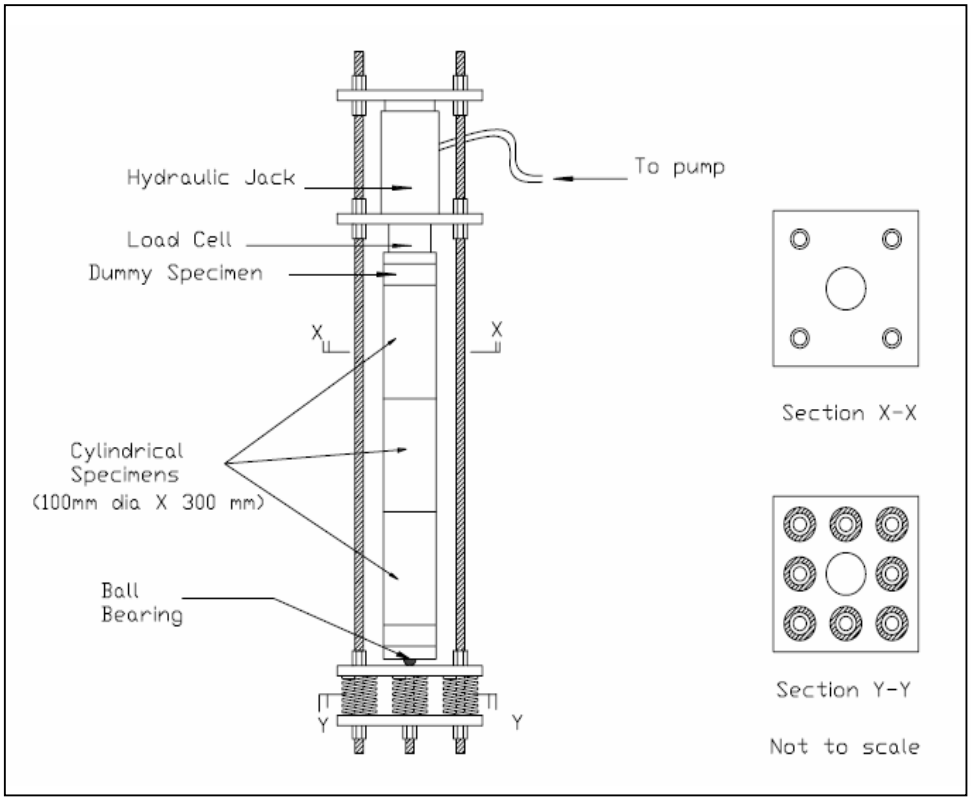

Figure 4.3: Typical creep test set-up for standard size specimens

After the stress applied has stabilised, the hydraulic jack is removed. The load is then held by the upper and lower metal plate through tightening the nuts on the threaded reaction rods. The strain was immediately recorded by the strain gauges and displayed through the data logger throughout the whole loading process. The measurement using the Demec gauge was carried out before loading as a reference datum. After the load has been fully applied, strain measurement was immediately taken. It was then measured again two to six hours later, then daily for one week, weekly for one month and monthly until the completion of test. The duration of loading for this set of testing was up to ten months.

4.8.4 Creep Calculations

The creep strain was calculated as an average of 12 measurement points for each set of testing series. The magnitude of creep was calculated by subtracting the initial elastic deformation and the shrinkage deformation of control samples from the total deformation measured from the creep specimens. The readings from Demec comparator is converted into strain value by using the following formula:

$$\varepsilon_{Total} = (Initial\ DRD - DRD) \times k_{Demec} \quad (4.2)$$

where

ε_{Total} = strain measured from the specimen

DRD = Demec reading taken from the specimen

k_{Demec} = strain conversion coefficient for Demec gauge = 7.94×10^{-6}

4.9 Shrinkage Test on Standard Size Specimens

The drying shrinkage test was performed on 100mm x 100mm x 500mm prisms with test method in compliance to ASTM C157–92. The test ambient condition for shrinkage specimens is the same as creep test.

4.9.1 Shrinkage Samples Preparation

The shrinkage specimens were cast in steel moulds, as shown in Figure B11 in Appendix B. Before concrete casting, the inner surfaces of the moulds were thinly covered with mineral oil. Thereafter, the gauge studs were fixed at both ends of the moulds with partial embedment to a depth of 30mm into the specimens and 20mm pin protruded out. The studs were fixed with proper care to keep it clean and free of oil, grease and foreign matter. This is to ensure a good bonding between the concrete and the studs for a precise measurement. The studs were fixed on the center point of the end plates to set its principal axis to coincide with the principal axis of the test specimen during casting. This step was to ascertain that the length change measured is the axial shrinkage of specimens.

The concrete was then cast horizontally in two layers with 30 times compaction for each layer, by using the tamper rod. No vibrator was used for the casting. After the process, surfaces of the specimens were smoothened and covered with wet gunny sacks and plastic sheets to prevent evaporation. Prior to curing, the protruded pins of shrinkage gauge studs were coated with mineral oil to prevent it from rusting during the curing period.

4.9.2 Shrinkage Test Apparatus

The comparator used for shrinkage measurement is shown in Figure B12 in Appendix B. The comparator consists of a fixed terminal at one end and a dial micrometer with accuracy of 0.001mm at the opposite end to record the length of specimens.

4.9.3 Shrinkage Test Procedures

Prior to taking the reading of length change of specimens with the comparator, a reference bar of 53mm in length is used to check the dial gauge setting of the device. The specimens were placed in the instrument with the same end each time the comparator reading was taken. Upon removal of the specimens from moulds at the age of 24 hours, a comparator reading was taken as the reference point, corresponding to 'zero' strains for the measurement. Therefore, the strains attributed to the fresh and setting concrete such as autogenous, plastic and thermal shrinkage were not considered in the deformations measured. By the end of the moist curing period, the specimens were stored either in the control room or under natural environment. Shrinkage reading was taken every day for two weeks, weekly for one month and monthly up to a period of ten months.

4.9.4 Shrinkage Calculations

The length change of the specimens at any age after initial comparator reading is calculated as follows:

$$\delta L_x = \frac{CRD - Initial\,CRD}{G} \; x \; 100 \qquad (4.3)$$

where

δL_x = length change of specimen at any age (%)

CRD = difference between the comparator reading of the specimen and reference bar at any age

G = the gauge length = 500mm

4.10 Time-dependent Deformation Test on Concrete Columns

4.10.1 Structural Columns Preparation

The laboratory scaled column is designed according to Eurocode 2 method. Detailed drawing of the column is shown in Figure 4.4 and the design calculation is attached in Appendix C. The preparation of the columns started with the assembly of nominal reinforcement and shear links according to the design details. Thereafter, the steel reinforcements were installed into the formwork together with 30mm thick spacer blocks. The spacer blocks were used to accommodate the nominal distance between the steel reinforcements and formworks. Figure B15 and B15 in Appendix B show the preparation of the columns prior to being loaded.

Prior to casting, the formworks were cleaned and applied with mineral oil to help ease the subsequent removal of formwork. Two numbers of columns were cast for each concrete strength of C40/50 and C65/80. Six numbers of 150mm cubes and 100mm ϕ x 300mm cylinders, each were prepared for every batch of concrete for 7 and 28 day compressive strength test. The columns were compacted using poker vibrator. Upon completion of concrete casting, the columns and accompanying cube and cylinder specimens were covered with polythene sheets to prevent moisture loss. The cube and cylinder samples were demoulded after approximately 24 hours whereas the column formworks were removed after 3 days.

After the moist curing period, gauge studs with effective length of 200mm and 600mm were fixed on all the four surfaces of the concrete columns. The positions of the studs are as shown in Figure 4.5. The gauge studs were bonded on the column surface using rapid setting epoxy under the brand name of Araldite. Prior to fixing of the studs, the concrete surface was smoothened using abrasive paper and cleaned with acetone.

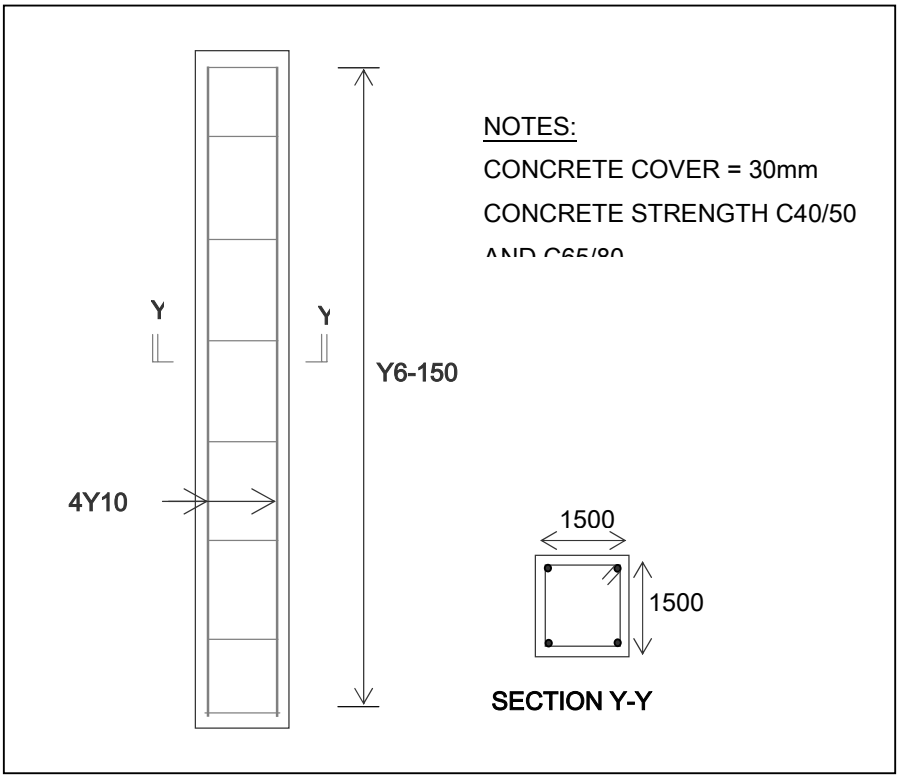

Figure 4.4: Details of columns tested for time-dependent deformation

4.10.2 Columns Test Apparatus and Instrumentation

The loading apparatus for the concrete column was the spring loaded frame which is the same as the creep loading frame. The initial compression was applied by a portable jack and the load was maintained by the header plates on ends of loaded specimens and kept constant by coil springs. Spherical head or ball joint was provided to ensure uniform loading to the specimens. The loading apparatus was the same as the creep testing and the test set-up is as shown in Figure 4.5. Photo of the set-up in the laboratory is shown in Figure B17 in Appendix B. The concrete strain was measured using Demec comparator (Mayes) with effective gauge length of 200mm and 600mm.

4.10.3 Columns Test Procedures

At the age of 7 days, the columns were removed from moist curing. Prior to loading the concrete columns, three numbers of cubes and cylinder specimens were each tested for ultimate compressive strength. This is to ensure that the concrete has achieved the desired strength before load is applied to the columns.

Similar to the loading procedures for creep testing of standard size specimens, load was applied through a hydraulic jack with hand pump. The loading rate is approximately 1kN/s. The magnitude of stress applied was at 40% of the ultimate design load capacity of the columns. The load increment was displayed and recorded by the data logger through the load cell. Precaution was exercised to ensure that the loading was uniform and directly axial to avoid eccentricity. This was practiced by applying small preload not exceeding 1.38 N/mm^2 and strain reading was then recorded to check on strain variation on each side of the column. After this step, the load was removed and specimens were realigned for better loading uniformity.

After the stress applied has stabilised, the hydraulic jack is removed. The load is then held by the upper and lower metal plate through tightening the nuts on the threaded reaction rods. The magnitude of load was captured by the load cell and displayed through the data logger throughout the whole loading process. The measurement using the Demec gauge was carried out before loading as a reference datum. After the load has been fully applied, strain measurement was immediately taken to determine the elastic strain. It was then measured again two to six hours later, then daily for one week, weekly for one month and monthly until the completion of test. The duration of loading for this set of testing was up to three months.

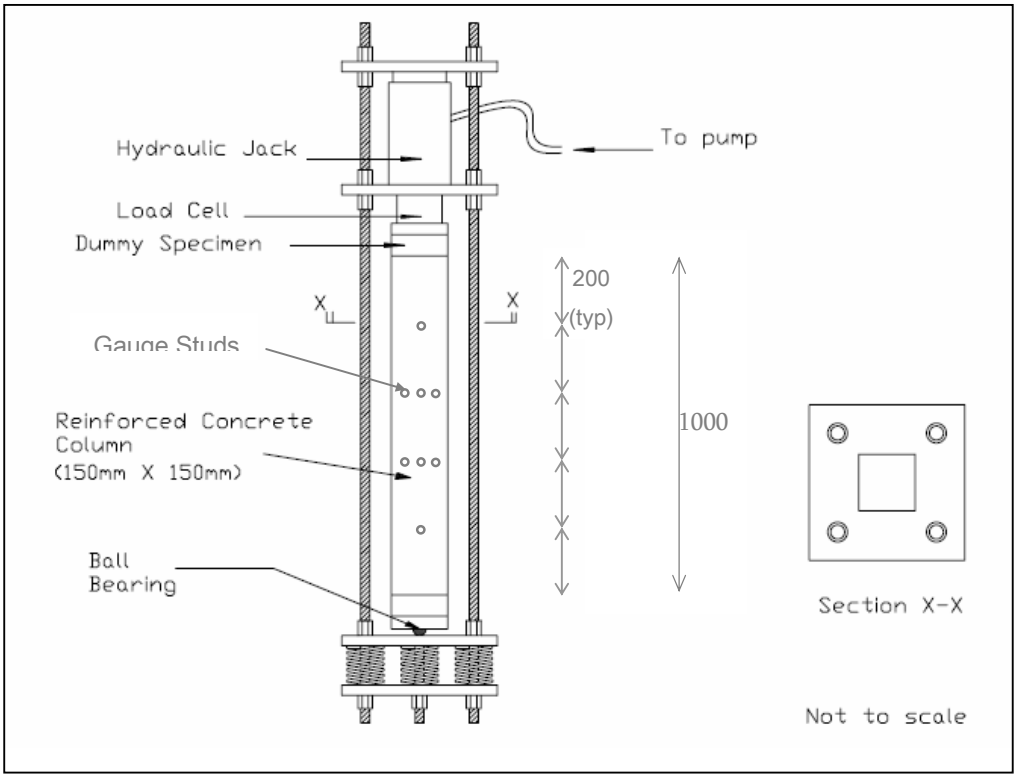

Figure 4.5: Creep test set-up for reinforced concrete columns

4.11 Pre-tensioned Prestressed Beams Test

The prestressed concrete beams were tested to investigate the structural performance of prestressed members under the effects creep and shrinkage. The test results obtained were used in the assessment of precamber, time-dependent deformation and prestress losses, mainly on concrete creep and shrinkage.

4.11.1 Prestressed Beams Preparation

Two numbers of pre-tensioned prestressed beams were designed, cast and tested under similar conditions to check on the reliability and consistency of results obtained. The beams were designed as uncracked section in accordance to Eurocode 2 (2004) with concrete C65/80. Therefore the

targeted strength at transfer of 7 days was 50 N/mm^2. The calculation sheet is attached as Appendix D. The beam cross section was designed as I-shaped and the dimensions were scaled down from a full-scale standard I-section beam with a ratio of 1:5. The cross sectional dimension of the beam and the detailing of tendons and reinforcements are shown in Figure 4.6. The length of the beam was at 2.5m. Two strands of 9.53mm diameter prestressing tendons of Grade 270 with low relaxation were fixed at the distance of 110mm from the neutral axis of each beam. No debonding was required as the tendon profile is within the calculated allowed cable zone limit.

Preparation for the prestressed beams prior to casting involves careful installation of formwork in the prestressing bed, tensioning of the prestressing strands and installation of reinforcement bars. The prestressing bed used in this study holds a maximum force capacity of 1000kN. The width of the bed is about 2.0m, the overall length of the bed is at 13.0m and the internal length available to fit prestressed concrete members is 9.0m. Therefore both the beams with the length of 2.5m each could be cast simultaneously.

The formwork for the beams was constructed using 18mm thick plywood. Prior to concrete casting, the internal joining sides of the formworks were sealed using rubber tapes to prevent leakage during casting. In addition to that, the internal surfaces of the formworks were also brushed with mineral oil to ease the removal of the formwork.

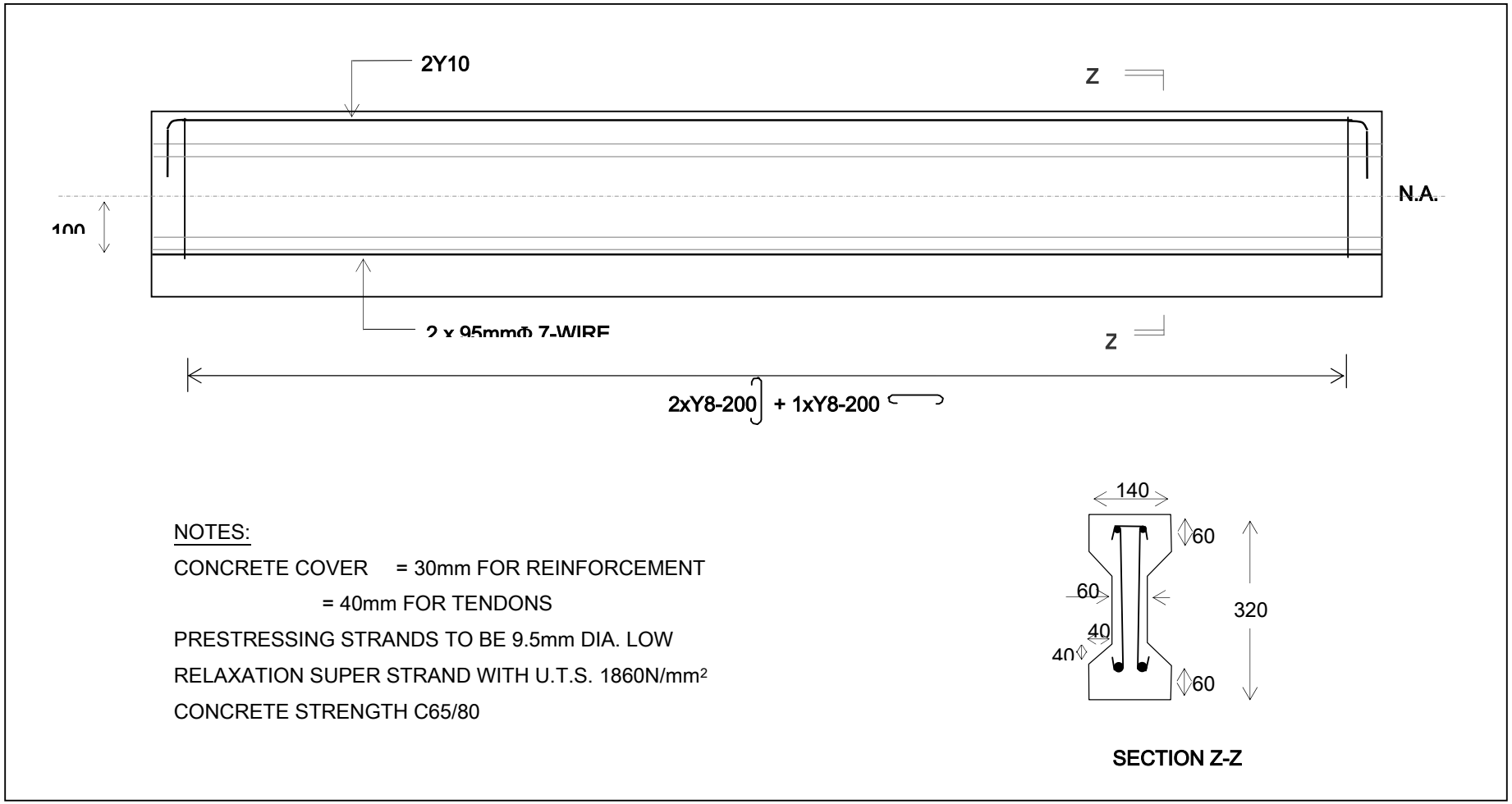

Figure 4.6: Details of prestressed beams designed and tested in the laboratory

4.11.1.1 Prestressing Work

Prior to prestressing, the strands were checked and wiped clean to remove loose rust, oil, dust or other lubricants that may reduce the efficiency of the grips. Thereafter, anchor grips were installed at both ends of the prestressing strands. The wedges and barrels were checked to ensure that there were no crack, worn teeth or other bad conditions and is fit for use. Good condition of anchor grips and proper installation of the grips are important to provide a safe state for stressing, casting and detensioning work.

Prestressing of the strands was carried out using a TITAN 20 jack, which is operated by high-pressure hydraulic pumps. The jack is capable of stressing strands up to 16mm in diameter and it has automatic front-full gripping for which 300mm of projecting strand is sufficient. Figure B18 in Appendix B shows the photo of the jack while the specifications are given in Table 4.9. The force applied is at 77kN on each tendon, equivalent to 70% of the tendon ultimate tensile strength. During prestressing, the force was increased at an interval of 12.7kN (500psi) and the increment pressure was measured by the dial gauge on the hydraulic pump. Figure B19 shows the photo of the formwork set-up and prestressed tendons on the prestressing bed.

Table 4.9: Specifications of hydraulic prestressing jack, TITAN 20

Type of Prestressing Jack	**TITAN 20**
Maximum Jack Force	225 kN
Jack Piston Area	3684 mm^2
Maximum Hydraulic Pressure	60 N/mm^2
Closed Length	550 mm
Jack Stroke	225 mm
Jack Weight	27 kg

The efficiency of the hydraulic jack was checked through monitoring of elongation of the prestressing strands. The experimental elongation was

obtained directly from the extension scale on the prestressing jack. The difference between theoretical and experimental elongation was compared. The theoretical elongation was calculated using the following formula:

$$\text{Elongation, } \delta = \frac{PL}{AE} \tag{4.4}$$

where

P = applied load (kN)

L = total stressing length of strand (mm)

A = sectional area of strand (mm^2)

E = modulus of elasticity of strand (kN/mm^2)

4.11.1.2 Prestressed Beams Concrete Casting

Upon completion of the beam reinforcements and prestressing setting up, concrete casting commenced. In order to keep to consistent and comparable results, the concrete mix proportion used for the prestressed beams was the same as the other C65/80 mix in this study. A total number of six 150mm cubes and six 100mm Ø cylinders were also cast to determine the 7 and 28 day concrete strength. Immediately after concrete batching, slump test was carried out to check the concrete workability. Each beam was cast and compacted using vibrating poker in two layers in order to prevent the formation of honeycomb, especially at the junction between the web and bottom flange. Upon completion of the compaction and surface finishing of the beams and accompanying cubes and cylinders, the specimens were covered with plastic sheets to avoid excessive loss of moisture. The beam formworks were removed 3 days after concrete casting whereas the cube and cylinder samples were demoulded after approximately 24 hours. In order to maintain a consistent development of concrete strength between the beams, cubes and cylinder specimens, all were cured under similar conditions. The specimens were moist cured using wet burlap until the age of 7 days.

4.11.1.3 De-tensioning Process

After the curing period of 7 days, three number of cubes and cylinder specimens, each were tested for concrete compression to determine the transfer strength of the beams. After the confirmation on achieving the allowed transfer strength limit, de-tensioning work was carried out individually for each strand. A de-tensioning chair and the prestressing jack were installed at one end of the strand, as shown in Figure B20 in Appendix B. The instruments were used to hold the strands from immediate release, which may cause failure to the beams. The anchorage grip was then slowly knocked out from its place using a hammer and chisel. After the prestressing force were slowly transferred into the beams through the release of the anchorage grips, the remaining length of the strands were cut off.

4.11.2 Pre-camber Test Procedures

Prior to the de-tensioning process, three units of LVDTs, were set-up at the top surface of each beam, at three different locations for the purpose of pre-camber measurement. The first location was at the middle-span of the beams while the other two were located at a quarter distances from left and right supports. The locations of the LVDTs are illustrated in Figure 4.7(a). The LVDTs were connected to Tokyo Sokki Kenkyujo (TDS 303) data logger to record the upward deflection, immediately after detensioning. The deflections were measured immediately after detensioning, two hours after and subsequently, everyday for duration of four days. The photo of LVDT and the setting up for beam pre-camber measurement is shown in Figure B21 and B22 in Appendix B.

4.11.3 Time-dependent Deformation Test Procedures

The beams were removed from the prestressing bed upon completion of pre-camber measurement at the age of 10 days. The full set-up for the

beam specimens two-point loading testing is illustrated in Figure 4.7(b). The test frame, specially assembled for the purpose of this testing was constructed on the strong floor in the laboratory. The frame was made up of steel plates with high strength bolt connections with the capacity of approximately 200 ton. Each test beam was simply supported over the span of 2.3m with 100mm projection from each end. A centrally applied load was transferred through a spreader beam of stiffened steel I-beam to form two equal vertical loads 150mm on either side of the mid-span. Due to the uneven surface of the specimen, steel plate was placed between the steel rollers and the specimen's surface to stabilise the applied load.

The load was applied using ENERPAC hydraulic pump jack ram of 200 ton capacity. A load cell with the capacity of 20 ton (Kyowa 20) was placed in between the jack and the beam to register the load that was applied. The total load applied was 60kN with the rate of 1kN/s. Three units of LVDTs were fixed at the soffit of the beam; at one-third, middle-span and two-third regions of the beam length to record for downward deflection due to the load applied. The deflection, concrete strain and steel strain were recorded at every 10kN increase in the loading, up till the full load was applied. Thereafter the deformation measurements were taken two hours after loading and subsequently everyday for a duration of 60 days. Photo of the test set-up is shown in Figure B23 and B24 in Appendix B.

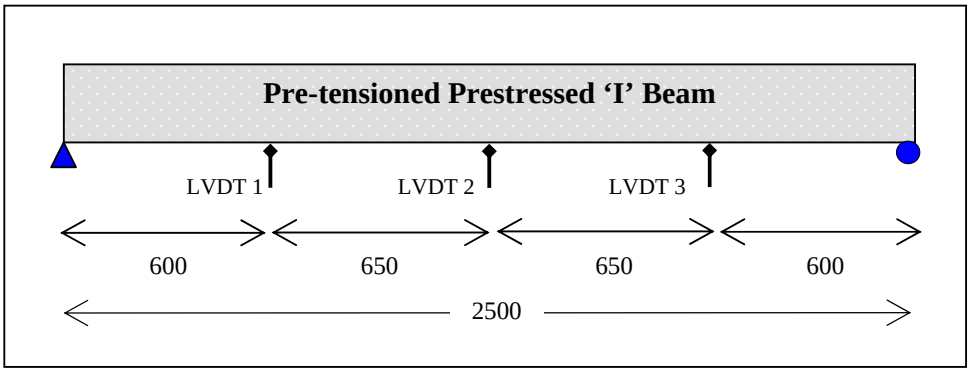

(a)

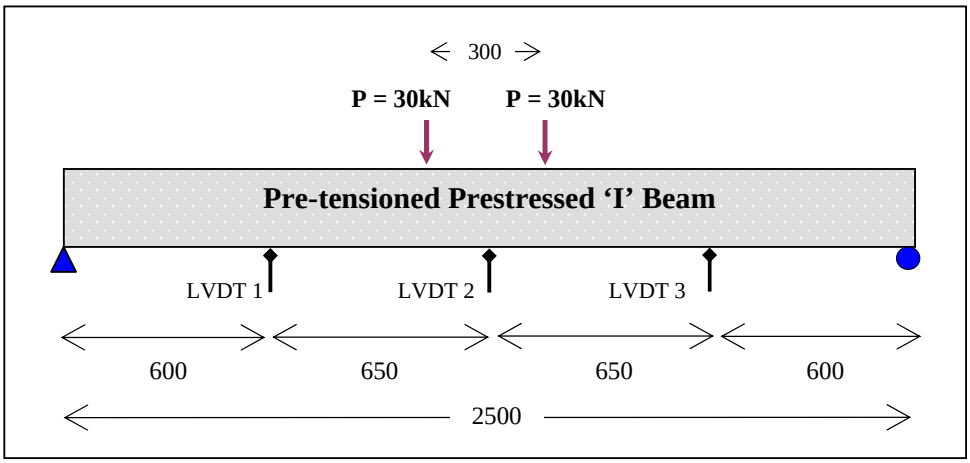

(b)

Figure 4.7: Illustration of prestressed beams set-up for (a) pre-camber test (b) deflection test

4.12 Pre-camber of Prestressed Beams on Site

The monitoring of pre-camber on actual prestressed beam members on site was conducted on post-tensioned 'I' beams. Besides site measurement, laboratory testing was also carried out on the concrete sampled from the prestressed beam casting on site to obtain concrete strength and modulus of elasticity. These concrete properties, known to directly affect the deflection of post-tensioned beam were useful in contributing towards better pre-camber prediction of the prestressed beams. In addition to that, the

concrete properties were also important in assisting to explain the magnitude of deflection that occurred. Figure B25 to B29 in Appendix B shows the photos taken during the construction of the prestressed beams on site.

In Figure 4.8, the typical cross sectional details of the prestressed beams is presented. The beams are at an overall height of 1.98m and 36m in length. The prestressed tendons used are 12.7mm Ø low relaxation super strands with ultimate tensile strength of 183kN per strand and the strands are prestressed at 75% of the ultimate strength.

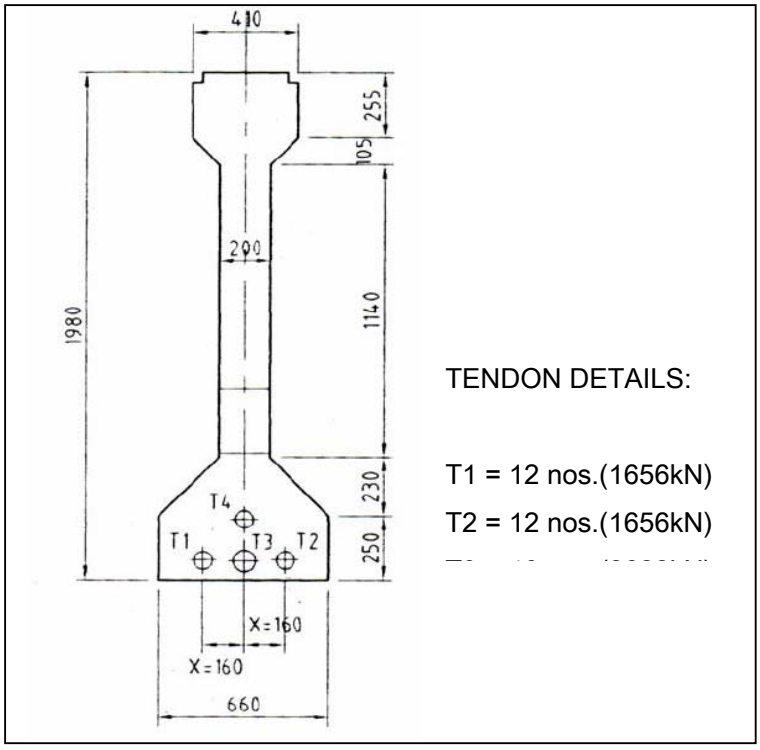

Figure 4.8: Cross-section of post-tensioned prestressed beam tested on site

4.12.1 Procedures of Monitoring of Pre-camber on Site

The actual pre-camber were monitored on four numbers of post-tensioned ‘I’ beam for a duration of 15 days after prestressing, by measuring

the movement of top level of the beams. The beams were cast with C40/50 concrete and prestressing work was conducted at the age of 28 days. Five points on the top of each beam with equal distance of 8.95m were chosen as the leveling reference points, as shown in Figure 4.9. The maximum pre-camber is determined from the difference between point No. 3 to the average of point No. 1 and No. 5. The leveling points were measured on every two days interval using the theodolite and a reference datum was established to counter check for vertical movement or settlement of the beam during monitoring.

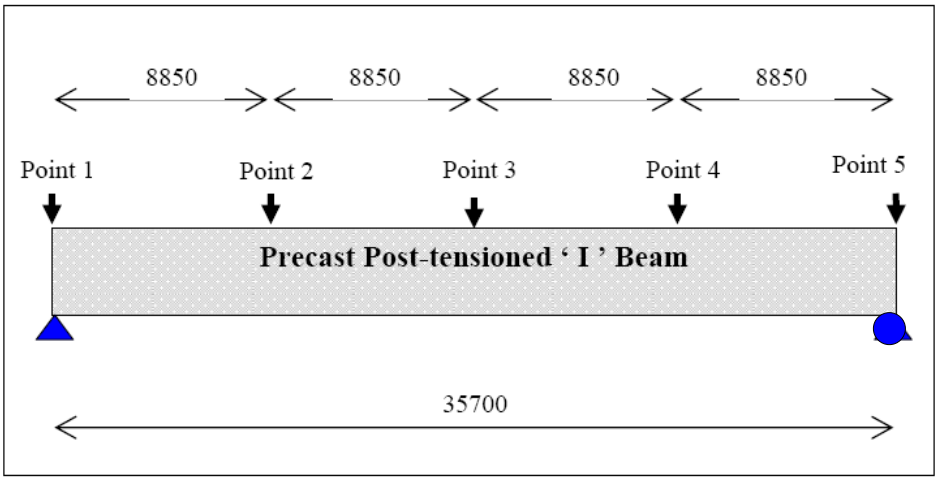

Figure 4.9: Illustration of survey reference points on post-tensioned beam

4.12.2 Mechanical Properties Test on Concrete Sampled from Site

Mechanical properties test were conducted on cube and cylinder specimens sampled from the same batch of concrete used for casting the prestressed beams. Laboratory testing was conducted on cube and cylinder specimens prepared using the ready-mixed concrete to obtain the actual compressive strength and elastic modulus. The specimens were cast and cured on site before being sent to be tested in the Structures and Materials Laboratory in Civil Engineering Faculty, Universiti Teknologi Malaysia. The compressive strength was tested on both 150mm cubes and 100mmØ cylinders at 7 and 28 days and test on elastic modulus were conducted on 100mm diameter x 300mm cylinders at the concrete age of 28 days. The

concrete properties tests were conducted according to the procedures explained in this chapter.

CHAPTER 5

RESULTS AND DISCUSSION FOR PRELIMINARY AND SUPPLEMENTARY CONCRETE TESTING

5.1 Preliminary Test Results

5.1.1 Creep Size Effect Test

In the testing of specimen size effect on creep, the properties for C32/40 concrete are presented in Table 5.1. During casting, the measured slump was at 165mm. It is observed that the cube and cylinder strength achieved at the age of 28 days was at 49.1 N/mm^2 and 32.6N/mm^2, respectively. The creep and shrinkage strain of both 100mmØ x 300mm and 150mmØ x 300mm cylinders are presented in Figure 5.1 and Figure 5.2, respectively. Through the graphs, it is observed that smaller size specimen, 100mmØ cylinder exhibit higher strain than 150mmØ cylinders. The results obtained are in agreement with the general theoretical understanding as presented by Neville (1990) as well as the findings by Bryant and Vadhanavikkit (1987), Mazloom et al. (2003) and Morita et al. (1994).

Table 5.1: Mechanical and physical properties of P1 concrete (C32/40)

Concrete Properties	**7 days**	**28 days**
Compressive strength (N/mm^2)		
Cube (150mm)		49.1
Cylinder (150mm Ø)	27.3	32.6
Cylinder (100mm Ø)	24.7	
Density (kg/m^3)	2421	2475
Modulus of Elasticity (kN/mm^2)	**7 days**	
Cylinder (150mm Ø)	27.1	
Cylinder (100mm Ø)	26.5	

On average, the smaller specimen exhibit approximately 4.4 % to 13.7% higher in creep strain as compared to 150mmØ specimen, depending on the time after loading. For shrinkage, the strain of smaller specimens is approximately 0.8% to 24.1% higher than the 150mmØ specimens. The mechanism of creep and shrinkage is highly related to mobility of moisture in the member. The lower the evaporable water content the lower the creep whereas the greater the drying, the greater the creep. Shrinkage and creep of concrete are greatly affected by the size of the parts because they are linked to the drying of the material. Higher strain in smaller specimens is likely due to the accelerated drying process from the relatively higher surface to cross section ratio. Thus for larger members, it takes a longer time for the drying effect to reach the interior region, thus lower rate of strain. Acker (2001) recommended the duration of drying varies roughly as the inverse of the square of the thickness.

Creep is greatly affected by the concrete constituent. Different mechanisms such as long term hydration of cement and drying make the influence of the size of member larger. At higher concrete strength, the controlling factor of shear-friction interaction between the aggregate and cementitious paste becomes more significant than the specimen size (Nawy, 2001). Therefore, it is expected that effect of specimen size will be reduced for the creep and shrinkage specimens tested in this research due to the higher concrete strength.

With the objective to obtain a correlation of creep strain between the two specimen sizes, a linear regression analysis was conducted. Figure 5.3 shows the creep strain of 100mmØ specimen with corresponding strain for 150mmØ. The linear correlation obtained based on the graph plotting is presented in Table 5.2. It is observed that all the findings by standard codes and experimental work agree that 100mmØ specimen exhibit higher strain value. This is shown in Table 5.2 as the gradient for all linear correlations is more than 1.0 and the correlated ratio of 100mmØ to 150mmØ cylinder strain are scattered above the reference line being more inclined to the 100mmØ axis in Figure 5.3. The correlation from the standard codes and experiment are within the same range and this result is useful in determining the strain value of 150mmØ cylinder when 100mmØ specimen is tested.

As the main emphasis of this research is to assess the effect of tropical environment on time-dependent deformation of concrete, specimen size is not a critical parameter as long as it is kept constant throughout the study for relative comparison and specimen size is accounted for in the analysis of results. In view of the consistent manner of the results from this study, it is concluded that a reduction in specimen size for creep test is acceptable and the 100mmØ cylinder is appropriate to replace the 150mmØ specimens. Moreover, this reduction in the size is within the limitation allowed in ASTM C192-90a for nominal maximum coarse aggregate of 20 mm. A reduction of 55.5% in materials could be achieved when the specimen size is reduced. Moreover, the rig capacity for small specimen also can be reduced about half of the bigger specimen capacity.

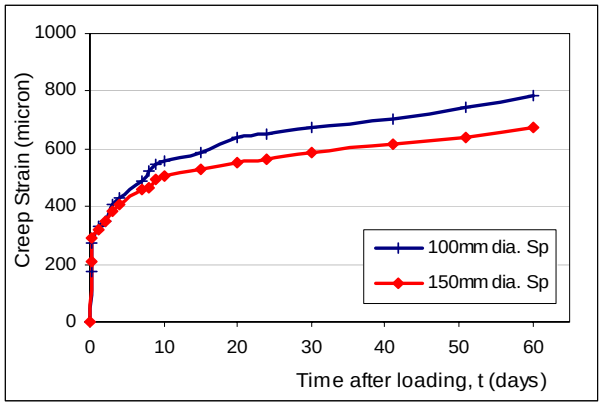

Figure 5.1: Creep strain of 100mmØ and 150mmØ specimens

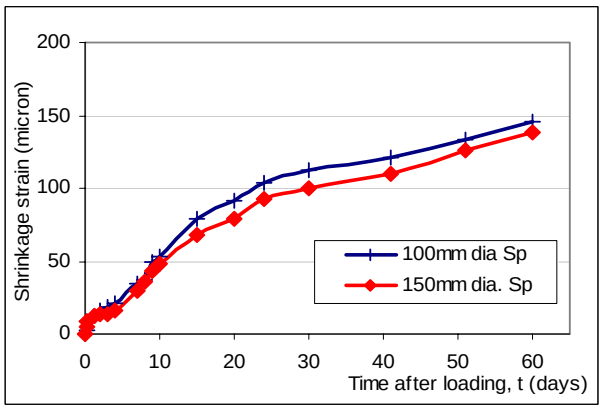

Figure 5.2: Shrinkage of control specimens for 100mmØ and 150mmØ cylinders

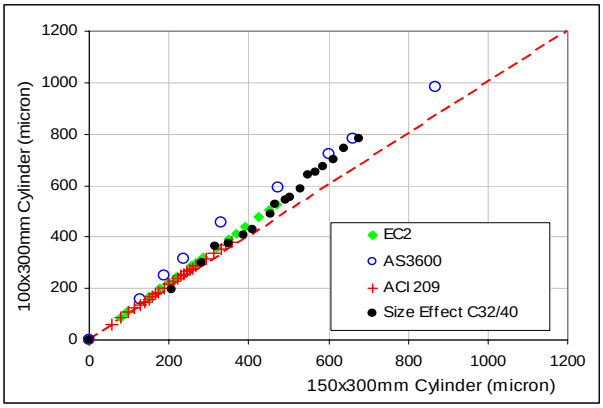

Figure 5.3: Correlation of creep strain between 100mmØ and 150mmØ cylinders by various codes and experimental findings

Table 5.2: Correlation of creep strain between 100mmØ and 150mmØ specimen

Experiments/Codes Recommendation	**Correlation**
Eurocode 2	$\varepsilon_{100} = 1.12\ \varepsilon_{150} + 0.74$
AS 3600	$\varepsilon_{100} = 1.13\ \varepsilon_{150} + 32.86$
ACI 209	$\varepsilon_{100} = 1.07\ \varepsilon_{150}$
Experiment C32/40	$\varepsilon_{100} = 1.19\ \varepsilon_{150} - 35.02$

5.2 Results of Material Testing

5.2.1 Results of Coarse Aggregate Properties

The result of sieve analysis for coarse aggregate with maximum nominal size 20mm is shown in Table 5.3. It is observed that the size distribution of the coarse aggregate is within the size distribution envelope. The grading of the coarse aggregate is according to the specification in BS 3797 (1990). The specific gravity of the coarse aggregate obtained from test was 2.66.

Table 5.3: Sieve analysis for coarse aggregate

Sieve Size	Weight retained (g)	Weight passing (g)	Percentage of retained (%)	Percentage of passing (%)
37.5 mm	0	4000	0	100
20 mm	523	3477	13.1	86.9
10 mm	3077	400	90.0	10.0
5 mm	276	124	96.9	3.1
Pan	122	2	99.95	0.05
Total	3998			

Percentage of loss during sieve = 0.05%

5.2.2 Results of Fine Aggregate Properties

Result of the sieve analysis for fine aggregate is shown in Table 5.4. The fine aggregate is categorised as Grade M and it meets the requirements as prescribed in BS 882 (1992).

Table 5.4: Sieve analysis for fine aggregate

Sieve Size	Weight of retained aggregate (g)	Weight of passing aggregate (g)	Percentage of retained aggregate (%)	Percentage of passing aggregate (%)
5 mm	8	492	1.6	98.4
2.36 mm	62	430	14.0	86.0
1.18 mm	105	325	35.0	65.0
600 μm	90	235	53.0	47.0
300 μm	79	156	68.8	31.2
150 μm	88	68	86.4	13.6
Pan	62	6	98.8	1.2
Total	494			

Percentage of loss during sieve = 1.2%

5.2.3 Results of Prestressing Strands Properties

A summary of tensile properties results for the five prestressing tendon specimens tested is presented in Table 5.5. The strands were tested to failure and the average breaking load from the five samples is 109.7kN with standard deviation of 0.59. Based on this result, the tendon tensile property is considered consistent. The strand elongation recorded at every 12.7kN interval during the process of pretensioning is presented in Table 5.6. The elongation obtained through the experiment is compared to the theoretically calculated values. It is observed that the result obtained from the experiment is slightly lower than the theoretical values. The percentage of difference is within the range of 0% to 4.7% as shown in Table 5.6 and the differences are within an acceptable range.

Table 5.5: Results of tensile properties of prestressing strands

Samples	Breaking Load (kN)	Maximum Stress (N/mm^2)	Maximum Extension before failure (mm)
Strand 01	109.42	1989.5	33.2
Strand 02	108.83	1978.7	30.8
Strand 03	110.23	2004.1	32.4
Strand 04	109.66	1993.8	33.7
Strand 05	110.25	2004.5	30.2

Table 5.6: Prestressing strand elongation during pre-tensioning

Pressure (psi)	Force (kN)	Theoretical Elongation (mm)	Experimental Elongation (mm)	Difference (%)
500	12.7	15	14.3	4.7
1000	25.4	30	30	0.0
1500	38.1	45.02	44.5	1.2
2000	50.8	60.04	59.5	0.9
2500	63.5	75.05	72	4.1
3000	76.2	90.05	87.5	2.8

5.3 Results of Concrete Mechanical Properties

The results of concrete properties for concrete batches A1, A2 and A3 are summarised in Table 5.7 and for concrete B1, B2, B3 and D1, the results are summarised in Table 5.8. The concrete properties reported in Table 5.7 and Table 5.8 comprises of properties of fresh concrete as well as the mechanical properties such as ultimate compressive strength, modulus of elasticity, Poisson's ratio, density and porosity content. As the same concrete mixture was used for both concrete batches A and B according to the concrete strength, properties such as modulus of elasticity, Poisson's ratio and porosity were only conducted in Batch A. The results for Batch B are considered to be similar as Batch A. Based on the concrete mechanical properties results, it is concluded that the designed concrete mixes with slagcement, inclusion of silica fume and superplasticiser are effective in achieving good workability and designed high strength.

In order to assess the consistency of the laboratory results recorded, statistical analysis consisting of standard deviation, s_d is carried out. The standard deviation calculation as shown by Equation (5.1) represents the spread of the concrete properties results around the mean value. If the data measured is close to the mean value, the standard deviation is small.

$$s_d = \sqrt{\sum \frac{(x - x')^2}{n - 1}} \tag{5.1}$$

where

x = individual measured data

x' = mean measured data

n = number of data points

Table 5.7: Concrete physical and mechanical properties for Batches A1, A2 and A3

Concrete Batch	Compressive Strength (N/mm^2)						Modulus of elasticity (kN)		Poisson's Ratio		Porosity (%)		Density (kg/m^3)	Slump (mm)
	150 Cube		Cylinder 150		Cylinder 100									
	7d	28d	7d	28d	7d	28d	7d	28d	7d	28d	7d	28d		
A1 - C40/50	**47.2**	**58.6**	**33.8**	**41.1**	**34.9**	**45.2**	**30.0**	**34.9**	**0.18**	**0.20**	**10.76**	**10.53**	**2392**	**55**
s_d	*(1.0)*	*(0.9)*	*(1.8)*	*(2.3)*	*(1.6)*	*(2.4)*	*(0.4)*	*(0.3)*						
A2 - C50/60	**54.3**	**62.5**	**40.3**	**52.3**	**41.0**	**52.1**	**32.7**	**35.7**	**0.18**	**0.18**	**9.26**	**9.79**	**2399**	**22**
s_d	*(2.4)*	*(4.4)*	*(4.9)*	*(4.2)*	*(2.9)*	*(2.5)*	*(1.0)*	*(0.5)*						
A3 – C65/80	**65.1**	**78.8**	**47.6**	**54.7**	**48.3**	**62.6**	**35.0**	**38.3**	**0.19**	**0.19**	**9.67**	**9.29**	**2433**	**225**
s_d	*(1.1)*	*(0.9)*	*(1.5)*	*(4.1)*	*(2.9)*	*(2.4)*	*(1.2)*	*(0.3)*						

Note: A1, A2 and A3 are concrete batches tested for creep and shrinkage on standard size specimens

s_d = Standard Deviation

Table 5.8: Concrete physical and mechanical properties for Batches B1, B2, B3 and D1

Concrete Batch	Compressive Strength (N/mm^2)						Modulus of elasticity (kN)	Slump (mm)
	150 Cube			Cylinder 100				
	7d	**28d**	**56d**	**7d**	**28d**	**56d**	**28d**	
B1 C40/50	**45.5**	**55.0**	-	**29.0**	**28.4**	-	-	**60**
s_d	*(2.3)*	*(2.2)*		*(1.4)*	*(3.4)*			
B2 C65/80	**65.1**	**75.8**	**84.4**	**44.4**	**47.0**	**61.4**	-	**200**
s_d	*(2.9)*	*(3.8)*	*(2.5)*	*(1.4)*	*(1.0)*	*(3.6)*		
B3 C65/80	**66.5**	**80.6**	-	**45.7**	**53.3**	-	-	**130**
s_d	*(1.3)*	*(1.2)*		*(4.6)*	*(3.5)*			
D1 C40/50	**47.3**	**59.1**	-	-	**43.9**	-	**35.0**	**115**
s_d	*(1.6)*	*(0.8)*			*(2.1)*		*(1.8)*	

Note: B1 and B2 are concrete batches prepared for columns tested in the laboratory

B3 is the concrete batch prepared for pre-tensioned prestressed beams tested in the laboratory

D1 is the concrete batch prepared for post-tensioned prestressed beams tested on site

s_d = Standard Deviation

5.3.1 Compressive Strength

As it was mentioned earlier, the compressive strength results for batches A1, A2 and A3 and batches B1, B2, B3 and D1 are presented in Table 5.7 and Table 5.8, respectively. Three different specimen sizes were tested for compressive strength. The cube strength was the main compressive strength referred to in this study as it was tested for all the different concrete batches studied. The standard deviation for each batch of concrete is also presented in Table 5.7 and Table 5.8.

Superplasticizers and retarders are two common inclusions in concrete mix used in the industrial practice. Both admixtures are invariably added to reduce mixing water content, produce good workability and delay the setting time of concrete. Therefore, the high strength for concrete samples was achieved through lower water content and also with the addition of silica fume (SF). The increase in strength as a result of utilizing SF in the mix can be attributed to the formation of new tobermorite gel as a result of the secondary hydration between the calcium hydroxide and silica at room temperature (Marzouk, 1991).

Generally, the targeted cube compressive strength for each batch of concrete was achieved, except for concrete C65/80 of batches A3 and B2. The cube strength result for batch A3 and B2 are at 78.8N/mm^2 and 72N/mm^2, respectively. However, the strength achieved for these two batches of concrete of C65/80 is within the high strength range and is acceptable for creep and shrinkage testing. The lower compressive strength result can be explained through the use of slag cement which is known to cause a slower rate of strength gain. As the concrete strength increase higher, more cement content is required and the effect of slower strength gain is more apparent; which was the case for concrete class C65/80. Concrete batch B2 was checked for cube compressive strength at the age of 56 days and the result was at 84.4 N/mm^2, achieving the targeted strength.

On average, the 7 to 28 days strength ratio obtained in this study is within the range of 0.77 to 0.90. This shows that the development of strength within the first 7 days was higher as compared to the general recommendation of 0.67 (Neville, 1981).

This can be attributed to the higher curing temperature in the tropical climate that causes rapid initial hydration process.

5.3.1.1 Cylinder-cube Strength Conversion Factor

Compressive strength of concrete changes based on specimen sizes and shapes due to its fracture characteristics (Yi et al., 2006). EC 2 specifies concrete strengths in cylinder and caters to design of high strength concrete up to maximum characteristic cylinder strength of 90N/mm^2. In order to facilitate the designers, EC 2 also provides equivalent cube strength besides the cylinder strength. However the suitability of the relationship is questionable as studies have shown that apparently different investigations resulted in different conversion. A general cylinder to cube strength conversion factor is usually taken to be 0.8 for normal strength concrete (Narayanan, 1994). This ratio however does not remain constant for all concrete strength as the influence of specimen shape decrease with higher concrete strength (Neville, 1981). As the cube-cylinder strength conversion factor has not be established, assessment on the relationship between cube and cylinder strength is necessary. This is to provide a better reference for the research as the current local practice is still referring to cube strength while the EC 2 specifies concrete in cylinder strength.

The variation of cylinder-cube ratio for HSC with respect to the compressive cube strength obtained from this study and findings by other existing literatures (Yi, et al., 2006; Rashid et al., 2002; L'Hermite, 1960; Neville, 1981) and EC 2 is shown in Figure 5.5. In general, it is observed that the experiment result for 100mmØ is comparable to the relationship given in EC 2. A slight increment in the cylinder-cube strength ratio with the increase of concrete strength is observed. It should be noted that it is not uncommon for different studies reported different conversion ratios for each concrete strength class.

The result of the 28 day cylinder-cube strength conversion ratio for concrete batches A is presented in Table 5.9. The average 28-day 150mmØ cylinder to cube strength ratio obtained is between 0.69 and 0.84. The compressive strength for

100mmØ cylinders appear to be more consistent as the average 28-day cylinder to cube strength ratio is within the range of 0.77 to 0.83. Based on Table 5.9, it is observed that the compressive strength of 150mmØ cylinder for batch A1 (C40/50) and A3 (C65/80) were lower than expected. Even though the cube specimens for the two batches achieved the targeted strength, the 150mmØ cylinders failed to achieve the targeted strength due to honeycombing in the specimens. The reason may be due to the fact that the 150mmØ cylinders were the last to be cast during concrete casting and each batch of casting involved of a big number of cube and cylinder specimens. As retarder was not included in the concrete mix, the concrete has started to harden with properties changed during casting of 150mmØ cylinders and this lead to improper compaction of specimens. This also explains the higher standard deviation for 150mmØ cylinders.

The range of cylinder-cube strength conversion for each concrete strength class obtained from the various literatures in Figure 5.4 is also summarised in Table 5.9. A wider range of difference is observed for concrete C40/50. A conversion to cylinder strength from 50N/mm^2 cube strength using the lowest and highest conversion ratio in Table 5.9 will result in 40N/mm^2 and 48N/mm^2, respectively. The differences are significant and may cause a major dispute during the construction process. This variability of results is believed to be due to the differences in materials and environment, mix proportions and the casting method between different experimental set-ups. The scatter also reveals that research conducted thus far have yet to agree on a specific conversion ratio for each concrete strength class. As this topic is not within the scope of this research, no further studies were conducted. Therefore base reference is made to the recommendation by EC2 since it is the most recently developed code which is to be adopted in the local industry. Subsequently reference is made to the experimental results obtained from the compressive strength test.

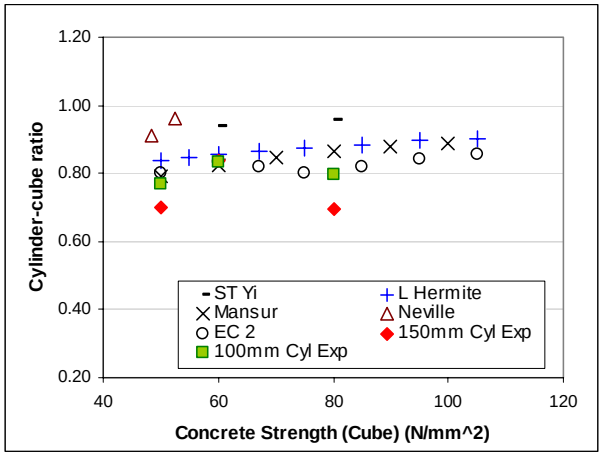

Figure 5.4: Cylinder-cube strength ratio from experiment and other investigations

Table 5.9: Cylinder-cube strength ratio from experiment and other investigations

Concrete strength class	150mmØ cylinder-cube ratio	100mmØ cylinder-cube ratio	Cylinder-cube ratio range by other investigations*
C40/50	0.70	0.77	0.80 – 0.96
C50/60	0.84	0.83	0.82 – 0.94
C70/80	0.69	0.80	0.87 – 0.96

**Note: Yi, et al., 2006; Rashid et al., 2002; L'Hermite, 1960; Neville, 1981 and EC 2*

5.3.2 Modulus of Elasticity

The results of modulus of elasticity for the three concrete strength classes are presented in Table 5.7. The modulus of elasticity test was conducted on concrete batches A1, A2 and A3 for both 7 and 28 days. As the materials and mix proportion for concrete batches A and B are the same for the same concrete class, the elastic property result is applicable to concrete batch B1, B2 and B3. The modulus of elasticity for concrete batch D on the other hand was tested only at the age of 28 days because the creep and shrinkage test for this particular batch was only tested at 28 days.

In general, it is reported that the main factor affecting the modulus of elasticity of concrete is the properties and volume of aggregate in the concrete mix. The increase in concrete strength also increases the modulus of elasticity. As the same type and size of aggregate was used throughout this study, the increase in the modulus of elasticity as the concrete class increases is due to concrete strength and higher aggregate volume. The effect of concrete strength on modulus of elasticity is clearly shown as higher elastic modulus is observed at the age of 28 days as compared to 7 days for the same batch of concrete. The modulus of elasticity is 10% to 15% higher at the age of 28 days. The increase in modulus of elasticity however, is progressively lower than the increase in compressive strength.

The standard deviation for modulus of elasticity ranges from 0.43 to 1.54, depending on the concrete batches. Similar to the results of compressive strength, it is observed that concrete C50/60 gives the highest standard deviation at both 7 and 28 days. Concrete C40/50 has proven to be the most consistent batch among the three with the lowest standard deviation. The values of modulus of elasticity obtained from test and the recommendation by other standard codes for concrete of different strength class is presented in Table 5.10. The values by B3 Model are with reference to ACI, which explains the same value provided by both models. The relationship between modulus of elasticity and compressive cylinder strength at the age of testing is plotted in Figure 5.5. It is clearly seen that the experimental results are within the range recommended by the standard codes investigated. Comparatively, ACI provides the lowest recommendation values for modulus of elasticity.

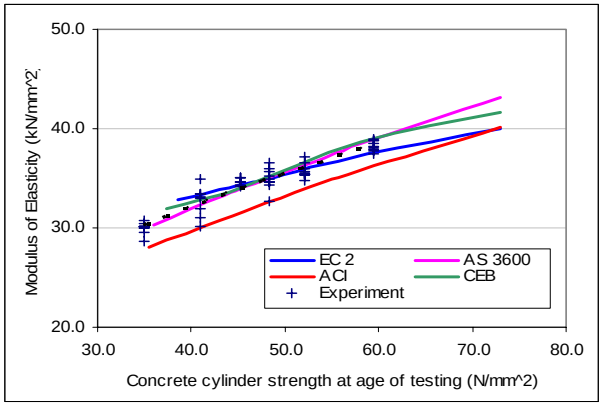

Figure 5.5: Relationship between modulus of elasticity and cylinder strength based on experimental results and standard codes

Table 5.10: Comparison of modulus of elasticity provided by standard codes and results from experiment

Concrete Class	C40/50		C50/60		C65/80	
	7 days	28 days	7 days	28 days	7 days	28 days
Experiment	30.2	34.7	32.7	35.7	35.0	38.3
EC 2	32.8	35.0	34.7	37.0	37.5	40.0
CEB-FIP	32.0	36.3	34.1	38.6	36.8	41.7
ACI	28.0	32.6	30.8	35.8	34.6	40.2
B3 Model	28.0	32.6	30.8	35.8	34.6	40.2
AS 3600	30.3	35.0	33.3	38.5	37.4	43.1

5.3.3 Poisson's Ratio

The results of Poisson's ratio tested on concrete batches A1, A2 and A3 are presented in Table 5.7. This ratio between the lateral strain and the strain in the direction of loading obtained from the test is within the range of 0.177 and 0.200. In Eurocode 2, the recommended Poisson's ratio for uncracked concrete is 0.200. The lower ratio obtained from the experiment is mainly due to high strength concrete tested in this study. There is no reliable information on the variation in Poisson's ratio with age or other properties of concrete. However, studies have proven that the ratio is lower in higher strength concrete (Brooks and Hynes 1993; Persson, 1999).

5.3.4 Porosity

Time-dependent deformation of concrete is highly related to its pore structure and total porosity. The percentage of porosity for concrete at 7 and 28 days are presented in Table 5.7 and values are also plotted in Figure 5.6 for a clearer illustration of the results. A comparison of the porosity results from this study to the results of the same test conducted in the University of Leeds by Mahir (1997) is also

presented in Figure 5.6. The comparison shows that the percentage of porosity from this study is in agreement with the trend obtained on concrete with water-cement ratio of 0.55 and cube strength of 55N/mm^2 at 28 days tested by Mahir (1997).

The percentage of porosity of concrete mainly depends on the water-cement ratio of the mix and also the degree of cement hydration. At higher age of testing and higher concrete strength, the percentage of porosity is lower due higher degree of hydration. This pattern is observed in the results as shown in Figure 5.6. However the porosity percentage for concrete C50/60 tested at the age of 7 days is lower than 28 days by 0.28%. This occurrence may be the explained with reference to the slump results, as shown in Table 5.7. The slump for C50/60 was at 22mm, the lowest among all the mixes. The lower slump may indicate that the water-cement ratio was sufficient to achieve a high degree of hydration with little excess water left and less capillary pores (Neville, 1990). As a result, the lower porosity content affects the creep strain deformation and this is discussed in the next chapter.

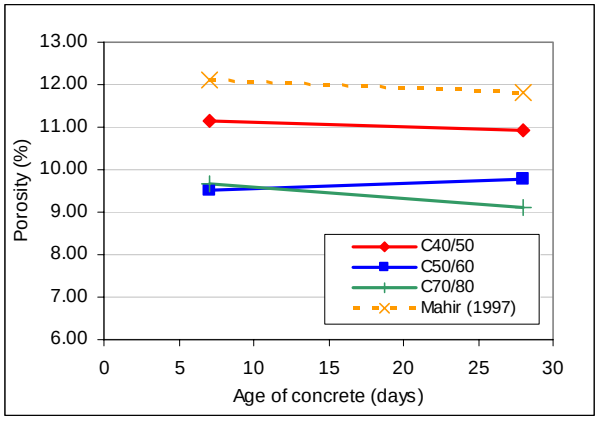

Figure 5.6: Concrete porosity from experiment results and comparison to results by Mahir (1997)

5.4 Summary on Preliminary Test and Concrete Properties Results

1. A reduction in specimen size from 150mmØ cylinder to 100mmØ cylinder for creep testing is adopted based on the consistent correlation results

obtained and also due to the practical and economical advantages. In addition, this reduction in specimen size is in compliance to ASTM C192-90a.

2. The overall concrete mechanical properties tested are within the designed range and the consistency of the results is also within good statistical range.

CHAPTER 6

RESULTS AND DISCUSSION ON CREEP AND SHRINKAGE

The results and analysis of investigation from creep and shrinkage test conducted on standard sized specimens tested under controlled and natural ambient condition are presented and discussed in this chapter. Besides the standard sized specimens, the time-dependent deformation of structural members tested in the laboratory and on site are also presented. In this chapter, assessment on the accuracy of standard codes recommendation to the time-dependent deformation of local concrete from this research is conducted using statistical analysis.

6.1 Temperature and Relative Humidity of Test Areas

As the influence of environment condition is one of the main parameters tested in this study, it is important to first determine the condition of test surrounding before analysing the results of concrete deformation. The temperature and relative humidity (RH) of the controlled room and the natural ambient test area for creep and shrinkage are shown in Figure 6.1 and 6.2, respectively. The RH of controlled room was kept at 50% with a variation within ±4%, as shown in Figure 6.1. This deviation is within the allowable range as stated in ASTM 512-87. As for the temperature, it was kept at 27^{o}C with a variation within the range of ±2^{o}C. On an average, the RH was at 49.9% whereas the average temperature of the controlled room was at 27.6^{o}C.

The average day time RH recorded for the test condition under natural ambient was at 65.9% whereas the temperature recorded was 28.6^{o}C. The result for the natural ambient test condition was recorded with a variation of ±15% of the average RH and ±3^{o}C of the average temperature condition, as shown in Figure 6.2. The vast difference is mainly due to the variation in the daily weather condition. Due to constrain in securing instruments outdoor, the condition for the natural ambient was recorded only during day time. It is worth noting that the natural ambient RH

recorded at the first 100 days shown in Figure 6.2 is erratic with higher RH due to the fact that it was during the rainy season in the month of January and February.

With reference to the Malaysian Meteorological Department, data recorded at the station in Senai, mean daily average temperature is 26^{o}C with RH of 86.7%. The mean monthly RH recorded is between 70% and 90%. It is also reported that the average daily maximum is in between 31 ^{o}C – 33 ^{o}C and average daily minimum is between 22 ^{o}C and 23.5 ^{o}C. (Malaysia Meteorological Department). The data obtained in the meteorological station in Senai best reflect the condition of the test surrounding as this station is the nearest to the laboratory testing site. Considering the fact that the ambient test area is sheltered, RH of 80% is adopted as the outdoor condition for tropical climate in this research.

Based on the data recorded for control condition and ambient testing environment, the average ambient temperature recorded is not significantly different from the control condition. This can be observed through Figure 6.3 when the condition of control and ambient are compared graphically. On an average, the difference in temperature between the control and ambient was 1.1^{o}C whereas the difference in RH was 30% when the RH for outdoor condition is taken as 80%. Hence the variation in the test results between ambient and control specimens were primarily due to the difference in the relative humidity.

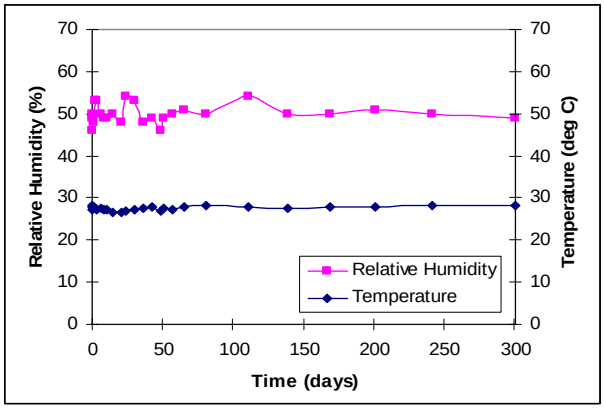

Figure 6.1: Temperature and relative humidity of controlled room

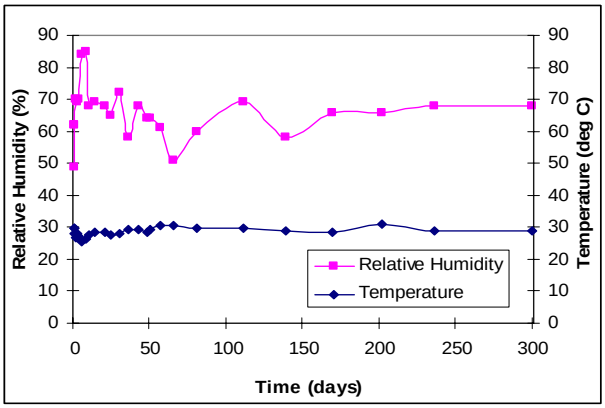

Figure 6.2: Temperature and relative humidity of test condition in natural ambient

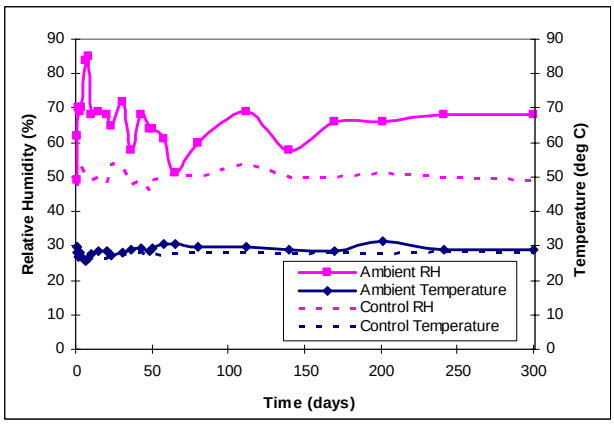

Figure 6.3: Comparison of temperature and relative humidity of control and ambient condition

6.2 Creep of Concrete

The results of creep of high strength concrete (HSC) loaded at the age of 7 and 28 days are discussed in this sub-chapter. The creep measurement comprising of total deformation values, strain of control specimens, and record of ambient temperature and RH for different concrete strength tested at age 7 days are given in Appendix D1. For concrete tested at age 28 days, the creep results are recorded in Appendix D2. The presentation of results is in creep coefficient, defined as creep strain to a fraction of the elastic strain. For creep coefficient, the effect of concrete stiffness is included by the means of initial strain. Thus the results of deformation with the inclusion of elasticity factor for different concrete strength are more

consistent as compared to specific creep. The creep coefficient results calculated is also included in Appendix D1 and D2.

Figure 6.4 and Figure 6.5 presents the result of creep coefficient of concrete loaded at the age of 7 days and 28 days, respectively. The results are based on a record of concrete specimens loaded for duration of 300 days. The slight scatter in the data observed instead of a smooth creep curve may be due to the influence of ambient as well as instrumentation variations. The magnitude of creep coefficient for the three concrete strengths studied is clearly plotted in the graphs. The deformation pattern in Figure 6.4 and 6.5 are not displayed as a smooth curve as a smooth pattern is only attainable upon formulation of creep prediction equation, which will be developed in Chapter 7. For both concrete tested at 7 days and 28 days, it is observed that the creep coefficient is lower as concrete strength increases for specimens tested in the controlled room. This pattern can be explained as higher strength concrete has lower water-cement ratio in the mix design. Thus fewer pores exist in the mature cement and this subsequently increases the rigidity of the solid matrix, decreasing the creep deformation (Smadi, 1987). The creep strain result obtained is in agreement with the trends obtained by other work conducted on concrete time-dependent deformation (Marzouk, 1991).

As for the concrete tested under natural ambient condition, the creep coefficient is the lowest as shown in Figure 6.4. Direct comparison to the C65/80 specimens tested under controlled condition also reveals that the ambient specimens exhibit lower strain. The concrete strain tested under natural ambient condition is approximately 10% to 30% lower than the controlled specimens, depending on the age after loading. The range in the percentage of deviation difference is attributed to the heteroscedacity behaviour of shrinkage and creep data. As explained by Bazant (1987), the spread of data is greater at the early age of deformation for percentage of deviation in the results calculated. This explains the range in percentage of difference in the comparison between different set of concrete.

Creep coefficient for ambient stored C65/80 specimens and the corresponding relative humidity is plotted in Figure 6.6 to show the influence of RH to the time-deformation of concrete. Through Figure 6.6, it is observed that under the condition

of higher RH, lower creep strain is obtained. Based on the temperature and relative humidity record, the results obtained are satisfactory to simulate the actual deformation for tropical concrete even though the specimens were not kept under direct effect of weather.

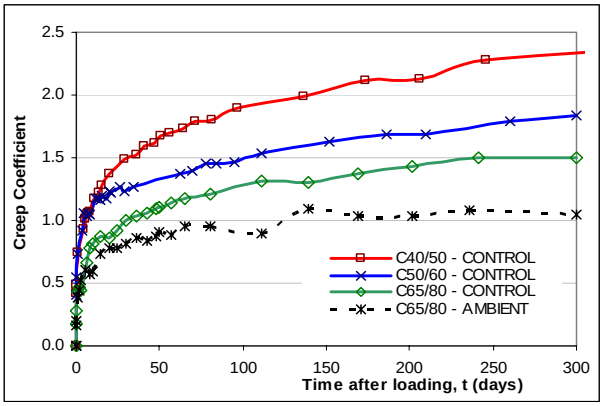

Figure 6.4: Creep coefficient for age at loading at 7 days

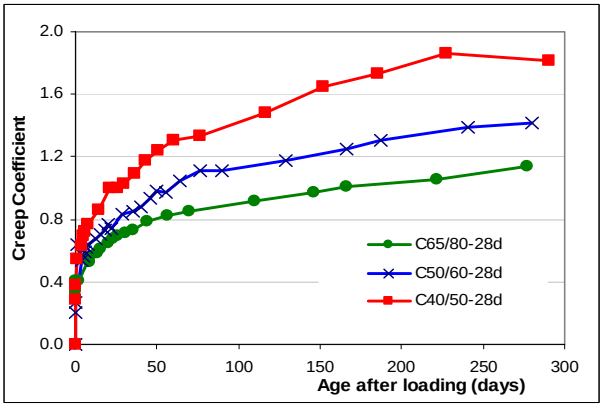

Figure 6.5: Creep coefficient for age at loading at 28 days

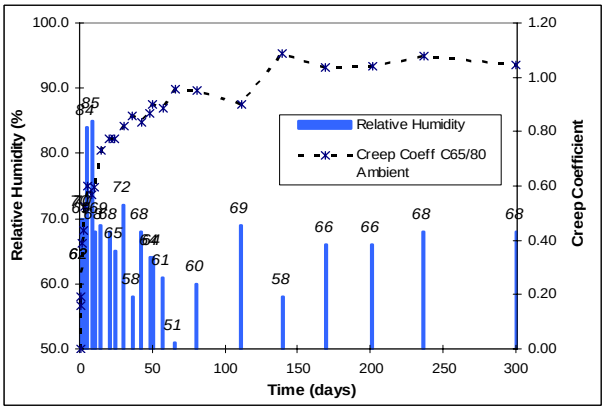

Figure 6.6: Creep coefficient for C65/80 with corresponding relative humidity for specimens tested under ambient condition

For creep behaviour which is time-dependent, the rate of creep is inversely proportional to time. Thus the creep coefficient can be expressed as a linear function of the logarithm of time (Neville et al., 1983). The translation into logarithmic graph provides a clearer comparison and analysis of the creep results as the gradient of the logarithmic graph indicates the rate of creep deformation. The intercept of log Y-axis represents the deformation constant which controls the magnitude of the deformation.

Figure 6.7 and 6.8 show the creep coefficient for concrete tested at age 7 days and 28 days, respectively expressed as a log creep coefficient versus log time graph. As mentioned above, the gradient of the log creep graph represents the rate of creep deformation. In Figure 6.7, it is observed that the rate of creep deformation for ambient specimens is lower compared to the controlled specimens, as shown by the gradient. This is due to the fact that under higher temperature, the initial strength gain of concrete is faster through the formation of tobormorite gel. In addition to that, higher moisture content in the ambient also causes lower rate of diffusion of water into the surrounding, subsequently lowering the magnitude of drying creep (Acker and Ulm, 2001). It is also noted that the gradient for concrete C50/60 is the lowest, indicating a lower rate of creep deformation as compared to the other concrete batches tested. This can be explained through the lowest porosity content of 9.26% for this batch of concrete at the age of 7 days, as reported in Chapter 5. In Figure 6.8, the lowest gradient is exhibited by concrete C65/80. Similarly this trend is explained through the porosity results. The porosity content for concrete C65/80 loaded at 28 days is the lowest at 9.29% as compared to the other concrete batches.

As stated earlier, the Y-intercept in the logarithmic plotting represents the magnitude of deformation. Thus in both Figure 6.7 and 6.8, the magnitude of Y-intercept values is higher for lower concrete strength, following the pattern of creep coefficient. Generally the consistency of the graph plotting to the equations is within a consistent range, having the Pearson residuals squared, R^2 between 0.95 and 0.99, as analysed through the Excel software.

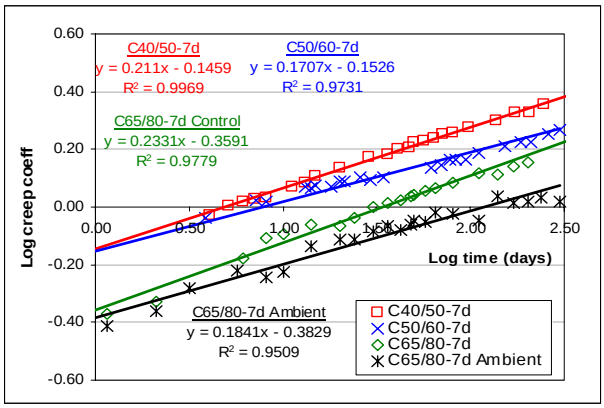

Figure 6.7: Log creep coefficient vs. log time after loading for concrete loaded at age 7 days

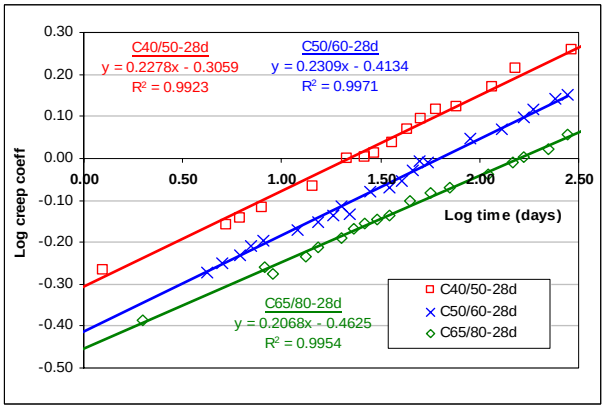

Figure 6.8: Log creep coefficient vs. log time after loading for concrete loaded at age 28 days

6.2.1 Statistical Analysis of Creep Results

The experimental results obtained for creep and shrinkage are statistically analysed. This step is important in order to establish the accuracy and consistency of the data collected and to verify the reliability of experimental results obtained in this study. The experimental creep results assessed are on the data of total deformation value and the controlled specimens strain collected in the laboratory testing.

The standard deviation is a statistical measure of variance from the mean, representing the dispersion of data from the mean value and the result is more precise with smaller values. Computation for standard deviation is based on Equation (5.1),

as discussed in Chapter 5. The coefficient of variation, *V* represents the ratio of the standard deviation to the average of the set of data, indicating the variability around the mean and is presented as Equation (6.1). The coefficient of variation is usually presented in percentage form.

$$s_d = \sqrt{\sum \frac{(x-\bar{x})^2}{n-1}} \tag{5.1}$$

$$V = \frac{1}{\bar{x}} \sqrt{\sum \frac{(x-\bar{x})^2}{n-1}} \tag{6.1}$$

where

x = individual measured data

$\bar{x}$ = mean measured data

n = number of data points

The standard deviation and coefficient of variation for concrete creep results are summarised and presented in Table 6.4 for concrete tested at 7 days and in Table 6.5 for concrete tested at 28 days. The standard deviation and coefficient of variation of creep is assessed on total strain measured directly from the specimens to prevent deviation to the statistical accuracy upon conversion to creep coefficient. In addition to that, statistical assessment in strain will also enable direct comparison to the standard deviation of shrinkage strain.

With reference to Table 6.1 and 6.2, it is observed that the standard deviation is proportionally higher under the cases when the magnitudes obtained from experimental results are higher. This is observed for both 7 and 28 days specimens whereby the total deformation leads to higher standard deviation of more than 100×10^{-6} as compared to the control specimens with standard deviation less than 40×10^{-6}. The higher deviation is also observed for concrete with lower strength as the total time-dependent strain is higher at lower concrete strength.

The coefficient of variation is a good indication of consistency in the results collected due to the fact that it is presented in percentage to capture the extent of deviation. The pattern of coefficient of variation is noted to be in line to the standard deviation, lower value for relatively smaller standard deviation. This trend of results is consistently observed for concrete tested at both 7 days and 28 days, except for the set of specimens tested under ambient condition. The analysis demonstrated that the coefficient of variation for ambient stored specimens is the highest even though the standard deviation is small. The lower value for standard deviation is due to the fact that the magnitude of data collected under ambient condition is low. The higher coefficient of variation can be explained due to the fact that the specimens were subjected to the fluctuation in temperature and ambient RH, as shown in Figure 6.2.

The coefficient of variation for laboratory measured shrinkage under stringent control in a statistically significant investigation conducted by Bazant (1987) was approximately 8%. This magnitude of coefficient of variation may be used as a benchmark for the statistical assessment on a single mixture of concrete. Based on Table 6.1 and 6.2, the average coefficient of variation for this research is at 13.9% for creep and the 18.2% for control specimens. In the laboratory work, creep and control specimens results were obtained from an average of 12 numbers of data collected for each set of concrete. Due to the small magnitude of strain measurement, the reading of data from the comparator is very sensitive, which may contribute to variation in data collection. In addition to that, the heterogeneous condition of concrete also contributed to the wider range of strain results. Accuracy of the measuring devices and defective measuring studs are also a factor for the deviation in results. Considering the coefficient of variation from this experiment is less than 20%, the results obtained are within an acceptable range.

Table 6.1: Standard deviation, s_d and coefficient of variation, V of creep specimens tested at 7 days

Concrete Batch	Creep specimens		Control specimens	
	s_d (x10^{-6})	V (%)	s_d (x10^{-6})	V (%)
C40/50 (7 days)	194.4	14.6	36.2	17.4
C50/60 (7 days)	141.5	11.6	29.0	16.4
C65/80 (7 days)	129.6	10.9	25.4	14.6
C65/80 (Ambient)	135.3	16.1	12.7	37.9
Average	150.2	13.3	25.8	21.6

Table 6.2: Standard deviation, s_d and coefficient of variation, V of creep specimens tested at 28 days

Concrete Batch	Creep specimens		Control specimens	
	s_d (x10^{-6})	V (%)	s_d (x10^{-6})	V (%)
C40/50 (28 days)	189.7	16.0	26.7	16.0
C50/60 (28 days)	169.8	14.3	22.9	15.3
C65/80 (28 days)	162.0	13.3	20.1	13.1
Average	173.8	14.5	23.2	14.8

6.3 Shrinkage of Concrete

Shrinkage of the concrete measured from the experimental work is presented in the form of shrinkage strain. The strain result is referring to drying shrinkage as the deformation for autogenous shrinkage is not considered in this study. The autogenous shrinkage is not taken into consideration because the initial shrinkage reading was taken after specimen curing and most of the hydration processes which causes autogenous shrinkage would have already occurred. Appendix D3 and D4 provide the data for concrete shrinkage strain tested at age 7 days and 28 days, respectively.

Figure 6.9 and 6.10 refer to the shrinkage strain for specimens exposed to drying at the age of 7 and 28 days, respectively. With reference to the graphs, the shrinkage strain of different concrete strength follow the trend with higher strain for lower concrete strength. The mechanism of shrinkage in concrete is different from creep phenomena. As it is well known, shrinkage mainly occurs in the cement paste and is mainly controlled by the volume of water in the concrete mix. At higher concrete strength, even though the cement content is higher, lower water content in the mix restricted the shrinkage through less water loss into the surrounding ambient. In addition to that, a stiffer matrix of material with higher density and lower pore content act as a restraint to the deformation of concrete with higher strength.

However the lowest strain in Figure 6.9 is observed to be C65/80 concrete specimens tested under ambient condition, simulating concrete under tropical environment. This proves that the influence of ambient RH is more definite as compared to the effect of concrete strength. At the age of 250 days, shrinkage strain for specimens stored under ambient condition is at 173 x 10^{-6} whereas under controlled condition is at 366 x 10^{-6}. On an average, the ambient stored concrete is 54% lower in strain for ambient stored concrete as compared to the controlled specimens. The difference was very apparent and this finding is important in the prediction of shrinkage for concreting work in the tropical countries.

As the variation between ambient and control condition was primarily the difference in the RH, the main factor for the lower shrinkage in the ambient is due to the influence in RH. The natural ambient RH which is higher resulted in less diffusion of moisture from the specimen to the surrounding. The prevailing conditions of warm and humid weather ensure a continuous supply of water into the pore structure of cement gel, thus reducing shrinkage strain. This phenomenon is clearly observed in Figure 6.11 where the shrinkage for C65/80 ambient stored specimens is plotted with corresponding ambient RH. Through Figure 6.11, it is observed that under the condition of higher RH, lower shrinkage strain is obtained. Based on the temperature and relative humidity record, the results obtained are satisfactory to simulate the actual deformation for tropical concrete even though the specimens were not kept directly under direct effect of weather. This finding agrees with the test results conducted by B. Barr, S.B. Hoseinian and M.A. Beygi who

conducted shrinkage testing on concrete stored in natural environment in Iran and also control environment of 23°C and 60% RH. The lowest shrinkage strain from the study occurred on specimens stored in the highest RH environment while the highest shrinkage occurred on specimens stored in lowest RH (Barr et al., 2003).

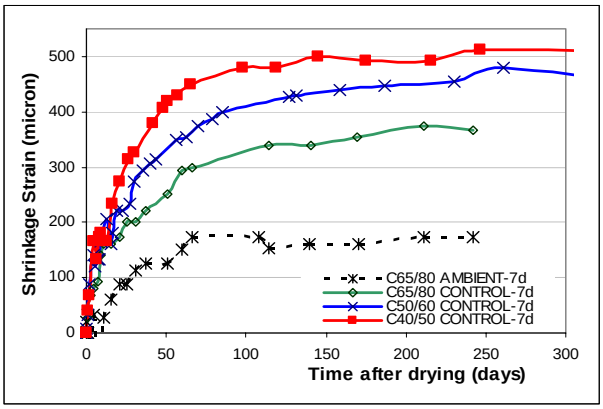

Figure 6.9: Shrinkage for concrete age at drying of 7 days

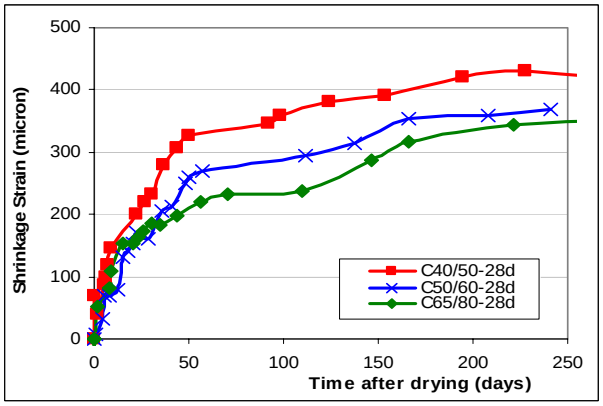

Figure 6.10: Shrinkage for concrete age at drying of 28 days

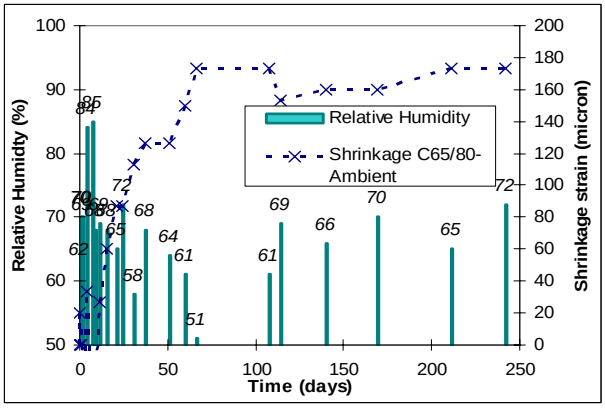

Figure 6.11: Shrinkage for concrete C65/80 with corresponding relative humidity for specimens tested under ambient condition

Shrinkage curves, which is time-dependent rise smoothly through the entire logarithmic time range (Bazant and Baweja, 2000). Thus similar to the creep analysis, the shrinkage strain can be plotted linearly in logarithmic graphs to provide clearer comparison and analysis. In Figure 6.12 and 6.13, the shrinkage results are plotted in logarithmic format to observe the divergence in the results. The gradient of the logarithmic plot represents the rate of shrinkage deformation whereas the Y-axis intercept represents the magnitude of the shrinkage deformation.

As predicted, the rate of shrinkage deformation for C65/80 concrete specimens stored under ambient condition is lower than the C65/80 specimens stored in the controlled room. This is observed through the lower gradient for the ambient specimens as plotted in Figure 6.12. Under the ambient condition, the RH is generally higher, thus lowering the rate of shrinkage strain in concrete, as opposed to the manipulated moisture movement under controlled room. Similar to the pattern for creep results, the lowest shrinkage rate for specimens tested at age 7 days occurred on C50/60 concrete. The lowest rate of deformation is attributed to the lowest porosity content for C50/60 concrete tested at age 7 days. In Figure 6.13, on logarithmic plot for shrinkage tested at age 28 days, the lowest rate of deformation occurred on C65/80 specimens due to the low porosity content in the concrete.

As it was explained earlier, the Y-axis intercept represents the deformation constant which control the magnitude of deformation. For both shrinkage testing at age 7 and 28 days, it is observed that the Y-intercept in the logarithmic plotting is higher with lower concrete strength, similar to the trend from shrinkage strain results. The consistency of the analysis is within a consistent range, having the Pearson residuals squared, R^2 within the range of 0.88 and 0.96, as analysed through the Excel software. However it is worth noting that creep results demonstrate better consistency than shrinkage strain as shrinkage is highly dependent on the influence of surrounding condition and is sensitive to the concrete composition.

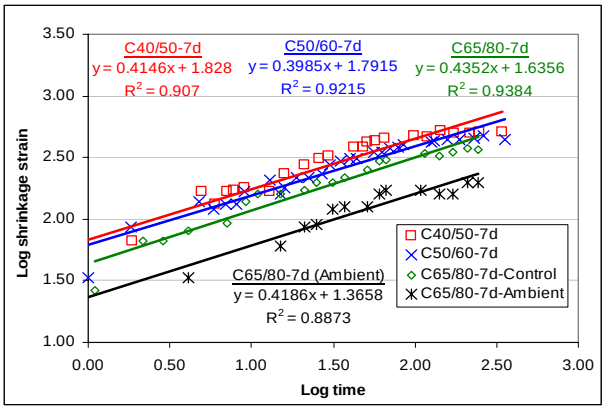

Figure 6.12: Log shrinkage vs. log time after drying for concrete tested at 7 days

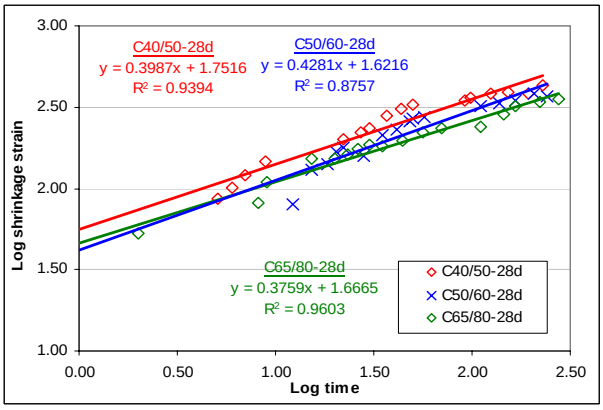

Figure 6.13: Log shrinkage vs. log time after drying for concrete tested at 28 days

6.3.1 Statistical Analysis of Shrinkage Results

Shrinkage results are further analysed statistically and presented through standard deviation and coefficient of variation. The statistical accuracy was assessed from an average of 3 axial shrinkage strain measured for each set of concrete tested. Table 6.3 and 6.4 presents the statistical analysis of shrinkage results.

Similar to the statistical results for creep, the standard deviation is proportionally higher under the cases when the magnitudes obtained from experimental results are higher. Based on Table 6.3 and 6.4, the standard deviation for 7 days shrinkage specimens are higher than for 28 days because the results of shrinkage for 7 days exhibit higher strain. The consistency in results for ambient specimens is similar to the results for creep, with the highest variation as the

specimens were exposed to natural ambient with fluctuating temperature and RH. Considering the fact that the coefficient of variation is less than 20%, the data measured is within the acceptable range of results.

Table 6.3: Standard deviation, s_d and coefficient of variation, V for shrinkage specimens tested at 7 days

Concrete Batch	**Shrinkage Specimens**	
	s_d **(x10^{-6})**	V **(%)**
C40/50 (7 days)	51.8	16.1
C50/60 (7 days)	50.1	15.7
C65/80 (7 days)	34.7	15.1
C65/80 (Ambient)	21.4	19.7
Average	39.5	16.7

Table 6.4: Standard deviation, s_d and coefficient of variation, V for shrinkage specimens tested at 28 days

Concrete Batch	**Shrinkage Specimens**	
	s_d **(x10^{-6})**	V **(%)**
C40/50 (28 days)	47.8	18.6
C50/60 (28 days)	25.7	15.3
C65/80 (28 days)	44.6	13.5
Average	39.4	15.8

6.4 Comparison of Experimental Results to Existing Prediction Models

Experimental work is the fundamental step towards a better prediction of time dependent deformation of high strength concrete in Malaysian climate and its application to structures. Comparison of creep and shrinkage value between the measured laboratory test data to prediction value by other prediction methods available will verify the accuracy of each prediction model to local concrete deformation. In addition, the comparison will also lead to establishing correction

factors and modification equations of the current standard code models for high strength concrete under local environment application. Modification factors are important in developing an accurate concrete time-dependent deformation prediction model for concrete structures in tropical climate.

The capabilities of five existing prediction models were first evaluated through graph plotting to determine the percentage of difference between the model predictions to experimental data. Subsequently, the accuracy and precision of each model were systematically assessed through statistical indicators to establish the best prediction model with regard to deformation of concrete in the tropical climate. The five prediction models assessed on creep and shrinkage prediction are from Eurocode 2, ACI 209 Code Model, B3 Model, CEB-FIP 1990 Code Model, and the Australian Standard 3600. The statistical indicators adopted are Residuals Analysis, Residuals Squared, Error Percentage and coefficient of variation.

The statistical analyses were assessed into two stages to determine the best prediction model available for local concrete. The first part consists of evaluation of experimental data through comparing the experimental results to the prediction values of the five models studied. Comparison of experimental data and model prediction were conducted through Residuals Analysis. Residual, *Re* is the difference between the experimental and model prediction values, as indicated in Equation (6.2). It identifies over-prediction or under-prediction of a particular model. Positive value of mean residual indicates over-prediction of a model whereas negative value indicates under-prediction. The result of this analysis however is limited to identifying if the prediction model is conservative or otherwise and does not distinguish the best model.

$$Re = c' - c \tag{6.2}$$

where

c = measured data from experimental work

c' = prediction value from calculation models

The second step of analysis involves the ranking of prediction model. Error Percentage Method, Residuals Squared analysis and coefficient of variation were

used to determine the best prediction model for local concrete. The Error Percentage, *E (%)* is obtained based on Equation (6.3) with the smallest error percentage indicating the best fit model. The Residuals Squared, Re^2 is obtained based on the summation of the residuals squared as shown in Equation (6.4). Residuals squared defines the precision of the prediction to experimental results. Therefore model with the smallest value is identified to be the best prediction model. This method is widely used for model accuracy and was also adopted by Townsend (2003) in his research.

$$E\,(\%) = \frac{\mathrm{Re}}{c}\,x\,100 \tag{6.3}$$

$$Re^2 = \sum\left[(\mathrm{Re})^2\right] \tag{6.4}$$

where

c = measured data from experiment

Re = residuals as identified in Equation (6.2)

Coefficient of variation is a common tool to gauge the accuracy of prediction models for creep and shrinkage (Fanourakis and Ballim, 2003; Bazant and Baweja, 2000; Lockman, 2004). Prediction models such as Eurocode 2, CEB-FIP 1990, B3 Model and AS 3600, benchmark the accuracy of the assumptions using coefficient of variation when compared to the RILEM Data Bank. It should be noted that the formulation of the coefficient of variation, V_m in assessing prediction accuracy differs from Equation (6.1). The coefficient of variation which was suggested by Muller and Hilsdorf (1990) is presented as Equation (6.5). V_m is calculated in six time ranges, from 0 to 10 days, 11 to 100 days, 101 to 365 days, 366 to 730 days, 731 to 1095 days, and above 1095 days. The final value is the coefficient of variation of the six interval values. The time ranges is essential considering the ascending magnitude in the creep and shrinkage strain with time. In this research, the coefficient of variation is captured in three interval ranges i.e. 0 to 10 days, 11 to 100 days, 101 to 365 days since the data collected is only up to 350 days,.

$$V_m = \sqrt{\frac{1}{N}\sum V_i^{\,2}} \tag{6.5}$$

where

V_i = coefficient of variation in a specific time range, i

$$= \frac{1}{\bar{c}}\sqrt{\sum \frac{(c-c')^2}{n-1}}$$

N = number of time range considered

c = individual measured data

c’ = predicted value to the corresponding measured data

$\bar{c}$ = mean measured data

n = number of data points

The combination of these three methods gives an overall ranking of the five prediction models studied. These statistical evaluations are applicable for both creep and shrinkage predictions.

6.4.1 Graphical Comparison on Creep Coefficient

The comparison of experimental results to codes recommendation is first assessed and explained through graphical presentation. The creep coefficient of experimental results and standard codes against the time after loading for concrete C40/50, C50/60 and C65/80, tested at the age of 7 days are plotted in Figure 6.14 (a) to (c), respectively. In Figure 6.14 (d), the comparison for creep coefficient of C65/80 specimens tested under ambient condition is presented.

The comparison of the codes prediction and experimental results for concrete tested at the age of 28 days are plotted in Figure 6.15 (a) to (c). Various codes provide different prediction results for creep coefficient, as shown in Figure 6.14 and Figure 6.15. The pattern of creep prediction by various codes is considerably similar for age of loading at 7 and 28 days as observed in Figure 6.14 and Figure 6.15. The difference in the recommendation by the various codes ranges up to 50%. Generally, AS 3600, CEB-FIP 90 and B3 Model provide the higher range in creep prediction whereas the ACI code provides the lowest prediction value. However, ACI prediction is the lowest only for concrete C40/50 and C50/60 because ACI does not

cater for concrete strength beyond C50/60. Therefore at C65/80, the prediction by ACI does not differ much from C50/60.

On an average for concrete loaded at the age of 7 days, the prediction by EC 2 is at 2% higher than the experimental results. The prediction by CEB and AS 3600 is higher than the experimental results within the range of 20% to 25% whereas the prediction by ACI for C40/50 and C50/60 is at 23% lower. For concrete loaded at the age of 28 days, the prediction by EC 2 is at 8% higher than the experimental results and the prediction by ACI is at 4% lower than the experimental results. As for CEB and AS 3600, the prediction by the three models is higher than the experimental results within the range of 28% to 35%. ACI refers to concrete slump as part of indicative parameter for concrete strength. However this parameter is no longer effective or accurate with the practice of addition of admixtures into the concrete mix that increases the slump for workability purposes. Therefore, in this analysis, the slump factor is taken out from the equation. The simple method in AS 3600 is only applicable for concrete up till $50N/mm^2$. This is because the basic creep factor provided caters up till $50N/mm^2$ and beyond that, the proposed basic creep factor stays constant at 2.0.

Through the comparison, on an overall, it is observed that the prediction by EC 2 exhibit the closest value to the experimental results for all the concrete strength tested. Subsequent assessments through statistical analysis provide a systematic comparison and recommend the best fit prediction for the experimental data.

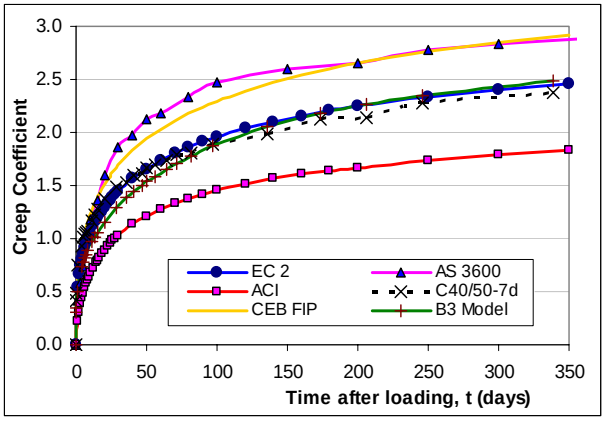

(a) C40/50 concrete tested in controlled room

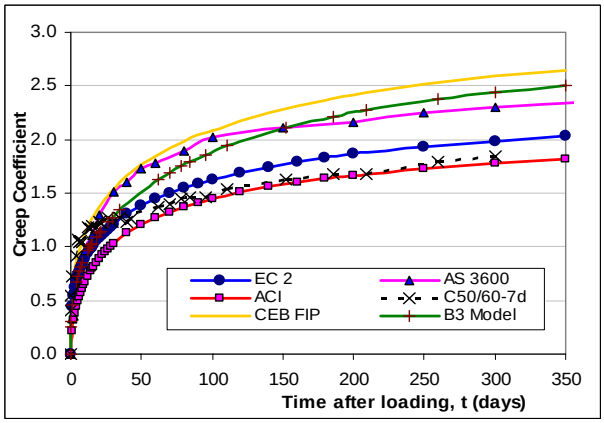

(b) C50/60 concrete tested in controlled room

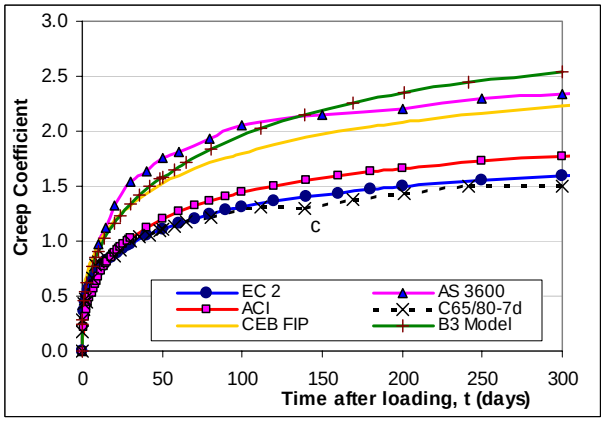

(c) C65/80 concrete tested in controlled room

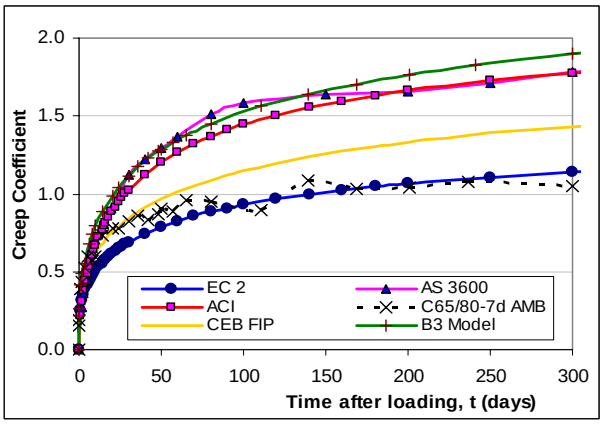

(d) C65/80 tested under ambient condition

Figure 6.14 (a)-(d): Comparison of creep coefficient between experiment results and standard codes for concrete tested at 7 days

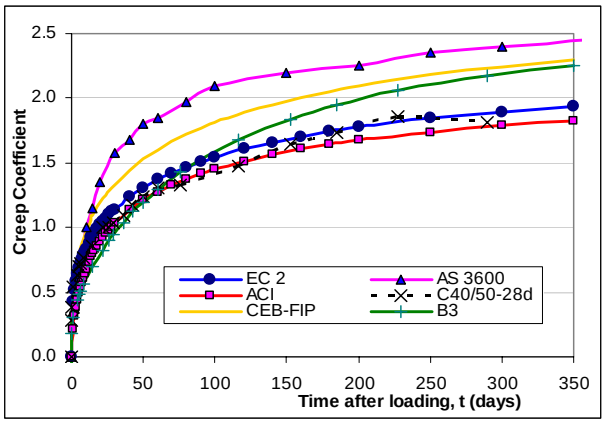

(a) C40/50 concrete tested in controlled room

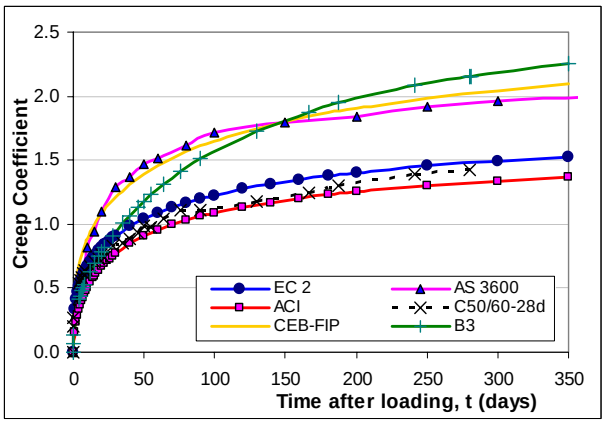

(b): C50/60 concrete tested in controlled room

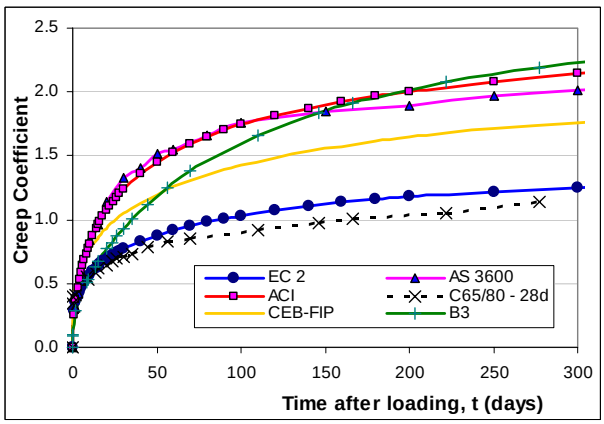

(c) C65/80 concrete tested in controlled room

Figure 6.15 (a)-(c): Comparison of creep coefficient between experiment results and standard codes for concrete tested at 28 days

6.4.2 Statistical Comparison for Creep Coefficient

Statistically, the actual creep coefficients were compared to the prediction models through Residuals Analysis and the results are presented in Table 6.5. Negative values denote under-prediction by the codes as compared to the deformation of local concrete whereas the positive values denote over-prediction. With reference to the summary in Table 6.5, the most prediction models generally over-predict the creep values, except for ACI Model. One of the explanations to the over-prediction is attributed to the high ambient humidity in the tropical condition which lowers the deformation in concrete.

The best prediction model for creep of local concrete is subsequently assessed through Error Percentage, Residuals Squared analysis and coefficient of variation. Results of the analysis are presented in Table 6.6. Based on the analysis, it is found that the EC 2 provides the best prediction for creep of Malaysian concrete. The EC 2 creep equations cater for a wide range of concrete parameters, which in return produces more definite and precise prediction. In addition to that, the recommendations in EC 2 are up-to-date and caters for concrete with the most recent technology, especially the inclusion of high strength concrete that covers up to C90/105. Based on the statistical analysis, the coefficient of variation for EC 2 prediction as compared to experimental measurements is within the range of 8.0% to 23.5%.

ACI 209 and CEB-FIP Models are both ranked second and third, respectively in the prediction accuracy, followed by the B3 Model in the forth ranking. The accuracy of AS 3600 model ranked fifth. AS 3600 model does not provide correction factors in its equation and the prediction values are obtained through graphs reading. A large degree of accuracy is compromised when the prediction is determined from graphs. Therefore, on an overall, it is concluded that the prediction by EC 2 consistently exhibit the closest value to the experimental results for all the concrete strength tested.

Table 6.5: Creep coefficient mean residual for specimens loaded at 7 and 28 days

Prediction Models	Age of loading = 7 days				Age of loading = 28 days		
	C40/50	C50/60	C65/80	C65/80 (Ambient)	C40/50	C50/60	C65/80
EC2	-0.03	-0.07	0.005	-0.08	0.05	0.05	0.05
ACI209	-0.47	-0.27	-0.18	0.24	-0.08	-0.10	0.29
CEB-FIP	0.21	0.26	0.36	0.08	0.24	0.36	0.33
B3	-0.11	0.07	0.42	0.35	-0.05	0.17	0.32
AS3600	0.26	0.15	0.43	0.29	0.38	0.37	0.55

Table 6.6: Overall creep coefficient prediction models ranking

Age at test	Concrete grade	Prediction Model														
		EC2			ACI209			CEB-FIP			B3			AS3600		
		E (%)	R^2	V_m	E (%)	R^2	V_m	E (%)	R^2	V_m	E (%)	R^2	V_m	E (%)	R^2	V_m
7 days	C40/50	-5.80	0.01	11.2	-37.46	0.22	41.3	10.22	0.08	19.0	0.89	0.03	16.0	10.46	0.17	53.8
	Ranking	2	1	1	5	5	4	3	3	3	1	2	2	4	4	5
	C50/60	-10.01	0.03	21.2	-27.53	0.11	37.3	14.97	0.17	32.1	12.23	0.18	28.8	19.91	0.16	48.8
	Ranking	1	1	1	5	2	4	3	4	3	2	5	2	4	3	5
	C65/80	-2.56	0.005	8.2	-15.49	0.04	21.8	35.76	0.17	41.4	53.20	0.45	48.9	35.44	0.30	50.3
	Ranking	1	1	1	2	2	2	4	3	3	5	5	4	3	4	5
	C65/80 (Ambient)	-13.02	0.01	19.8	19.01	0.13	45.2	6.97	0.02	20.0	41.92	0.18	51.9	27.31	0.19	53.3
	Ranking	2	1	1	3	3	3	1	2	2	5	4	4	4	5	5
28 days	C40/50	2.49	0.01	8.8	9.09	0.02	23.6	19.88	0.08	25.3	14.28	0.11	34.1	27.93	0.22	40.4
	Ranking	1	1	1	2	2	2	4	3	3	3	4	4	5	5	5
	C50/60	3.19	0.005	7.9	-17.82	0.01	24.7	38.14	0.16	43.9	38.41	0.27	38.2	34.42	0.18	37.6
	Ranking	1	1	1	2	2	2	4	3	5	5	5	4	3	4	3
	C65/80	2.40	0.01	23.4	30.34	0.16	57.9	40.00	0.15	55.2	61.52	0.48	71.1	66.21	0.40	70.0
	Ranking	1	1	1	2	3	3	3	2	2	4	5	5	5	4	4
Sum		23			60			63			80			89		
Ranking		**1**			**2**			**3**			**4**			**5**		

6.4.3 Graphical Comparison on Shrinkage

The comparison of shrinkage results to the models prediction are plotted in Figure 6.16 and 6.17, for age of drying at 7 days and 28 days. Although all prediction models provide similar shrinkage curve pattern, each model provide different rate and magnitude of deformation. It shall be noted that shrinkage is difficult to predict as it is easily affected by the influence from fluctuation of ambient condition. This explains the wide variation in the prediction of different models, unlike the prediction for creep coefficient which is more uniform.

With reference to Figure 6.16 (a) to (c) and Figure 6.17 (a) to (c), it is interesting to note that the ACI 209 prediction is not sensitive to the change in concrete strength. At the same age of drying, the magnitude of strain is observed to be similar. This is due to the fact that concrete strength parameter is not included in the prediction formula and the influence of concrete strength is only capture through correction factors for percentage of cement and fines content in the concrete mixture. Similar condition of having the same shrinkage magnitude for different concrete strength is also seen for the prediction by AS 3600. For this case, the influence of concrete strength and the age of concrete at start of testing are not considered in the prediction.

Based on an overall observation on Figure 6.16 and Figure 6.17, the prediction by EC 2 and CEB-FIP are rather close to the laboratory tested shrinkage strain. In actual fact, the shrinkage prediction in the EC 2 is developed based on the CEB-FIP Model, which explains the similarity in the results of the two models. Rough observations made through the graphs will not be able to distinguish the best prediction model between the two. Thus confirmation of the best prediction model for the shrinkage strain can only be gathered from a systematic statistical comparison discussed in the following section.

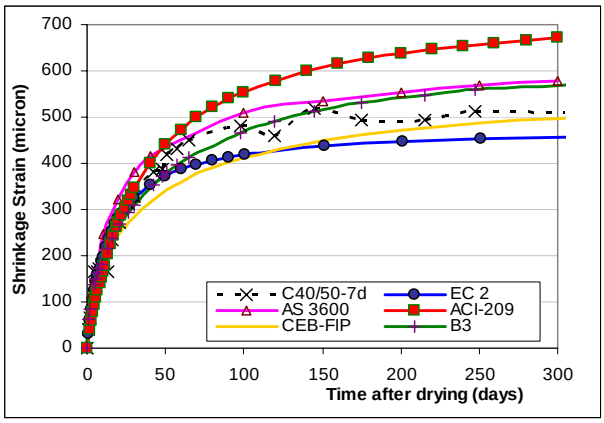

(a) C40/50 concrete tested under controlled condition

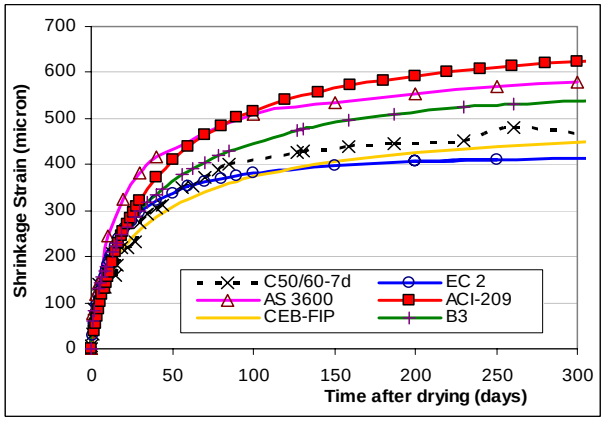

(b) C50/60 concrete tested under controlled condition

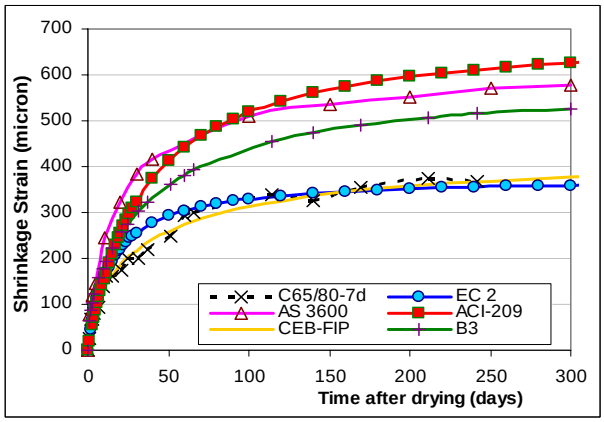

(c) C65/80 concrete tested under controlled condition

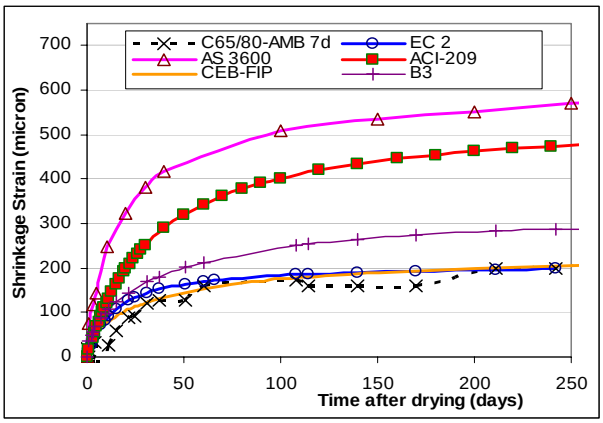

(d) C65/80 concrete tested under ambient condition

Figure 6.16 (a)-(d): Comparison of shrinkage between experimental results and standard codes for concrete tested at age 7 days

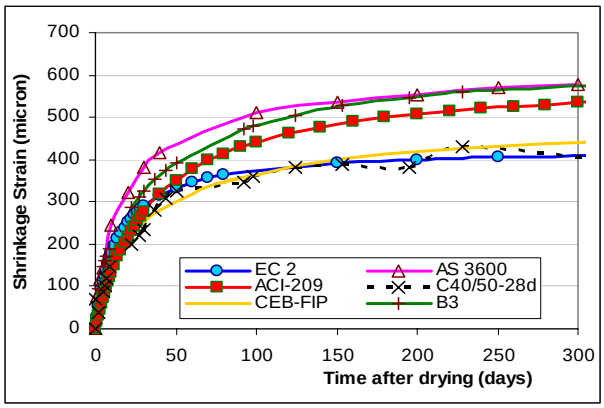

(a) C40/50 concrete tested under controlled condition

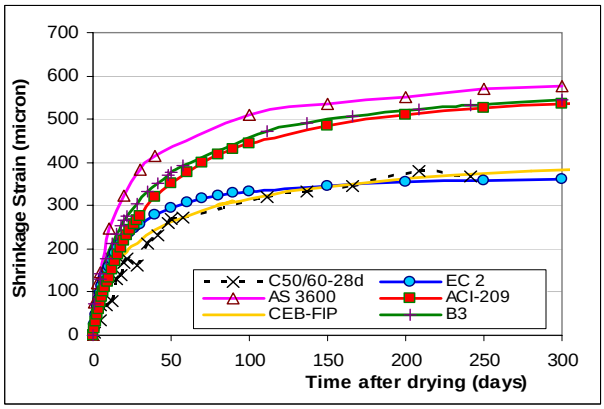

(b) C50/60 concrete tested under controlled condition

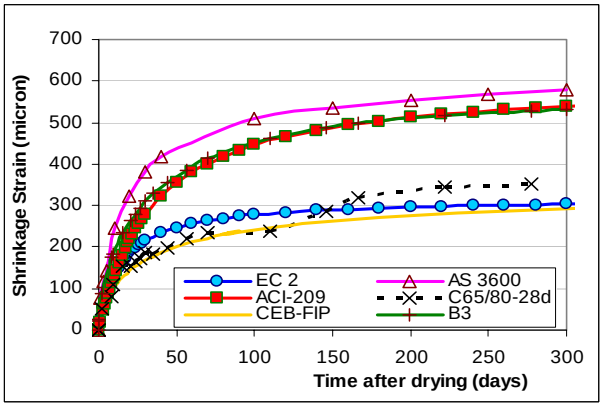

(b) C65/80 concrete tested under controlled condition

Figure 6.17 (a)-(c): Comparison of shrinkage between experimental results and standard codes for concrete tested at age 28 days

6.4.4 Statistical Comparison for Shrinkage

The comparison of shrinkage experimental results and standard codes against time after drying for the concrete batches, tested at the age of 7 and 28 days are summarized statistically in Table 6.7 and 6.8. In Table 6.7, the shrinkage mean residuals for the prediction models are presented and the negative values represents under-prediction whereas positive values signify over-prediction. It is observed that most of the prediction models such as the ACI 209, B3 Model and AS 3600 over-predicts the shrinkage strain. The EC 2 and CEB-FIP models also over-predict the shrinkage strain except for C40/50 and C50/60 concrete tested at age 7 days.

Table 6.8 shows that the best shrinkage prediction for local concrete is the CEB-FIP Model, followed by the EC 2, ACI, B3 Model and AS 3600. The average coefficient of variation, V_m for concrete tested at both 7 days and 28 days for the CEB-FIP Model is at 26.7%. The average shrinkage V_m for 7 and 28 days for EC 2 is at 37.3%, slightly higher than the limit stated in the EC 2 code. It is interesting to note that the ranking for ACI and B3 Model is similar. However, based on the average coefficient of variation between ACI and B3 Model, the V_m for ACI is lower than the results by B3 Model. The average V_m for ACI is at 57.0% whereby the average V_m for B3 Model is at 63.2.

As observed in Table 6.8, large V_m occurs at concrete tested in the ambient, due to the fluctuation in RH that affect the concrete shrinkage and complicates prediction process. With reference to the statistical analysis and Figure 6.7 and 6.8, the prediction by CEB-FIP provides the closest values for shrinkage of local concrete. However, considering the impending adoption of the Eurocodes and the wider usage reference, EC 2 model is chosen for shrinkage modification instead of referring to CEB-FIP 1990. A close observation shows that the summation of ranking between the two models is rather close.

Table 6.7: Shrinkage mean residual for specimens loaded at 7 and 28 days

Prediction Models	age of drying = 7 days				age of drying = 28 days		
	C40/50	**C50/60**	**C65/80**	**C65/80 (Ambient)**	**C40/50**	**C50/60**	**C65/80**
EC2	-9.6	21.9	44.5	54.9	29.0	64.9	41.8
ACI209	34.7	58.9	103.7	160.2	42.5	89.8	106.8
CEB-FIP	-30.0	-12.1	-1.7	32.2	11.6	29.5	-13.4
B3	3.4	36.2	83.1	78.3	93.4	125.8	127.3
AS3600	34.8	70.6	137.8	190.8	121.5	157.8	172.6

Table 6.8: Overall shrinkage prediction models ranking

Age at test	Concrete grade	Prediction Model														
		EC2			ACI209			CEB-FIP			B3			AS3600		
		E (%)	R^2	V_m	E (%)	R^2	V_m	E (%)	R^2	V_m	E (%)	R^2	V_m	E (%)	R^2	V_m
7 days	C40/50	0.9	889	10.7	7.8	5516	26.0	-5.0	1933	13.8	0.6	938	10.8	11.4	2283	22.4
	Ranking	2	1	1	4	5	5	3	3	3	1	2	2	5	4	4
	C50/60	11.9	1417	16.7	11.8	7513	30.1	-1.0	575	10.5	12.7	1822	16.5	22.9	6636	36.4
	Ranking	3	2	2	2	5	4	1	1	1	4	3	3	5	4	5
	C65/80	22.3	2801	28.9	34.5	19038	54.5	6.4	191	12.8	40.6	8444	47.9	65.5	22410	95.1
	Ranking	2	2	2	3	4	4	1	1	1	4	3	3	5	5	5
	C65/80 (Ambient)	-1.1	4167	42.7	77.5	33061	157.4	-18.9	2554	19.4	48.3	7256	60.2	190.8	75783	285
	Ranking	1	2	2	4	4	4	2	1	1	3	3	3	5	5	5
28 days	C40/50	16.6	1335	20.5	9.3	3077	22.3	11.5	362	17.6	42.8	10070	89.1	64.6	15936	73.8
	Ranking	3	2	2	1	3	3	2	1	1	4	4	5	5	5	4
	C50/60	45.1	4977	86.6	46.7	10279	58.2	22.1	1320	74.9	73.6	16750	92.8	109.5	27587	169.9
	Ranking	2	2	3	3	3	1	1	1	2	4	4	4	5	5	5
	C65/80	15.8	2583	42.2	38.7	16476	60.2	-18.2	723	21.6	50.6	19378	95.9	88.2	35154	120.0
	Ranking	1	2	2	3	3	3	2	1	1	4	4	4	5	5	5
Sum		41			71			31			71			101		
Ranking		**2**			**3**			**1**			**3**			**5**		

6.5 Time-dependent Deformation of Reinforced Concrete Columns

Measurements on reinforced concrete columns captured the total deformation, a total of the elastic strain, shrinkage and creep due to the sustained load. The magnitude of the total deformation measured for C40/50 and C65/80 columns are shown in Appendix E1. In the analysis and as shown in Figure 6.18, creep deformation is presented instead of the total deformation. The effect from elastic and shrinkage strain are deducted is to control the variables in the assessment on the accuracy of the modified creep and shrinkage prediction, reducing the influence of other parameters such as elastic strain. The elastic strain of the columns is taken based on the first reading taken immediately after the columns were loaded.

As shown in Figure 6.18, the deformations of the columns follow the trend with lower strain for higher concrete strength. As expected, the C40/50 columns exhibit highest strain value as compared to the C65/80 columns. The lowest strain is observed for the column stored under ambient, with approximately 20% to 30% lower than the C65/80 control column, depending on the age after loading. This range is similar to the difference between the control and ambient C65/80 specimens tested for creep. It is also observed that the initial strain for C65/80 ambient column exhibit higher strain during the initial loading period. The difference is approximately 10% and occurs during the first 10 days of loading. One of the reasons for this occurrence may be due to the fluctuation of temperature and RH of the ambient surrounding during that time period.

Statistically, accuracy of the data measured within the same batch of concrete is assessed through standard deviation and coefficient of variation. The results are as presented in Table 6.9. Similar to the trend for creep and shrinkage statistical evaluation, the standard deviation and coefficient of variation is higher for control specimens that exhibit higher strain. The deformation for column C40/50 has a wider range in results as it is taken from an average of two columns tested. This explains the higher statistical variability. Fluctuation in the surrounding temperature and RH leads to a higher coefficient of variation for the column tested in the ambient.

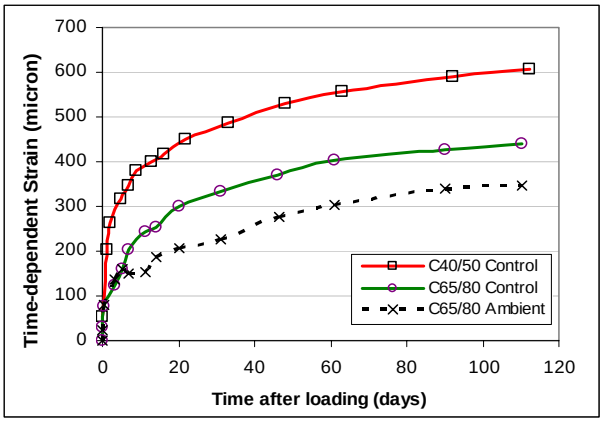

Figure 6.18: Time-dependent deformations for C40/50 and C65/80 columns tested under controlled and ambient condition

Table 6.9: Statistical results of columns tested

Columns	**Standard Deviation ($x10^{-6}$)**	**Coefficient of Variation (%)**
C40/50	128.6	25.3
C65/80 – Control	85.1	19.4
C65/80 – Ambient	71.5	22.5
Average	95.0	22.4

6.6 Pre-camber of Pre-tensioned Prestressed Concrete Beams

Initial pre-camber of two laboratory scale prestressed beams tested are presented and discussed in this section. In order to ease the comparison study and for presentation purpose, the magnitude of pre-camber reported in this thesis is shown as negative values unless otherwise stated. The initial pre-camber were monitored for a total period of 4 days, from the time immediately after transfer until the time the beams were prepared for deflection testing. The results of pre-camber at midspan of the two beams at different time after transfer are presented in Table 6.10. Evaluation of the measurement accuracy is also shown in Table 6.10. Detailed information on the pre-camber at different measuring points are presented in Appendix E2.

It is observed that the magnitude of pre-camber is low. At four days after transfer, the average upward deflection at midspan is 1.23mm. The main reason for the small magnitude is the short span length of the beam, at 2.5m. In addition to that, the low pre-camber value was also due to the straight tendon profile with constant eccentricity exerting uniform tendon force along the beam, as opposed to a curved profile with higher eccentricity at the midspan producing greater prestressing force. However the results obtained provide a good indication on the pre-camber behaviour on prestressed beams and in assessing the accuracy of the current prediction calculation. Therefore for comparison purposes, the results are presented in two decimal points even though two decimal points in millimeter is difficult to be comprehensible.

Besides evaluating the pre-camber based on an average from two sets of beams, reference to available results conducted by other researcher is also made to establish the confidence in the results measured. In the University of New South Wales, Zou (2003) conducted short-term and long term deflections monitoring on laboratory scaled prestressed concrete beams. The main focus of his study was to evaluate the effect of fiber reinforced polymer tendons on prestressed beams and it was reported that the initial pre-camber measured for the prestressed beam with concrete strength 80N/mm^2 is at 1.70mm. The initial pre-camber measured by Zou is comparable to the data obtained in this study. Zou's pre-camber is higher due to the longer beam span of 6.0m and also due to the differences in the beams design properties. Thus it can be concluded that the measured pre-camber is correct within acceptable range.

For a clearer illustration of the development of beam pre-camber, the deflection taken at different time is shown in Figure 6.19. It is observed that the elastic deformation occurred during the rapid pre-camber increase in the first 1.2 hours (0.05 days), approaching an average deflection of 1.17mm. The short period evaluation with displacement reading taken in short interval gave a good demarcation between elastic strain and time-dependent strain, as it is clearly shown in Figure 6.19. Subsequently the increase was more gradual and the final value recorded at the end of 4 days is at 1.24mm. Besides the elastic strain which caused the sharp increase

in deformation at the beginning, inexperienced skills in the release of prestressing tendons during the experimental work also contributed the high initial up-surge.

It was undeniable that the total duration for pre-camber monitoring of 4 days is short, due to the time constraint in the laboratory work. With reference to the graph plotting in Figure 6.19 and Table 6.10, the pre-camber reading has stabilized within the first 48 hours of detensioning. Thus any observation beyond the age of 4 days is expected to be within the same magnitude as at the age of 4 days with slight increase due to creep, which is computable as shown in Chapter 7. The objectives of the pre-cambering measurement are to verify the accuracy of the proposed modified creep and shrinkage data and also the accuracy of proposed modified calculation method, which is to be discussed in Chapter 7. In addition to that, the pre-camber results also provide a good indication of the initial hogging and verified the accuracy of the current simplified prediction method in BS 8110 to actual beam behaviour.

Table 6.10: Pre-camber of prestressed beams at mid-span

Time after prestressing (days)	**Beam Pre-camber (mm)**			**Std Deviation**	**Coeff. of Variation (%)**
	PSB 1	**PSB 2**	**Average**		
0.00	0.00	0.00	0.00	0.00	0.0
0.05	-1.45	-0.88	-1.17	0.29	24.5
0.70	-1.47	-0.94	-1.21	0.27	22.0
0.90	-1.45	-0.96	-1.21	0.25	20.3
1.50	-1.47	-0.97	-1.22	0.25	20.5
2.00	-1.50	-1.02	-1.26	0.24	19.0
2.50	-1.51	-1.03	-1.27	0.24	18.9
3.00	-1.50	-1.01	-1.26	0.25	19.5
3.50	-1.51	-1.00	-1.26	0.26	20.3
4.00	-1.51	-1.00	-1.26	0.26	20.3
Average				0.26	20.6

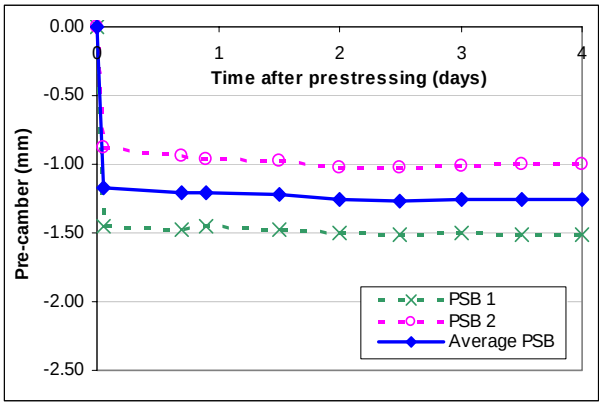

Figure 6.19: Mid-span beam pre-camber monitored in the laboratory at different days after de-tensioning

6.7 Deflection of Prestressed Pre-tensioned Concrete Beams

Subsequent to the pre-camber monitoring, vertical deflection due to sustained concentrated load of 60kN was measured at the mid-span of the prestressed beams PSB1 and PSB2. The duration for loading and measurement taken was for a period of 28 days and is presented in Table 6.11. The deflection value recorded is the total deformation due to the load applied which include the elastic, creep and shrinkage deformation, without subtracting the hogging induced by pre-camber. The mid-span deflection due to concentrated load dependent deflection is plotted against time after loading in Figure 6.20. For the ease in analysis, sagging of beam due to the applied load is represented by positive value as plotted in Figure 6.20.

Immediate downward deflection when the load is applied represents the elastic deformation, which is recorded at 2.76mm. It is observed in Figure 6.20 that the sagging of the beams increased continuously with time throughout the loading period. However this deflection is recorded with declining rate of increment. The subsequent increment after elastic deflection can be attributed to the time-dependent deformation. At the age of 28 days after the load application, the average sagging increased by 15% increase in deflection from the elastic deformation to 3.16mm.

Taking pre-camber into account to evaluate the actual deflection from the initial beam soffit level, the final pre-camber for the respective beams is deducted from the total sagging measured. The hogging of the beams due to pre-camber

followed by sagging of the beams due to the applied load is plotted against time after prestressing in Figure 6.21. The hogging pre-camber is plotted as negative values while the sagging is denoted as positive deflection in Figure 6.21. It is worth noting that the final sagging of the beams upon subtracting the respective pre-camber deformation exhibit relatively close results. The coefficient of variation computed for the deflection upon subtracting the respective pre-camber deformation is at 0.5%.

Table 6.11: Deflection of prestressed beams at mid-span

Time after loading (days)	Beam Deflection (mm)			Std Deviation	Coeff. of Variation (%)
	PSB 1	PSB 2	Average		
0.0	0	0	0	0	0
0.1	2.97	2.55	2.76	0.21	7.69
0.8	3.05	2.62	2.84	0.22	7.63
1.0	3.09	2.64	2.86	0.22	7.86
1.5	3.13	2.70	2.92	0.22	7.56
3.0	3.11	2.68	2.90	0.22	7.42
3.5	3.15	2.72	2.94	0.21	7.24
4.0	3.19	2.77	2.98	0.21	7.11
6.0	3.20	2.76	2.98	0.22	7.41
8.0	3.26	2.81	3.04	0.23	7.52
9.0	3.28	2.82	3.05	0.23	7.47
10.0	3.31	2.84	3.07	0.23	7.62
11.0	3.31	2.86	3.08	0.23	7.32
12.0	3.33	2.87	3.10	0.23	7.38
14.0	3.34	2.88	3.11	0.23	7.32
15.0	3.35	2.90	3.12	0.23	7.23
16.0	3.37	2.91	3.14	0.23	7.32
18.0	3.36	2.90	3.13	0.23	7.36
20.0	3.38	2.94	3.16	0.22	6.95
22.0	3.39	2.92	3.15	0.23	7.45
28.0	3.39	2.94	3.16	0.22	7.06
Average				0.22	7.40

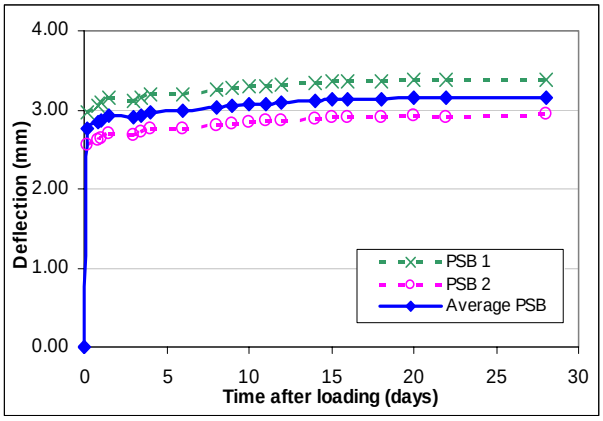

Figure 6.20: Deflection of prestressed beams due to applied concentrated load

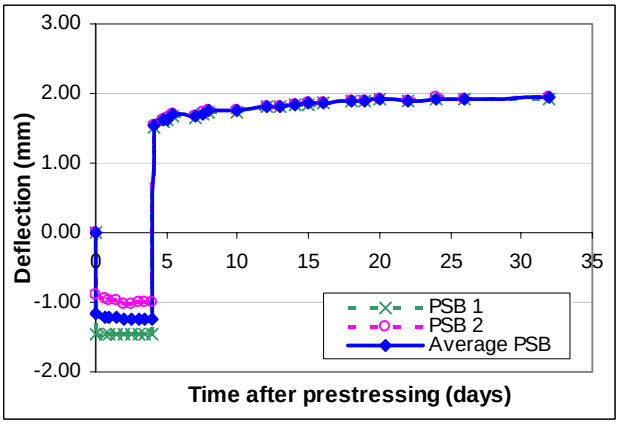

Figure 6.21: Mid-span deformation of PSB1 and PSB2 due to pre-camber and applied concentrated load

6.8 Pre-camber of Post-tensioned Prestressed Beams on Site

As elaborated in Chapter 4, a total of four post-tensioned beams of 36m in length were assessed for pre-cambering immediately after post-tensioning on site. The results from this monitoring will provide an indication of the actual deflection of prestressed beams on site and the degree of accuracy for the theoretical calculation. Table 6.12 shows the results of the pre-camber measurement at the mid-span of the four beams throughout the monitoring period of 15 days after prestressing. As mentioned in earlier, the pre-camber is presented in negative values. With reference

to the measurements, it is observed that the upward deflection of the four beams continue to increase after day one until day 15. Immediately after prestressing, the mid-span camber of the four beams reached a magnitude within 37mm to 57mm. At day 15, the mid-span camber of the beams increased to an average of 63mm with a maximum of 75mm. The detailed pre-camber curve is presented in Appendix E4.

It is observed that substantial increase of the upward deflection occurred during the first three days after prestressing, and after which, it increased steadily within a small margin. This increment is evidently seen in Figure 6.22 with pre-camber values of the beams plotted against different time after prestressing. This steep increment at the initial stage is due to the elastic strain of concrete when prestressing load is first applied. Thereafter, the increment is lower under the influence of time-dependent deformation of creep and shrinkage.

It is worth noting that Beam 2 gives the highest pre-camber whereas Beam 4 exhibits the smallest value among the four beams. Beam 1 and Beam 3 on the other hand exhibit similarly close pre-camber. The differences in the deformation may be attributed to the variation in material quality and variance in workmanship during construction. The standard deviation of all camber measurement obtained from the four beams is within the range of 7.1 to 8.7, as indicated on Table 6.12. The standard deviation represents the consistency of the measured data from the four beams and the result is more precise with smaller standard deviation values. This variation is within an acceptable range as the coefficient of variation is under 20% at between 12.2% and 15.5%.

Table 6.12: Pre-camber and statistical accuracy of post-tensioned beams measured on site

Time (day)	Beam Pre-Camber Measured on Site (mm)					Statistical Accuracy	
	Beam 1	Beam 2	Beam 3	Beam 4	Average	Standard Deviation	Coefficient of Variation
I**	-45	-57	-45	-37	-46.0	7.1	15.5
3	-55	-71	-56	-47	-57.3	8.7	15.1
6	-59	-73	-57	-49	-59.5	8.6	14.5
9	-58	-74	-57	-51	-60.0	8.5	14.2
12	-60	-75	-59	-55	-62.3	7.6	12.2
15	-62	-75	-59	-56	-63.0	7.3	11.5
Average						8.0	13.8

* Between predicted value and average pre-camber measured on site

** Immediately after transfer

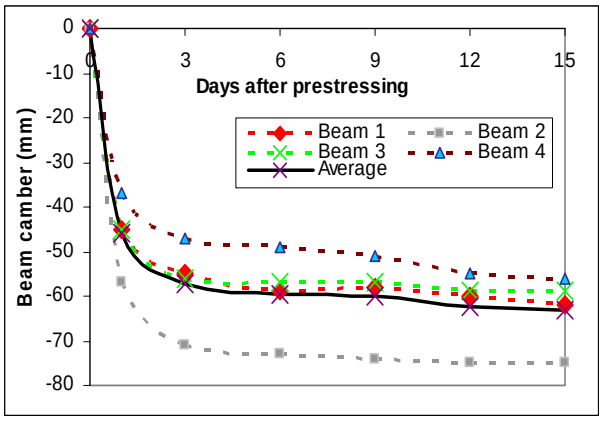

Figure 6.22: Mid-span beam pre-camber monitored on site at different days after prestressing

6.9 Summary of Results on Creep and Shrinkage Analysis

1. A total of 433 standard size specimens and 10 numbers of structural members were cast and tested under the scope of this research. From the total number of specimens, 24 numbers were tested for creep while 48 numbers were tested for shrinkage. Each specimen carries at least four measurement points, indicating a good figure for a reasonably dependable statistical analysis. The duration of testing for time-dependent deformation of standard size specimens were between 300 days to 339 days and the structural members testing is between 4 days, for pre-camber monitoring and 112 days for columns testing.

2. The main environment influence is the RH as variation between the ambient and controlled condition for RH is at 30% while the difference in temperature is only at 1.1^{o}C. Thus, it is concluded that variation in the test results between ambient and control specimens were primarily due to the difference in the relative humidity.

3. Generally, the trend for concrete deformation measured from the experimental results shows that creep and shrinkage strain is lower as concrete strength increases for specimens tested in the controlled room. However under the influence of higher RH and temperature, concrete exhibit lower strain. The experiment results proved that a reduction in 10% to 30% strain is observed for the concrete stored under the tropical ambient as compared to the concrete of the same batch, tested under the controlled condition of 27^{o}C and 50% RH.

4. The higher temperature led to faster initial strength gain of concrete from the formation of tobormorite gel. Higher moisture content in the ambient also causes lower rate of diffusion of water into the surrounding, subsequently lowering the magnitude of drying creep.

5. Both statistical results and graph comparison between experimental results and existing models recommendations show that creep and shrinkage for concrete tested in tropical condition is closer to the recommendation by EC 2, as compared to the other models. One of the obvious reasons is because the model is contains the most up-to-date information on the influencing parameters and full coverage of concrete strength.

6. Due to the increasing importance on time-dependent deformation and the considerably big difference between the experimental measurements to codes recommendations, modification factors are introduced for local concrete applications based on the best prediction model available, which is the EC 2. The development of modification factors and verification on the accuracy and applicability of the prediction equation are discussed in Chapter 7.

CHAPTER 7

PROPOSED TIME-DEPENDENT DEFORMATION MODIFICATION FACTORS FOR CONCRETE IN TROPICAL CLIMATE

With the increasing emphasis on accurate time-dependent deformation prediction on concrete structures, reliable prediction model for concrete in the tropical climate is vital for structural design. Due to the considerable difference between the experimental measurements to codes recommendations observed in the analysis in Chapter 6, an improved prediction model for local concrete is introduced in this chapter. The proposed improved creep and shrinkage prediction is developed based on the prediction model from EC 2 with incorporation of modification factors to cater for concrete in the tropical environment. As proven in the statistical analysis conducted in Chapter 6, the EC 2 clearly exhibits close results to experimental values. The move of adopting Eurocodes to replace the British Standards adds to the advantage of modifying the Eurocode model for prediction values.

To predict creep and shrinkage of concrete, two distinctly different approaches to formulate the material laws have been adopted by various researchers previously. Firstly it is the empirical approach in which time functions are determined from a number of tests by curve fitting. Secondly is the analytical approach in which the time functions are obtained by solving differential equations of postulated processes governing creep and shrinkage behaviour. In either case, the model parameters are obtained by best-fitting a number of test results available (Ojdrovic and Zarghamee, 1996). In this research, the first approach, which is the empirical data fitting is adopted. With the EC 2 model as the reference code, creep and shrinkage modification factors for concrete in the tropical climate, TROPCS is introduced in this research. These modification factors are tailored to be included in the National Annex of Malaysia for Eurocode 2 as an option for engineers' reference and applications.

7.1 Development of TROPCS Creep Factors

The progress of creep with time is observed to follow a definite pattern in which can be translated into equation for the purpose of obtaining good prediction values without having to conduct laboratory testing. Based on the results obtained, it is observed that the creep deformation curve is best expressed using double power hyperbolic function as adopted by EC2, ACI 209 and CEB-FIP Models. Having the ultimate goal in this study oriented towards the application in structural design, modification factors for creep is developed based on the practical approach of curve fitting. The TROPCS creep modification factors are obtained empirically by best-fitting the laboratory results to the prediction by EC 2. Logarithmic data fitting is recognized as a common tool used to develop creep and shrinkage empirical coefficient (Neville et al., 1983).

TROPCS creep factors are used with reference to the prediction formula in Appendix B of EC 2, as presented in Equation 7.1. The modification coefficients are introduced at RH effect factor, ϕ_{RH} and also at the power coefficient for duration of loading, which controls the creep coefficient curve pattern. In EC 2, the power coefficient for duration of loading is a constant for all concrete strength recommended at 0.3. Through the empirical analysis, a new power coefficient is recommended to modify the current EC 2 model. This TROPCS power coefficient is referred to as C_1 for the convenience of distinction.

Equation 7.1 is rearranged to Equation 7.2, with the power coefficient C_1. Subsequently Equation 7.2 is reestablished into logarithmic expression as shown in Equation 7.3. With reference to creep experiment results, graphs with $\text{Log}\dfrac{\phi(t,t_o)}{\beta(f_{cm})\cdot\beta(t_o)}$ representing the Y-axis and $\text{Log}\left[\dfrac{(t-t_o)}{(\beta_H+t-t_o)}\right]$ as the X-axis are plotted for the three concrete strength; C40/50, C50/60 and C65/80. The high Pearson residuals squared, R^2 from the logarithmic graphs indicates that a consistent linear relationship can be established. The intercept and gradient of slop provide

values of modified constants ϕ'_{RH} and C_1, respectively. The empirical ϕ'_{RH} is obtained through the antilog of the intercept of Y-axis.

$$\phi(t, t_o) = \left[\frac{(t-t_o)}{(\beta_H + t - t_o)}\right]^{0..3} . \beta(f_{cm}) . \beta(t_o) . \phi_{RH} \quad (7.1)$$

$$\frac{\phi(t,t_o)}{\beta(f_{cm}) \cdot \beta(t_o)} = \left[\frac{(t-t_o)}{(\beta_H + t - t_o)}\right]^{C_1} . \phi_{RH} \quad (7.2)$$

$$\text{LOG } \frac{\phi(t,t_o)}{\beta(f_{cm}) \cdot \beta(t_o)} = C_1 . \text{ LOG } \left[\frac{(t-t_o)}{(\beta_H + t - t_o)}\right] + \text{LOG } \phi'_{RH} \quad (7.3)$$

where

$\beta(f_{cm}) = \dfrac{16.8}{\sqrt{f_{cm}}}$

= coefficient for the effect of concrete strength

$\beta(t_o) = \dfrac{1}{0.1 + t_o^{0.2}}$

= coefficient for the effect of age of concrete during loading

$\phi_{RH} = 1 + \dfrac{1 - RH/100}{0.1 \cdot \sqrt[3]{h_o}}$

= coefficient for the effect of surrounding ambient on structural members, referring to RH and member size as the main parameters

ϕ'_{RH} = empirically modified coefficient on effect of surrounding ambient

β_H = correction factor for ambient relative humidity

$= 1.5 * \left[1 + (0.012 * RH)^{18}\right](h_o) + 250 \cdot \alpha_3$; with $\alpha_3 = \left(\dfrac{35}{f_{cm}}\right)^{0.5}$

t = age of concrete at the time considered (days)

t_o = age of concrete at loading (days)

f_{cm} = mean concrete cylinder strength (N/mm^2)

RH = ambient relative humidity (%)

h_o = specimen notional size (mm)

C_1 = empirically modified power coefficient

Based on the empirical analysis, the creep coefficient equation with incorporation of TROPCS modification factors for concrete in the tropical environment is as given in Equation 7.4. The factor C_1, representing the modified power coefficient for the duration of loading is determined from the gradient of the logarithmic graph plot, as explained in Suh-chapter 7.1. The second correction factor, C_2 is introduced to modify ϕ_{RH} for concrete in the tropics. Value C_2 is the ratio between ϕ'_{RH} and ϕ_{RH} .

$$\phi(t, t_o) = \left[\frac{(t-t_o)}{(\beta_H + t - t_o)}\right]^{C_1} . \beta(f_{cm}) . \beta(t_o) . C_2 . \phi_{RH} \qquad (7.4)$$

7.1.1 Development of TROPCS Creep Factors for Concrete Loaded at 7 Days

The analysis using logarithmic plotting to determine TROPCS creep factors for concrete loaded at age 7 days are presented in Figure 7.1 (a) to (d). The gradient of the graph represents the power coefficient for duration of loading for concrete in the tropics, C_1 whereas the antilog of the intercept represents the empirically modified factor to allow for RH effect, ϕ'_{RH} . Results of the gradient and intercept are generated for each of the respective graphs in Figure 7.1 (a) to (d). As it was mentioned in Chapter 6, Bazant (1987) reported that shrinkage and creep data behave heteroscedacity. That is, as the time increases, the spread of data increases. Thus, when linear regression is used, the later data with larger deviation lead to a wider range of scatter in the logarithmic plots at different age of loading, as shown in Figure 7.1.

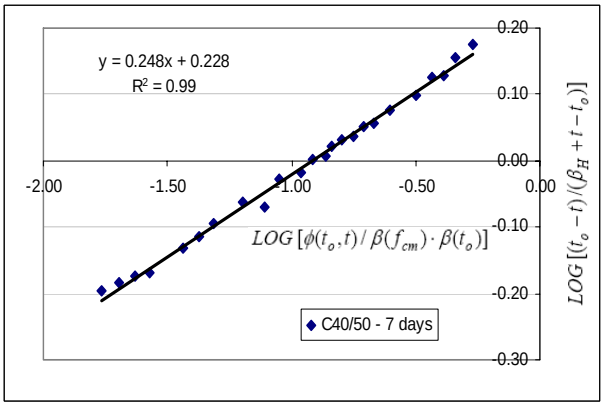

(a) C40/50 tested under control RH of 50%

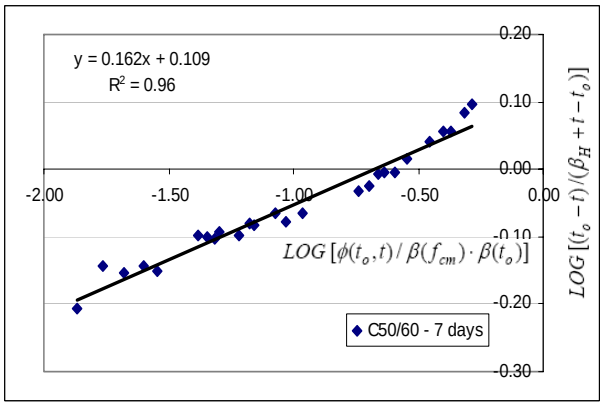

(b) C50/60 tested under control RH of 50%

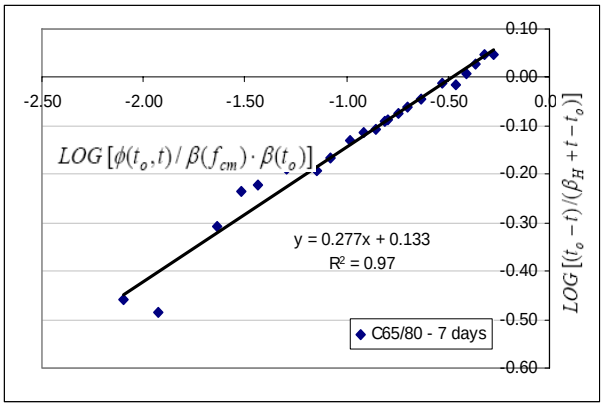

(c) C65/80 tested under control RH of 50%

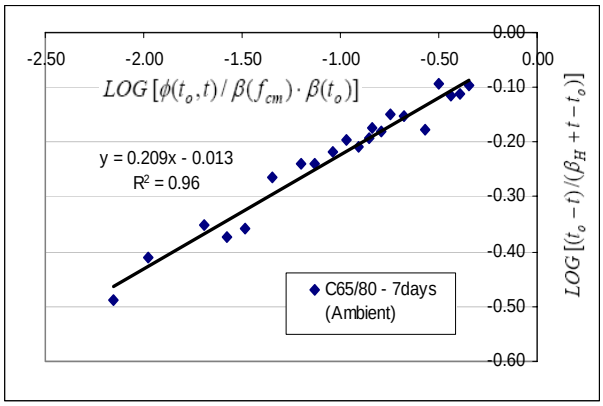

(d) C65/80 tested under ambient condition

Figure 7.1(a)-(d): Creep modification analysis to determine TROPCS factors for concrete tested at 7 days

Table 7.1 summarises the average TROPCS factors of C_1 and C_2 for concrete loaded at the age of 7 days for the three concrete grades tested under control RH of 50±4% and temperature at 27±2^{o}C and for C65/80 specimens tested under ambient condition. Based on Table 7.1, the common power coefficient, C_1 is found to be within the ranges of 0.21 to 0.28 whereas the RH ratio, C_2 is within the ranges of 0.80 to 0.83. It is also observed that the factors for C50/60 is lower as compared to other concrete strengths, with C_1 at 0.16 and C_2 at 0.69.

As a simplification to the modification prediction formula, average values for C_1 and C_2 for the concrete tested at 7 days are introduced through the average of the three concrete strengths. The results from C50/60 however are excluded from the average of TROPCS creep factors due to the inconsistency in the results. The significant difference in results for C50/60 is due to the comparatively slower rate of increase in concrete strength from 7 days to 28 days tested, as shown in Table 5.7 in Chapter 5. The increase in concrete strength from 7 days to 28 days for C50/60 is at 15% higher as opposed to C40/50 and C65/80 which are at 24% and 21%. Thus with lower rate in the increase in concrete strength, creep at the initial stage is significantly higher than the EC 2 prediction, resulting in a lower power coefficient, C_1. It is also worth noting that comparatively, the porosity of C50/60 is low which attributes to the lower creep strain beyond the age of 28 days.

Therefore for concrete tested at the age of 7 days, the TROPCS creep factors, C_1 and C_2 are found to be at 0.24 and 0.81, respectively. It should be highlighted however that the accuracy of the modified equation is slightly compromised through this simplification exercise of averaging C_1 and C_2 as opposed to providing individual modification factors as reflected in Table 7.1. Simplification of prediction models and equations however are essential for application purposes as long as the coefficient of variation is within an acceptable range of 20% (Bazant and Baweja, 2000).

Table 7.1: TROPCS creep factors for concrete tested at the age of 7 days

Concrete Class	C_1	ϕ'_{RH} (empirical analysis)	ϕ_{RH} (by EC 2)	C_2 $\left(\phi'_{RH}/\phi_{RH}\right)$
C50	0.25	1.69	2.03	0.83
C60	0.16	1.29	1.87	0.69
C80	0.28	1.36	1.69	0.80
C80 Ambient	0.21	0.97	1.21	0.80
Average	**0.24**	1.33	1.70	**0.81**

7.1.2 Development of TROPCS Creep Factors for Concrete Loaded at 28 Days

The modification analysis using logarithmic plotting for concrete loaded at age 28 days are presented in Figure 7.2 (a) to (d). Similar to the analysis for concrete loaded at 7 days, the gradient of the graph represents the power coefficient for duration of loading for concrete in the tropics, C_1 and the intercept represents the factor to allow for RH effect, ϕ'_{RH}. The ratio of ϕ'_{RH}/ϕ_{RH} results in the coefficient C_2. The gradient and intercept of the logarithmic analysis for each concrete class is shown in the graph and the summary for all is compiled in Table 7.2. The average creep modification factors for high strength concrete tested at age of 28 days are also provided in Table 7.2.

As observed in Table 7.2, the range of correction factors, C_1 and C_2 for different concrete strength are rather close. Power coefficient C_1 is within the range of 0.26 to 0.30, with an average of 0.28. The RH correction factor, C_2 is within the range of 0.72 to 0.89 and the average value is calculated to be 0.80. Smaller range of correction factors allows for better accuracy in the prediction when simplification exercise in averaging C_1 and C_2 is practiced.

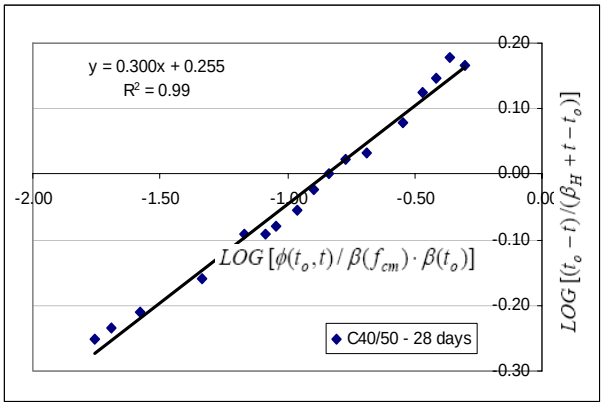

(a) C40/50 concrete tested in controlled room

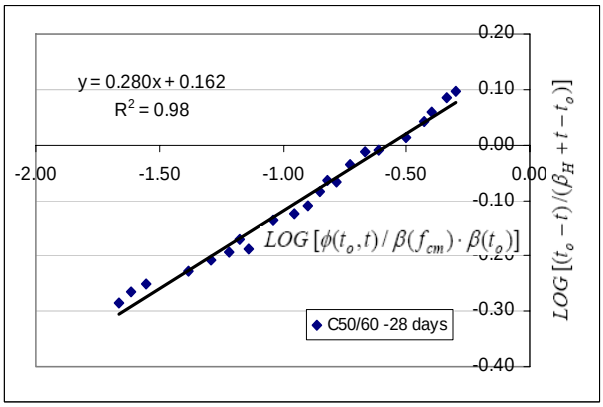

(b) C50/60 concrete tested in controlled room

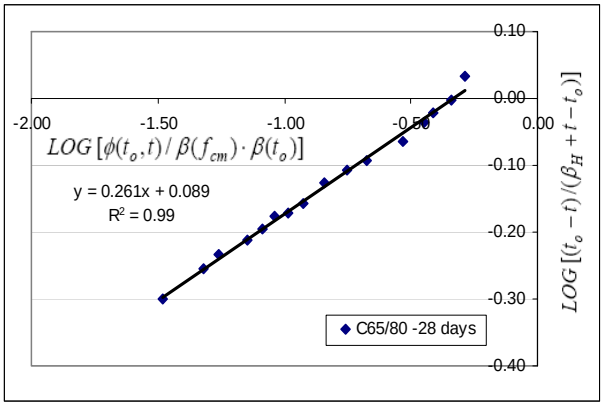

(c) C65/80 concrete tested in controlled room

Figure 7.2(a)-(c): Creep modification analysis to determine TROPCS factors for concrete tested at 28 days

Table 7.2: TROPCS creep factors for concrete tested at age 28 days

Concrete Class	C_1	ϕ'_{RH} (from empirical analysis)	ϕ_{RH} (recommended by EC 2)	C_2 $\left(\phi'_{RH}/\phi_{RH}\right)$
C50	0.30	1.8	2.028	0.887
C60	0.28	1.45	1.872	0.774
C80	0.26	1.226	1.694	0.724
Average	**0.28**	1.49	1.87	**0.80**

7.1.3 Discussion on TROPCS Creep Prediction Factors

The modified creep prediction equation based on the recommendation from EC 2 is shown in Equation 7.4. The TROPCS factors, C_1 and C_2 developed for creep of HSC under tropical condition is summaried in Table 7.3. The notations in the equation are as described in Equation (7.1).

$$\phi(t, t_o) = \left[\frac{(t-t_o)}{(\beta_H + t - t_o)}\right]^{C_1} . \beta(f_{cm}) . \beta(t_o) . C_2 . \phi_{RH} \qquad (7.5)$$

Table 7.3: Summary of TROPCS creep factors for concrete in tropical climate

Concrete Age at Loading (days)	C_1	C_2
7	0.24	0.81
28	0.28	0.80

TROPCS model basically corrected the early age deformation curve of EC 2. Based on the experimental results and analysis, it is found that creep in concrete under tropical condition is found to exhibit higher creep coefficient during the initial loading stage and subsequently beyond the age of approximately 50 days, a slightly lower value as compared to the recommendation by EC 2. Thus the TROPCS factors are developed based on this finding from the experiment results.

The modification resulted in lower power coefficient, C_1 with 0.23 and 0.28 for concrete loaded at age 7 and 28 days, respectively as opposed to the recommendation of 0.3 by EC 2. Based on the theory of power function, the power factor, C_1 mainly controls the graph pattern on the rate of initial and long term curve. The recommended modifications with lower power coefficient provide a higher surge during initial curve of the graph and a lower rate of creep after approximately 50 days of loading, as per the results from laboratory experiment. It is highlighted here that the power coefficient for concrete loaded at age 7 days is lower than for concrete loaded at age 28 days. This is due to the concrete strength at the specific age. At the age of 7 days, the concrete has not achieved its full design strength thus the initial rate of deformation is higher. At the age of 28 days, the concrete has already achieved its design strength which is approximately 20% higher than at the age at 7 days, as shown in Table 5.7. With the higher concrete strength and higher density at 28 days after curing, the rate of initial creep deformation is lower as compared to concrete at 7 days, as reflected in the experiment results.

The prediction of creep coefficient for each concrete strength from the modified equation, results from the experiment and also the recommendation from EC 2 are plotted for comparison purposes. In order to test the differences between the

new modified model and the EC 2 recommendation, the concrete properties are kept constant between the two models. Thus concrete properties for both predictions are with reference to the magnitude obtained from the experiment.

The plotting comparison between EC 2 and TROPCS modification to experiment measurements are presented in Figure 7.3 for concrete tested at age 7 days. Figure 7.4 presents the comparison for concrete tested at 28 days. With reference to the graph plotting, it is clearly shown that the experimental results exhibit higher rate of creep during the initial loading period for local concrete as compared to the recommendation by EC 2. Thus the introduction of lower power coefficient, C_1 to increase the initial gradient of the creep curve is justified. However lower power factor overestimate long term creep predictions. This over estimation is overcome through the empirical coefficient of RH correction factor, C_2. The C_2 values computed for concrete loaded at 7 days and 28 days are at 0.91 and 0.90 respectively, controlling the overestimation of long term creep. For reference purposes, the calculation for TROPCS and EC 2 creep predictions for concrete tested at 7 and 28 days are presented in Appendix F1 and F2, respectively.

As a summary, the modified results give a higher initial creep coefficient value and a slightly lower value beyond the age of approximately 50 days and subsequently lower magnitude for long term creep, as compared to the recommendation in EC 2. The statistical accuracy of TROPCS modification factors are analysed in the sub-chapter 7.1.4.

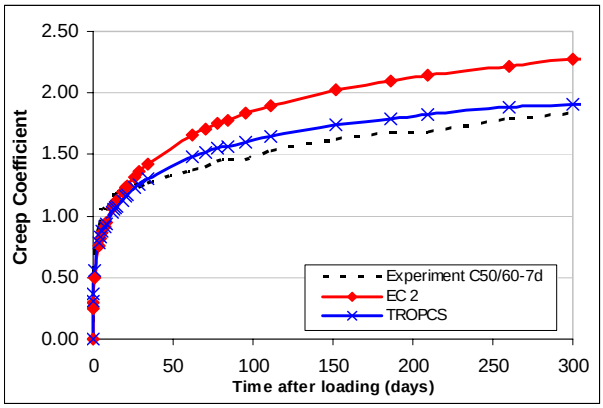

(a) C40/50 concrete tested in controlled room

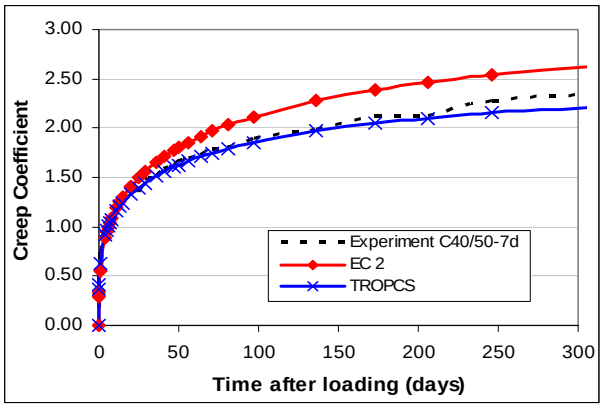

(b) C50/60 concrete tested in controlled room

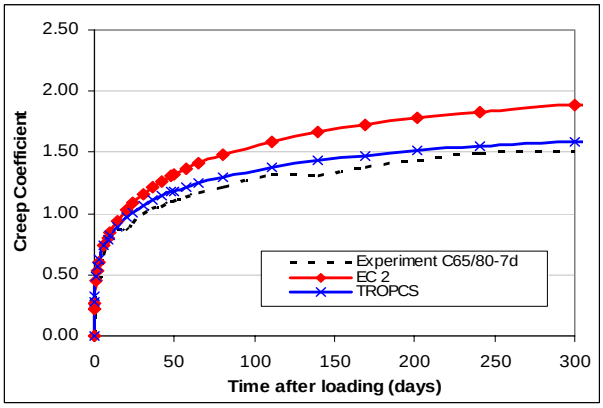

(c) C65/80 concrete tested in controlled room

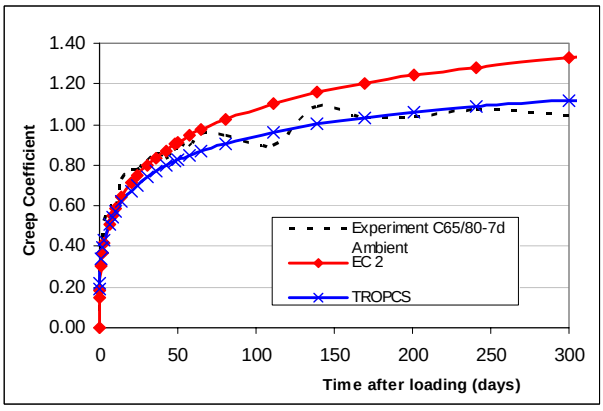

(d) C65/80 concrete tested in ambient condition

Figure 7.3 (a)-(d): Comparison between TROPCS creep modification and EC 2 predictions to experiment results for concrete tested at 7 days

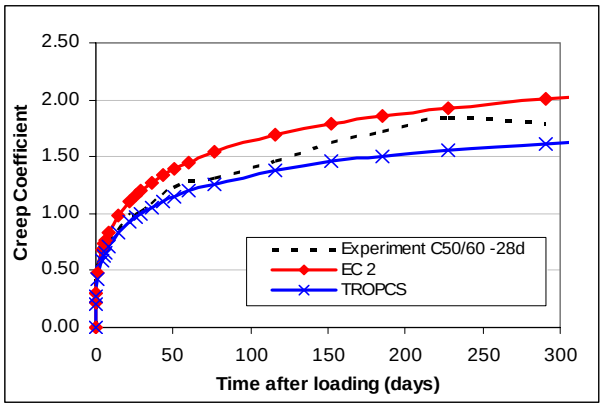

(a) C40/50 concrete tested in controlled room

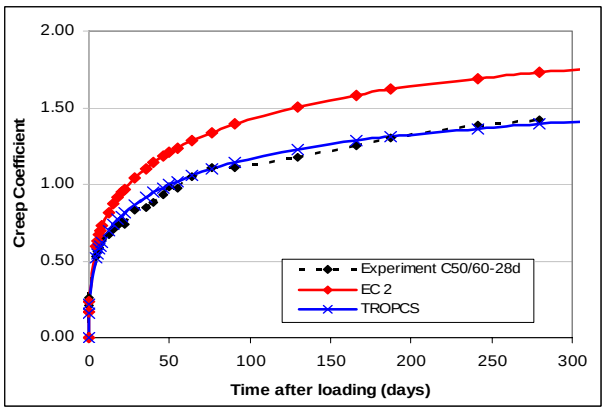

(b) C50/60 concrete tested in controlled room

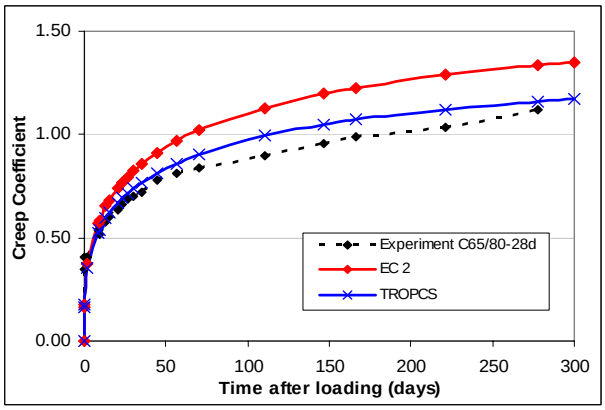

(c) C65/80 concrete tested in controlled room

Figure 7.4 (a)-(c) Comparison between TROPCS creep modification and EC 2 predictions to experiment results for concrete tested at 28 days

7.1.4 Statistical Verification of TROPCS Creep Prediction

Accuracy of the prediction by TROPCS and other codes predictions are assess through statistical analysis to the experiment results. Similar to the statistical methods adopted in sub-chapter 6.4, the assessment adopted are Residuals Analysis, *Re* which identifies over-prediction or under-prediction of a particular model, Error Percentage Method, *E(%)* Residuals Squared, Re^2 and coefficient of variation, V_m to determine the best prediction model ranking between the prediction models. The mean Residuals for TROPCS creep prediction and other models are presented in Table 7.4. The negative results denotes under prediction by the models as compared to the deformation of local concrete whereas positive values denotes over prediction. As shown in Table 7.4, it is observed that TROPCS generally exhibit the lowest *Re* values. This proves that the TROPCS prediction offers the closest recommendation to creep deformation of local concrete as compared to the other prediction models.

Table 7.4: Comparison of creep coefficient mean residuals, *Re* for TROPCS and other models for concrete tested at 7 and 28 days

Prediction Models	**Age of loading = 7 days**				**Age of loading = 28 days**		
	C40/50	**C50/60**	**C65/80**	**C65/80 (Ambient)**	**C40/50**	**C50/60**	**C65/80**
EC2	-0.03	-0.07	0.005	-0.08	0.05	0.05	0.05
ACI209	-0.47	-0.27	-0.18	0.24	-0.08	-0.10	0.29
CEB-FIP	0.21	0.26	0.36	0.08	0.24	0.36	0.33
B3	-0.11	0.07	0.42	0.35	-0.05	0.17	0.32
AS3600	0.26	0.15	0.43	0.29	0.38	0.37	0.55
TROPCS	**-0.04**	**-0.022**	**0.08**	**-0.04**	**-0.02**	**-0.01**	**0.01**

Error percentage indicates the percentage of residual from the prediction of each model, as given in Equation (6.3) and the Residuals squared defines the precision of the prediction to experimental results. Residuals squared is defined in Equation (6.4). As explained in sub-chapter 6.4, smaller Residuals squared signifies better prediction model.

Coefficient of variation is a common tool adopted by most models to measure the degree of accuracy of the prediction recommendation, as defined in Equation 6.5. The lower the value of V_m, the more accurate is the prediction. As proposed by ACI Committee 209, a model that could predict coefficient of variation for shrinkage within 15% would be excellent, and 20% would be adequate. This magnitude can be referred as a benchmark to assess the model accuracy. In Appendix B of EC2, it is stated that the mean coefficient of variation of the predicted creep data, deduced from a computerised data bank of laboratory test results, is of the order of 20%. As for shrinkage, it is stated in Clause 3.1.4 (6) in the EC2 that the coefficient of variation is at 30%. It should be noted that the accuracy of the models is limited by the many variables and measurement variability. Practically, based on the progress of current creep and shrinkage model development, models with coefficient of variation within 20% are recognised to be acceptable.

Table 7.5 presents the values of Error Percentage, *E(%),* Residuals squared, Re^2 and coefficient of variation, V_m of TROPCS and other models for creep predictions ranking. The ranking is determined from the model with lowest statistical values when compared to the actual experimental results. As observed, the best prediction model for concrete under tropical condition as shown in Table 7.5 is the TROPCS prediction developed from this research. The coefficient of variation for TROPCS creep prediction is at 10.8%, which is better than the proposed benchmark of 15%.

Table 7.5: Overall creep coefficient prediction models ranking

Age at test	Concrete grade	Prediction Models																	
		EC2			ACI209			CEB-FIP 1990			B3			AS3600			TROPCS		
		E (%)	R^2	V_m	E (%)	R^2	V_m	E (%)	R^2	V_m	E (%)	R^2	V_m	E (%)	R^2	V_m	E (%)	R^2	V_m
7 days	C40/50	-5.80	0.01	11.2	-37.46	0.22	41.3	10.22	0.08	19.0	0.89	0.03	16.0	10.46	0.17	53.8	-3.49	0.003	5.1
	Ranking	3	2	2	6	6	5	4	4	4	1	3	3	5	5	6	2	1	1
	C50/60	-10.01	0.03	21.2	-27.53	0.11	37.3	14.97	0.17	32.1	12.23	0.18	28.8	19.91	0.16	48.8	-1.96	0.01	13.1
	Ranking	2	2	2	6	3	5	4	5	4	3	6	3	5	4	6	1	1	1
	C65/80	-2.56	0.005	8.2	-15.49	0.04	21.8	35.76	0.17	41.4	53.20	0.45	48.9	35.44	0.30	50.3	6.18	0.01	14.5
	Ranking	1	1	1	3	3	3	5	4	4	6	6	5	4	5	6	2	2	2
	C65/80 (Ambient)	-13.02	0.01	19.8	19.01	0.13	45.2	6.97	0.02	20.0	41.92	0.18	51.9	27.31	0.19	53.3	-4.43	0.004	10.59
	Ranking	3	2	2	4	4	4	2	3	3	6	5	5	5	6	6	1	1	1
28 days	C40/50	2.49	0.01	8.8	9.09	0.02	23.6	19.88	0.08	25.3	14.28	0.11	34.1	27.93	0.22	40.4	-2.47	0.004	6.83
	Ranking	2	2	2	3	3	3	5	4	4	4	5	5	6	6	6	1	1	1
	C50/60	3.19	0.005	7.9	-17.82	0.01	24.7	38.14	0.16	43.9	38.41	0.27	38.2	34.42	0.18	37.6	-0.62	0.001	5.50
	Ranking	2	2	2	3	3	3	5	4	6	6	6	5	4	5	4	1	1	1
	C65/80	2.40	0.013	23.4	30.34	0.16	57.9	40.00	0.15	55.2	61.52	0.48	71.1	66.21	0.40	70.0	3.26	0.010	15.50
	Ranking	1	2	2	3	4	4	4	3	3	5	6	6	6	5	5	2	1	1
Sum		40			81			84			100			110			26		
Ranking		**2**			**3**			**4**			**5**			**6**			**1**		

7.2 Development of TROPCS Shrinkage Factors

The experimental results and codes evaluation on shrinkage models in Chapter 6 reveals that the prediction by CEB-FIP 1990 best exhibits the results of concrete in the tropical climate. However due to the fact that the British Standards are more commonly used in this region and local practices are more familiar with this code, TROPCS is developed with reference to EC 2, that supersedes BS 8110. The EC 2 is the second best prediction for shrinkage as assessed in sub-chapter 6.4.2. Based on the experimental results, TROPCS factors are introduced through empirical modification in order to improve the prediction of shrinkage for local concrete. The EC 2 shrinkage prediction equations are presented as Equation (7.6).

$$\varepsilon_{cd}(t) = \frac{(t - t_s)}{(t - t_s) + 0.04\sqrt{h_o^3}} \cdot k_h \cdot \varepsilon_{cdo} \qquad (7.6)$$

where

$$\varepsilon_{cdo} = \cdot 1.55\left[1 - \left(\frac{RH}{RH_o}\right)^3\right] \cdot 0.85\left[(220 + 110 \cdot \alpha_{ds1}) \cdot \exp\left(-\alpha_{ds2} \cdot \frac{f_{cm}}{f_{cmo}}\right)\right] \cdot 10^{-6}$$

t = age of concrete at the time considered (days)

t_s = age of concrete when drying begins (days)

k_h = is a coefficient depending on notional size and is provided in Table A1.1 in Appendix A1

ε_{cdo} = nominal unrestrained shrinkage strain

α_{ds1} = coefficient which depends on the type of cement

α_{ds2} = coefficient which depends on the type of cement

f_{cmo} = 10 MPa

RH_o = 100%

The modification introduced are the inclusion of a power coefficient at the time effect, S_1 and a correction factor for RH, S_2 as shown in Equation (7.7-a) or the simplification in Equation (7.7-b). The notations for these two equations are as defined in Equation (7.6).

$$\varepsilon_{cd}(t) = \left(\frac{(t-t_s)}{(t-t_s)+0.04\sqrt{h_o^3}}\right)^{S_1} . k_h . S_2 \cdot 1.55\left[1-\left(\frac{RH}{RH_o}\right)^3\right] .$$

$$0.85\left[(220+110\cdot\alpha_{ds1})\cdot\exp\left(-\alpha_{ds2}\cdot\frac{f_{cm}}{f_{cmo}}\right)\right]\cdot 10^{-6} \qquad (7.7\text{-a})$$

$$\varepsilon_{cd}(t) = \left(\frac{(t-t_s)}{(t-t_s)+0.04\sqrt{h_o^3}}\right)^{S_1} . k_h . S_2 \cdot \varepsilon_{cdo} \qquad (7.7\text{-b})$$

The TROPCS shrinkage factors are derived based on a two steps analysis method, involving experimental-prediction ratio and logarithmic expressions. The first step was to determine the RH correction factor, S_2 based on the experiment measurements. The shrinkage equation was rearranged from Equation (7.7-b) to Equation (7.8) to acquire the shrinkage RH coefficient, based on ratio method for every result recorded at different time period, $S_2(t)$. The correction ratio S_2 was then obtained based on an average of $S_1(t)$. Inclusion of these new parameters help in controlling the general magnitude of shrinkage prediction and will be discussed in detail in sub-chapter 7.2.3.

$$S_2(t) = \left[\frac{\varepsilon_{cd}(t)}{\left((t-t_s)/(t-t_s)+0.04\sqrt{h_o^3}\right)\cdot k_h\cdot\varepsilon_{cdo}}\right] \qquad (7.8)$$

Subsequently, incorporating the new RH correction factor, S_2 the second step involved converting Equation 7.7-b into a logarithmic expression to determine the power constant, S_1 for the hyperbolic time function. The logarithmic expression for the shrinkage prediction is as given in Equation 7.9. Referring to the logarithmic expression, the factor S_1 is determined from the gradient of Log $\left[\frac{\varepsilon_{cd}(t)}{k_h\cdot r'\cdot\varepsilon_{cdo}}\right]$ versus Log $\left(\frac{(t-t_s)}{(t-t_s)+0.04\sqrt{h_o^3}}\right)$ graph plotted based on the measured shrinkage results.

The results and discussion on TROPCS shrinkage factors based on empirical analysis for concrete with age of drying at 7 days and 28 days are discussed in sub-chapter 7.2.1 and sub-chapter 7.2.2, respectively.

$$LOG\left[\frac{\varepsilon_{cd}(t)}{k_h \cdot S_2 \cdot \varepsilon_{cdo}}\right] = S^1 . LOG\left(\frac{(t-t_s)}{(t-t_s)+0.04\sqrt{h_o^3}}\right) \quad (7.9)$$

7.2.1 Development of TROPCS Shrinkage Factors for Concrete Tested at 7 Days

The development of the TROPCS shrinkage factors involved two stages, as explained in sub-chapter 7.2. Thus the coefficient for RH, S_2 for different concrete strength developed based on empirical ratio are presented in Table 7.6. The multiplication factors computed are within the range of 1.14 to 1.33. The S_2 factor for C65/80 tested under ambient condition however varies further from the other concrete strengths, with a magnitude of 1.87. The range of results is anticipated between concrete of different strength as to the fact that the concrete were batched at different times. Moreover the heterogeneous nature of concrete and the manner in which it is affected by many variables, especially the different exposure condition are contributing factors to the deviation.

For the benefit of simplifying the prediction equations, one value for S_2 is introduced from averaging the values from C40/50, C50/60 and C65/80 tested under controlled condition. Thus the value for the coefficient S_2 developed from this research for the high strength concrete is 1.24.

Logarithmic graphs to determine the time function power coefficient, S_1 for different concrete strength with drying starting at the age of 7 days are plotted in Figure 7.5 (a) to (d). The gradient of each graph represents the power coefficient, S_1 for the time function of shrinkage strain. The consistency of the prediction through this analysis to experimental values is assessed through the Pearson residuals squared

plotted in each graphs. It is observed that the residuals squared are within the range of 0.90 to 0.96. The lowest residual squared value of 0.90 is from the analysis for specimens stored in the ambient condition. The irregularity in shrinkage deformation due to the variation in temperature and RH caused a higher dispersion of experimental results from the linear graph pattern.

The TROPCS factor S_1 derived from the analysis for each concrete strength is summarized in Table 7.6. It shall be noted that the power coefficient controls the magnitude of initial shrinkage and it is observed that these power coefficients are within the range of 1.48 to 1.33. Similar to the condition of S_2, the S_1 factor for C65/80 tested under ambient is much higher than the general range. The S_1 value is at 1.87. Higher power coefficients results in lower initial shrinkage strain and this explains the high S_1 value for the C65/80 specimens tested under ambient condition with high RH. For the benefit of simplification in prediction calculation, an average factor of 1.24 is adopted for S_1. The averaging of S_1 excludes the value from C65/80 tested under ambient due to the high magnitude. Comparison of the prediction model and the experimental results as well as the statistical analysis of the prediction model will be further discussed in sub-chapter 7.2.4.

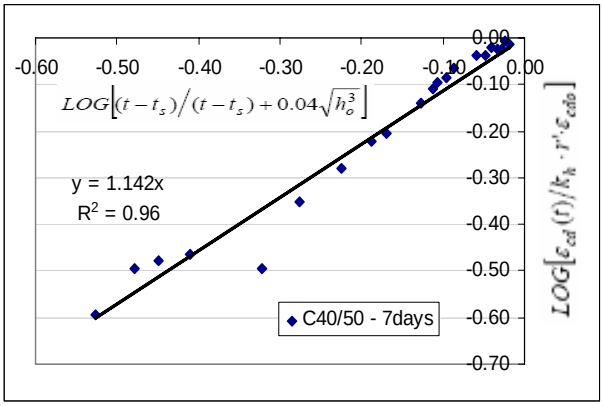

(a) C40/50 stored in controlled room

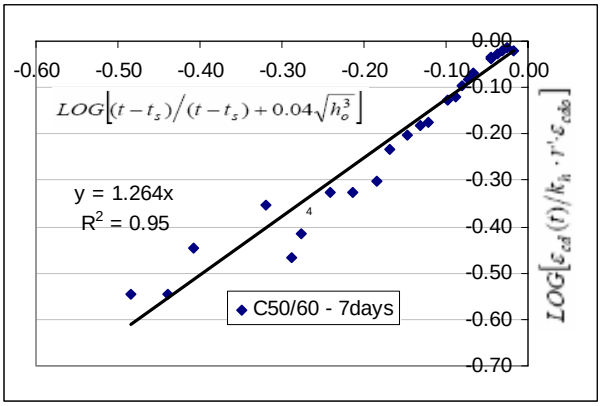

(b) C50/60 stored in controlled room

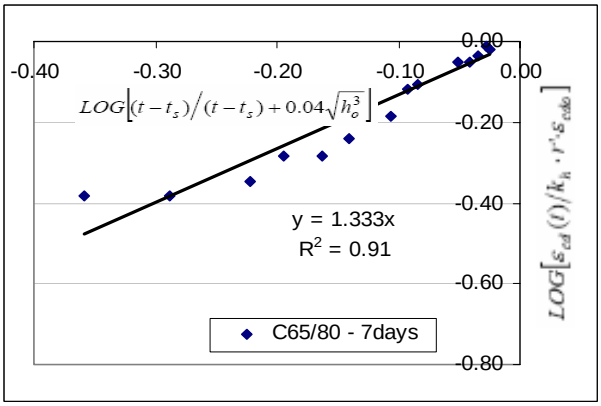

C65/80 stored in controlled room

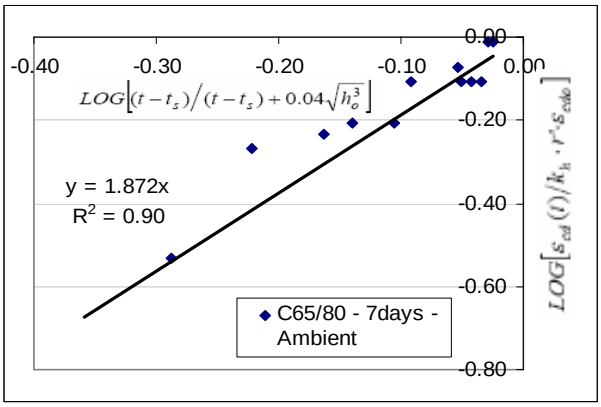

(d) C65/80 stored in ambient condition

Figure 7.5 (a)-(d): Logarithmic analysis for TROPCS shrinkage factors for concrete tested at 7 days

Table 7.6: TROPCS shrinkage factors for concrete tested at age 7 days

Concrete Class	S_1	S_2
C50	1.05	1.14
C60	0.99	1.26
C80	0.90	1.33
C80 Ambient	0.86	1.87
Average	**0.98**	**1.24**

7.2.2 Development of TROPCS Shrinkage Factors for Concrete Tested at 28 Days

The shrinkage modification factors for concrete dried at 28 days are presented in this section. Table 7.7 summarises the value of S_1 and S_2 for the three concrete classes tested at 28 days under controlled condition. Through the empirical ratio, the modification factor S_2 is found to be within the range of 0.89 to 1.00. The range of results for the three concrete classes is small. Therefore simplification process of averaging the modification factor of the three concrete classes is introduced. The average S_2 value is at 0.94, as shown in Table 7.7.

Figure 7.6 (a) to (c) presents the logarithmic plot for the empirical analysis of the time effect power coefficient, S_1. Values of the S_1 coefficient, which is obtained from the gradient of the graphs, are summarized in Table 7.7. Based on a range of results within 1.35 to 1.55, the average of the three concrete strength of 1.46 is adopted. The consistency of the logarithmic plot and also the accuracy of the analysis results to the experiment is assessed through the Pearsons residual squared. As presented in Figure 7.6 (a) to (c), the residual squared of the 28 day shrinkage analysis is between 0.88 and 0.95. With 1.0 indicating the best statistical consistency, the residual squared of this shrinkage analysis is within a reasonable range.

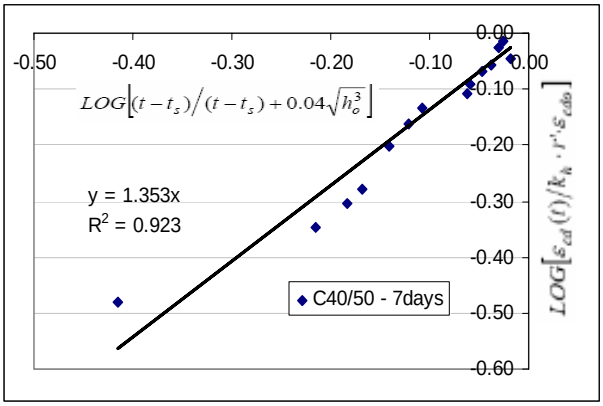

(a) C40/50 stored in controlled room

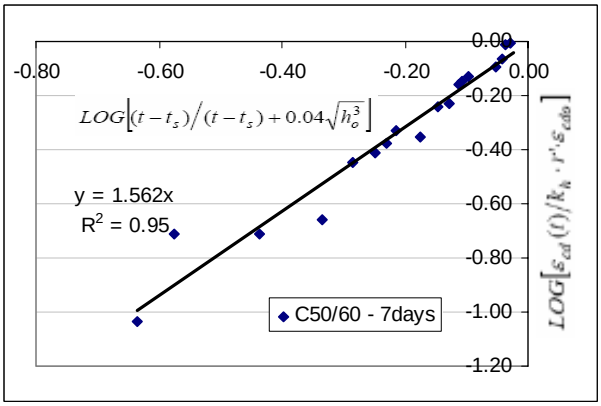

(b) C50/60 stored in controlled room

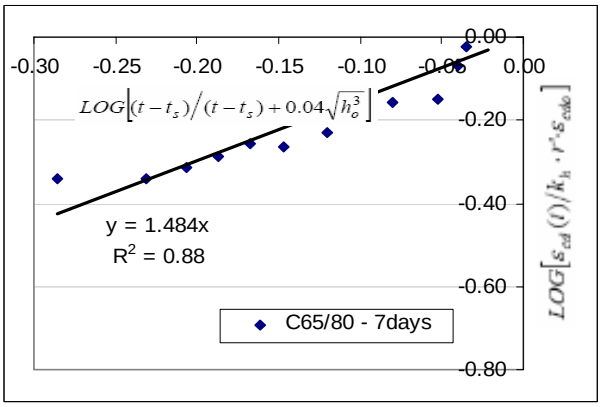

(c) C65/80 stored in controlled room

Figure 7.6 (a)-(c): Logarithmic analysis for TROPCS shrinkage factors for concrete tested at 28 days

Ultimately with the results from extensive experimental research and empirical analysis, the TROPCS time power factor, S_1 is at 1.24 and 1.46 for concrete tested at 7 days and 28 days, respectively. As for the TROPCS RH modification factor, S_2 is at 0.98 and 0.94 for concrete cured for 7 days and 28 days, respectively.

Table 7.7: TROPCS shrinkage factors for concrete tested at 28 days

Concrete Class	S_1	S_2
C50	1.00	1.35
C60	0.89	1.55
C80	0.93	1.48
Average	**1.46**	**0.94**

7.2.3 Discussion on TROPCS Shrinkage Prediction

Based on the codes comparison to shrinkage of concrete tested in this research, the prediction of EC 2 is proven to be the best suited prediction model for local concrete. Through the comparison study conducted in Chapter 6, it is obvious that improvement can be introduced to this prediction model to suit for concrete exposed to tropical climate. Generally it is observed that the experimental results of shrinkage exhibit lower rate of shrinkage for the first 50 days after being exposed for drying as compared to EC 2. Subsequently, the long term shrinkage strain measured at 300 days after drying is also lower than the prediction by EC 2. Therefore the modification factors introduced here is to correct the shrinkage versus time curve pattern to be applicable for tropical concrete.

The modified shrinkage prediction equation developed in this research based on EC 2 is shown in Equation (7.10). The modification factors, S_1 and S_2 developed for creep of HSC under tropical condition is summaried in Table 7.8.

$$\varepsilon_{cd}(t) = \left(\frac{(t-t_s)}{(t-t_s)+0.04\sqrt{h_o^3}}\right)^{S_1} . k_h . S_2 \cdot 1.55\left[1-\left(\frac{RH}{RH_o}\right)^3\right] .$$

$$0.85\left[(220+110\cdot\alpha_{ds1})\cdot\exp\left(-\alpha_{ds2}\cdot\frac{f_{cm}}{f_{cmo}}\right)\right]\cdot 10^{-6} \qquad (7.10)$$

Table 7.8: Summary of TROPCS shrinkage factors for concrete in tropical climate

Concrete Age at Loading (days)	S_1	S_2
7	1.43	0.97
28	1.46	0.94

The introduction of RH multiplication factor, S_2 of 0.97 and 0.94 for concrete dried at 7 and 28 days, respectively lowers the prediction of shrinkage strain to the magnitude measured from the experiment. The decline to the magnitude of prediction with the addition of S_2 resolves the long term under prediction of shrinkage by EC 2. It is observed however that the multiplication factor for concrete cured for 7 days is higher than for concrete cured at 28 days. The difference in the ratio may be attributed to the addition of slag in the concrete mixture, leading to a slower strength gain at the beginning of concrete age, thus more susceptible to shrinkage. At the age of 28 days, the concrete would have gained enough strength and even though the prediction by EC 2 is still lower than the actual case measured, the value of the RH multiplication factor is lower than the specified for 7 days.

With the long term prediction of shrinkage by EC 2 modified, the time effect power modification factor, S_1 is introduced to control the rate of initial shrinkage strain. Due to the fact that the time effect factor, bearing the function of $\left(\frac{(t-t_s)}{(t-t_s)+0.04\sqrt{h_o^3}}\right)$ results in more than 1.0, the power coefficients lowers the initial curve of the graph pattern. Through the empirical analysis the rate of initial

shrinkage prediction by EC 2 is reduced with the introduction of power modification factor, S_1 at 1.43 and 1.46 for concrete dried at age 7 and 28 days, respectively.

Figure 7.7 and Figure 7.8 compares the shrinkage strain from experiment results, prediction by EC 2 and also prediction with reference to TROPCS modification factors. The main objective is to examine the improvement introduced by TROPCS prediction. Figure 7.7 (a) to (d) presents the comparison for concrete of different strength with age of drying at 7 days while Figure 7.8 (a) to (c) presents the comparison for concrete with age of drying at 28 days. For reference purposes, the calculation for TROPCS and EC 2 shrinkage predictions for concrete tested at 7 and 28 days are presented in Appendix F3 and F4, respectively.

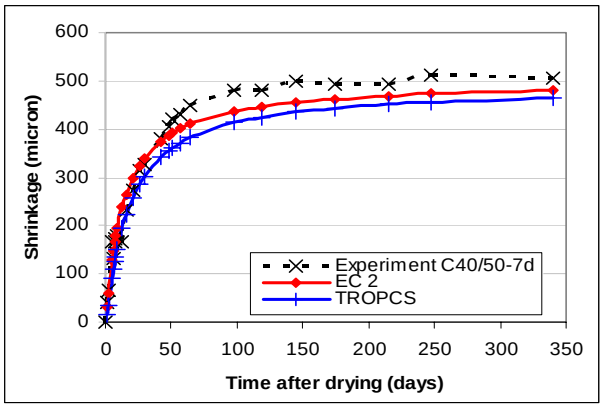

(a) C40/50 concrete in controlled room

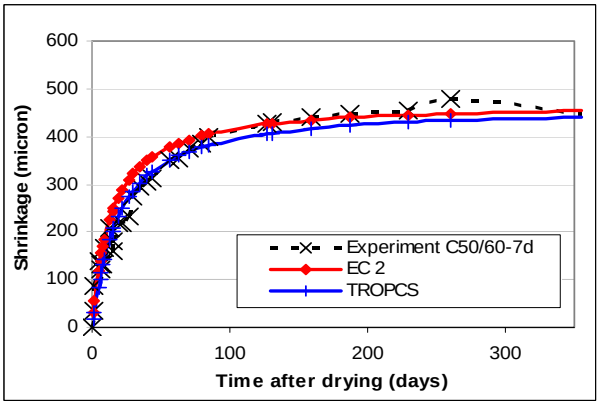

(b) C50/60 concrete in controlled room

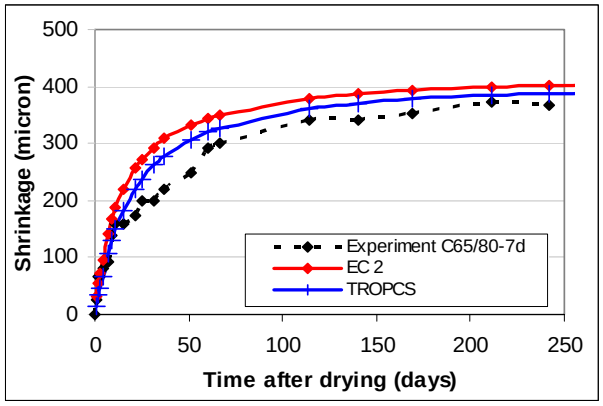

(c) C65/80 concrete in controlled room

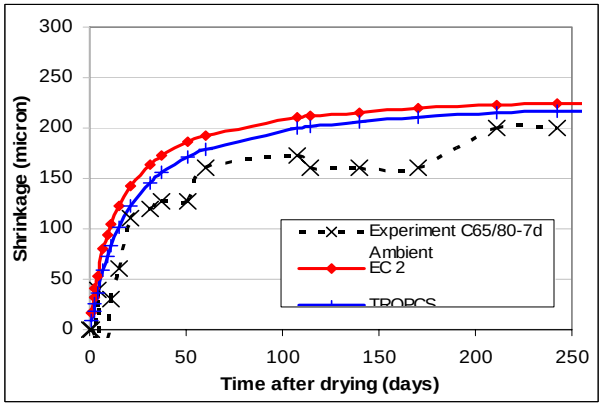

(d) C65/80 concrete in ambient condition

Figure 7.7 (a)–(d): Comparison between TROPCS shrinkage modification and EC 2 predictions to experiment results for concrete tested at 7 days

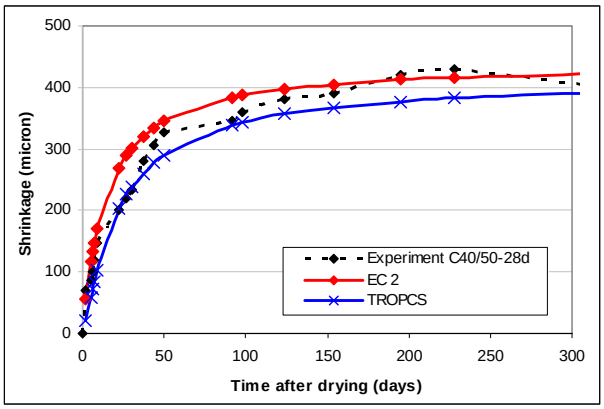

(a) C40/50 concrete in controlled room

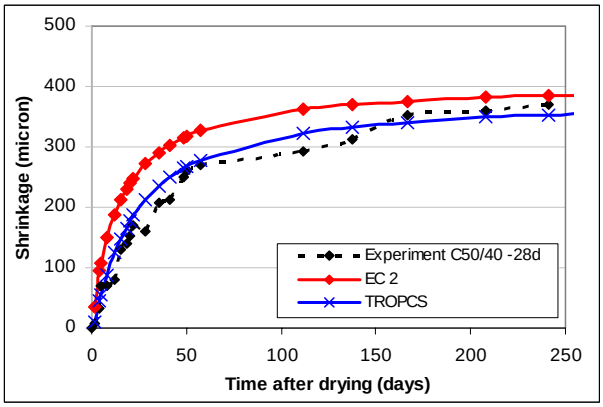

(b) C50/60 concrete in controlled room

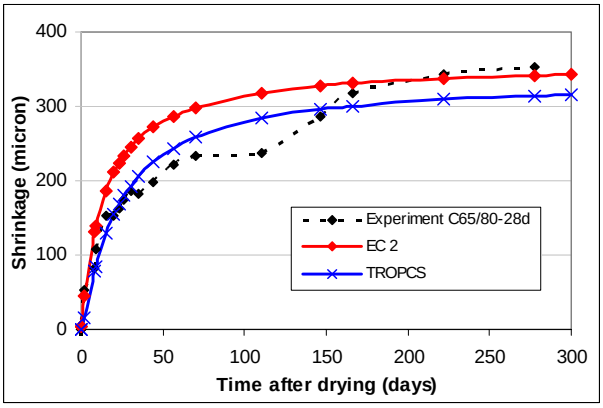

(c) C65/80 concrete in controlled room

Figure 7.8(a)–(c): Comparison between TROPCS shrinkage modification and EC 2 predictions to experiment results for concrete tested at 28 days

7.2.4 Statistical Verification of TROPCS Shrinkage Prediction

The accuracy of the modified shrinkage prediction to the experimental measurement is assessed through statistical analysis presented and discussed in this section. Similar to the statistical assessment conducted for creep prediction, the analyses involved are Residuals Analysis, Error Percentage and Residuals Squared. The statistical analysis of the other prediction methods discussed in Chapter 6 are also presented here as a guide to determine the level of accuracy of the modified prediction, for comparison purpose.

The Mean Residuals which identifies the over-prediction or under-prediction of the prediction models are presented in Table 7.9. Negative value signifies under-prediction of the model to experimental value whereas positive value indicates otherwise. With reference to Table 7.9, the mean residuals for TROPCS shrinkage prediction are within the range of -33.7 μm to 33.2 μm. Considering the final shrinkage measured is averagely at 400 μm, the percentage of mean residuals of TROPCS prediction is at an acceptable range of less than 10%.

Table 7.9: Comparison of creep coefficient mean residual for Modified Shrinkage and other Prediction Models for Concrete Tested at 7 and 28 days

Prediction Models	**Age of loading = 7 days**				**Age of loading = 28 days**		
	C40/50	**C50/60**	**C65/80**	**C65/80 (Ambient)**	**C40/50**	**C50/60**	**C65/80**
EC2	-9.6	21.9	44.5	54.9	29.0	64.9	41.8
ACI209	34.7	58.9	103.7	160.2	42.5	89.8	106.8
CEB-FIP	-30.0	-12.1	-1.7	32.2	11.6	29.5	-13.4
B3	3.4	36.2	83.1	78.3	93.4	125.8	127.3
AS3600	34.8	70.6	137.8	190.8	121.5	157.8	172.6
TROPCS	**-33.7**	**-3.2**	**18.2**	**33.2**	**-22.2**	**15.1**	**0.7**

Table 7.8 presents the shrinkage prediction ranking of TROPCS prediction and other prediction models. Similar to the analysis for creep, the ranking is made based on Error Percentage, *E(%)*, Residuals Squared, Re^2 and coefficient of variation,

V_m of each prediction models. As shown in Table 7.8, TROPCS shrinkage prediction developed in this research proves to provide the best prediction for concrete under tropical condition. It is then followed by the prediction by CEB-FIP 1990, EC 2, B3 Model, ACI-209 and lastly AS 3600. The average coefficient of variation for TROPCS is at 21.6%, lower than the range set by EC 2 at 30%. Thus it is concluded that the TROPCS prediction is the best prediction for shrinkage of concrete in the tropical climate.

Table 7.10: Overall shrinkage prediction models ranking

Age at test	Concrete grade	Prediction Models																	
		EC2			ACI-209			CEB-FIP 1990			B3			AS3600			TROPCS		
		E (%)	R^2	V_m	E (%)	R^2	V_m	E (%)	R^2	V_m	E (%)	R^2	V_m	E (%)	R^2	V_m	E (%)	R^2	V_m
7 days	C40/50	0.9	889	10.7	7.8	5516	26.0	-5.0	1933	13.8	0.6	938	10.8	11.4	2283	22.4	-11.1	1620	22.0
	Ranking	2	1	1	4	6	6	3	4	3	1	2	2	6	5	5	5	3	4
	C50/60	11.9	1417	16.7	11.8	7513	30.1	-1.0	575	10.5	12.7	1822	16.5	22.9	6636	36.4	-0.24	502	11.4
	Ranking	4	3	4	3	6	5	2	2	1	5	4	3	6	5	6	1	1	2
	C65/80	22.3	2801	28.9	34.5	19038	54.5	6.4	191	12.8	40.6	8444	47.9	65.5	22410	95.1	2.5	1056	19.8
	Ranking	3	3	3	4	5	5	2	1	1	5	4	4	6	6	6	1	2	2
	C65/80 (Ambient)	-1.1	4167	42.7	77.5	33061	157.4	-18.9	2554	19.4	48.3	7256	60.2	190.8	75783	285	-8.9	2337	30.0
	Ranking	1	3	3	5	5	5	3	2	1	4	4	4	6	6	6	2	1	2
28 days	C40/50	16.6	1335	20.5	9.3	3077	22.3	11.5	362	17.6	42.8	10070	89.1	64.6	15936	73.8	-13.0	749	17.2
	Ranking	4	3	3	1	4	4	2	1	2	5	5	6	6	6	5	3	2	1
	C50/60	45.1	4977	86.6	46.7	10279	58.2	22.1	1320	74.9	73.6	16750	92.8	109.5	27587	169.9	11.1	576	22.1
	Ranking	3	3	4	4	4	2	2	2	3	5	5	5	6	6	6	1	1	1
	C65/80	15.8	2583	42.2	38.7	16476	60.2	-18.2	723	21.6	50.6	19378	95.9	88.2	35154	120.0	1.0	542	24.6
	Ranking	2	3	3	4	4	4	3	2	1	5	5	5	6	6	6	1	1	2
Sum		59			90			43			88			122			39		
Ranking		**3**			**5**			**2**			**4**			**6**			**1**		

7.3 Verification of TROPCS Prediction to Structural Deformation

Models are always a compromise between accuracy and convenience. The accuracy of the models depends on the constitutive approach used and the size of the data referred for derivations. In most cases, variability in shrinkage and creep measurements and the heterogeneous structure of concrete inhibit prediction models from closely matching experimental data. The coefficient of variation for creep and shrinkage from this study, as presented in Chapter 6 is approximately 17.5% and 16.3%, respectively. Therefore due to the variability in concrete batches, it would be unrealistic to expect results from prediction models to be lower than ±20% of the test data. The applicability and accuracy of the proposed TROPCS creep and shrinkage prediction is assessed and the variation of prediction to the actual structural deformation of 20% is taken as an acceptable range.

7.3.1 Prediction for Columns Deformation

The columns were tested for total time-dependent deformation consisting of creep and shrinkage. Based on the modification model developed for local concrete, the prediction of column deformation is compared to the actual column strain measured from the laboratory experiment. For the convenience in calculation, the predicted time-dependent deformation is calculated based on principle of superposition and with incorporation of creep reduction coefficient to capture the effect from the steel reinforcements.

In the case of reinforced concrete section, the time-dependent deflection is a function of the steel reinforcement area (Neville, 1983; Zou, 2003). The deformation of reinforced concrete members reduces due to the enhancement in strength by the reinforcing steel. For axially loaded columns, reinforcement will generally carry between 10% and 30% of the total capacity of the column (MacGregor, 1997). Theoretically, the change in strain for both steel and concrete is equal under the condition of perfect bonding. The deformation prediction of these structural members however can be treated as plain concrete members with the incorporation of creep reduction coefficient. Under the case with symmetrical reinforcement, as in the case

for the columns in this study, the reduction in deformation can be captured through the introduction of creep reduction coefficient, α_1 as given in Equation (7.11) (Neville, 1983). This creep reduction coefficient, α_1 is provided to capture the reduction in deformation due to the provision of steel reinforcement. Thus Equation (7.11) is a function of the steel area ratio as well as the steel modulus. The total time-dependent axial strain of columns, ε_{col} with the incorporation of creep reduction coefficient is calculated from Equation (7.12).

$$\alpha_1 = \frac{1}{1+\rho n_o\left[1+\phi(t,t_o)\right]} \tag{7.11}$$

$$\varepsilon_{col} = \alpha_1\left[\frac{\sigma}{E_c}\phi(t,t_o)+\varepsilon_{sh}(t,t_o)\right] \tag{7.12}$$

where

ρ = steel reinforcement ratio

n_o = material modulus ratio = E_s/E_c

$\phi(t,t_o)$ = creep coefficient from at time t

σ = axial stress on columns

E_c = modulus of elasticity of concrete at 28 days

ε_{sh} = shrinkage strain at time t

The strain predictions are calculated with reference to the proposed TROPCS recommendations. Shrinkage strain, ε_{sh} is calculated based on Equation (7.10) and the creep coefficient, ϕ is calculated from the proposed creep coefficient as in Equation (7.5). The concrete properties referred for the prediction calculation are based on the results obtained from the laboratory concrete properties testing. The predicted time-dependent deformation of the columns, ε_{col} is then compared to the measured laboratory results as well as the prediction deformation by EC 2.

In Figure 7.9 (a) and (b), the new prediction results are compared to the laboratory measurements tested in controlled environment for C40/50 and C65/80 columns, respectively. The comparison between prediction and measured strain for C65/80 columns tested under ambient condition is presented in Figure 7.9 (c). The

prediction by EC2 is incorporated for comparison purpose to identify the better prediction model. With reference to Figure 7.9 (a) to (c), the general trend observed is that the measured strain is lower than the prediction values. On an average, the modified prediction is 13.4% higher than the experimental results whereas the prediction by EC2 is at 24.8% higher. Even with the inclusion of creep reduction coefficient, α_1 the actual column behaviour is still lower than theoretical calculation. One of the explanations may be due to the inclusion of shear links which help to enhance the strength of concrete, lowering the shrinkage strain of the specimens.

The coefficient of variation for TROPCS prediction and EC 2 prediction for the columns are summarized in Table 7.11. Practically, the coefficient of variation for TROPCS prediction is at a consistent 18% to 20% range with an average of 19.5%. With consideration that fluctuation of actual deformation is difficult to predict and common statistical variation is at the order of 20%, the deviation is considered as an acceptable range. However, as for EC2, the statistical analysis slightly exceeded the 20% limitation, with an average coefficient of variation at 26.9%. It can be concluded that TROPCS prediction provides better recommendation for time-dependent deformation when compared to EC 2 prediction.

Table 7.11: Coefficient of variation of TROPCS and EC 2 for columns specimens

Columns Specimens	**Coefficient of variation, V_m (%)**	
	TROPCS	**EC 2**
C40/50–Control	20.4	20.2
C65/80–Control	18.2	30.4
C65/80–Ambient	19.8	30.2
Average	**19.5**	**26.9**

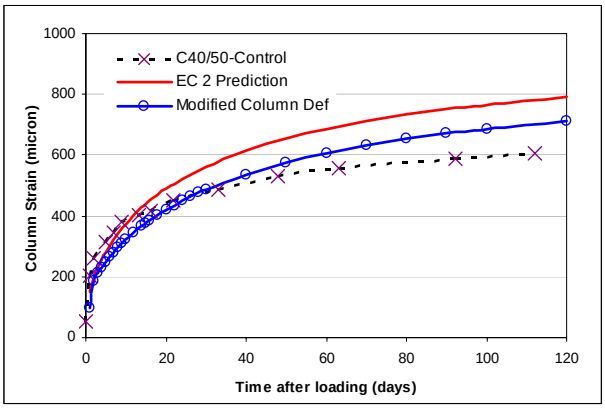

(a) C40/50 concrete tested in controlled room

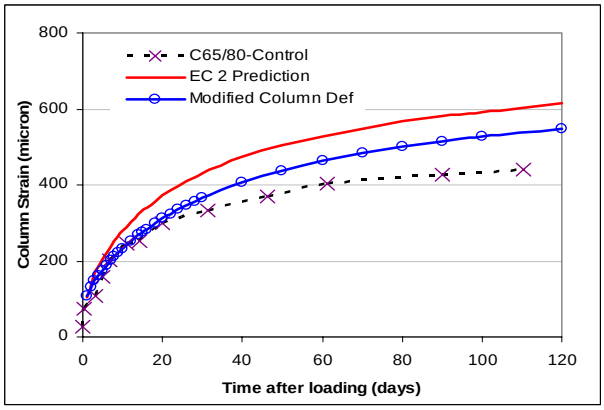

(b) C65/80 concrete tested in controlled room

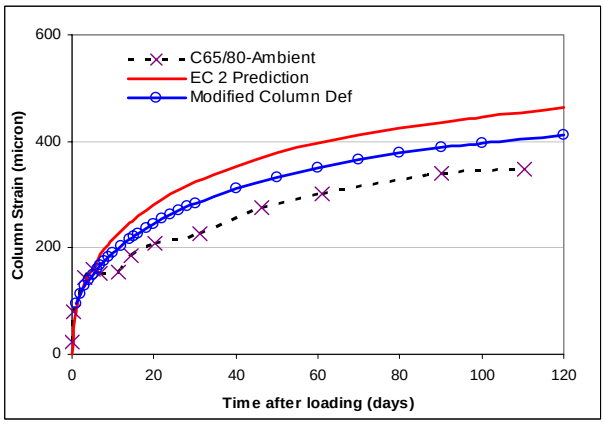

(c) C65/80 – concrete tested under ambient condition

Figure 7.9: Comparison of column deformation between TROPCS, EC 2 and experiment results for concrete tested at 7days

7.3.2 Pre-camber of Pre-tensioned Prestressed Concrete Beams

In the construction process, accuracy in the prediction of short-term deflection is important to ensure that the deflection of structural members is controlled within the allowable range and also to provide for the aesthetic values. Therefore a good accuracy on the short-term deflection, especially upward deflection is vital for a smooth construction process. Before the evaluation on the accuracy of TROPCS prediction on measured pre-camber is carried out, explanation on calculation method for pre-camber is first explained in sub-chapter 7.3.2.1.

7.3.2.1 Calculation Estimation for Pre-camber

Pre-camber resulting from prestressing force can be calculated either on the basis of curvatures, moment-area method, or based on the equivalent weight method (Nilson, 1978). The common practice in the local design context is based on the equivalent weight method in which the elastic modulus are usually taken directly from BS 8110 with reference to the respective concrete strength. Deflections due to the dead and live loads are calculated as of any other flexural members, and to obtain the total deflection, the deflection due to prestressing force and all the deflections that are calculated separately are superimposed.

According to the equivalent weight method, the upward deflection, δ_{pi} at the mid-span of a uniformly loaded simply supported beam is obtained from Equation (7.12), when the tendon profile is straight. The sagging of beam, δ_o is calculated based on Equation (7.13), which is developed from Equation (7.12) with *Pe* being substituted by moment due to the dead load. The resultant short-term or instantaneous deflection is obtained from Equation (7.14) in which the hogging produced by the prestressing force is deducted by the sagging due to the self-weight of the beam. These equations resulted in pre-camber at mid span. However the deflection at other locations can be obtained assuming that the deflection profile is a perfect parabolic curvature.

This brief calculation method only provides an approximate estimation as the accuracy is compromised due to the over simplified calculation. It is highlighted that none of the parameters in the equations are time-dependent and only short term prestress losses are taken into account through the prestressed force after initial losses, *P*. Based on this prediction, the pre-camber is not considered as a time-dependent behaviour. Another point to note is that elastic modulus is the only reference made to the concrete property and in most cases, this elastic modulus is determined from BS 8110 based on specified concrete strength. Deviation in elastic modulus taken from foreign codes further intensifies the digression.

$$\delta_{pi} = \frac{Pel^2}{8EI} \quad (7.12)$$

$$\delta_o = \frac{5wL^4}{384\,E_c I_c} \quad (7.13)$$

$$\delta_{c\text{-}short\text{-}term} = -\delta_{pi} + \delta_o \quad (7.14)$$

where

δ_{pi} = upward deflection of beam

δ_o = sagging of beam due to self-weight

$\delta_{c\text{-}short\text{-}term}$ = resultant deflection from hogging and sagging effect

L = beam length

E_c = elastic modulus of concrete

I_c = moment of inertia of section

P = prestressing force after initial losses

e = eccentricity of tendon

w = dead load computed from the self weight of the beam.

In achieving better prediction accuracy, creep factor has to be considered in the initial deflection prediction and in prestress losses calculation. This recommendation is valid as creep occurs even at an early stage during loading and has been widely adopted (Neville, 1990; Nilson 1978). Creep strain affects the deflection in two opposite ways. While it produces loss of prestress force, tending to reduce the pre-camber, creep strains in the concrete usually increase negative

curvatures and hence, increase the pre-camber. Generally the second effect predominates and pre-camber increases with time, in spite of the reduction of prestress loss (Nilson, 1978).

With the incorporation of creep coefficient in the prestress losses, the upward deflection is given as Equation (7.15), as proposed by Nilson (1978). δ_{pe} is the midspan deflection due to prestressing after taking prestress losses into consideration. Both δ_{pi} and δ_{pe} are calculated based on Equation (7.12) for prestress beam with straight tendon profile. The first term in Equation (7.15) is the initial negative curvature and the second term is the reduction in that initial curvature because of the loss of prestress. The third term is the increase in negative curve because of concrete creep through the incorporation of creep coefficient, ϕ. Important approximation made is that creep occurs under a constant prestress force, equal to the average of the initial and final values, as expressed in the equation.

The deflection due to self weight is also modified by creep and may be obtained by applying the creep coefficient to the instantaneous value. Thus the downward deflection is obtained through Equation (7.16) with δ_o being calculated based on Equation (7.13). Using the principle of superposition, the total member deflection formulated from the summation of Equation (7.15) and Equation (7.16) is given by Equation (7.17). Through the study conducted by Saiidi (1998), this calculation formula has been proven to be a simple yet reasonably accurate for the prediction of prestressed member deflection.

$$\delta_{upwards} = -\delta_{pi} + \left(\delta_{pi} - \delta_{pe}\right) - \frac{\delta_{pi} + \delta_{pe}}{2}\phi \tag{7.15}$$

$$\delta_{downwards} = \delta_o(1+\phi) \tag{7.16}$$

$$\delta_{total} = -\delta_{pe} - \frac{\delta_{pi} + \delta_{pe}}{2}\phi + \delta_o(1+\phi) \tag{7.17}$$

where

ϕ = creep coefficient

δ_{pi} = upward deflection of beam as given by Equation (7.12)

δ_{pe} = upward deflection of beam with consideration of losses as given by Equation (7.12)

δ_o = sagging of beam due to self-weight as given by Equation (7.13)

δ_{total} = resultant deflection from hogging and sagging effect

7.3.2.2 TROPCS Prediction of Prestressed Beam Pre-camber

Using the simplified calculation method from Equation (7.12), the calculated pre-camber for the pre-tension prestressed beam is -0.87mm. Hogging deformation is presented in negative values in this thesis to distinguish from sagging, which is in positive values. This simplified prediction does not consider pre-camber as a time-dependent deformation. Thus the estimated value is assumed to be constant throughout the time period.

A better pre-camber prediction is based on Equation (7.17), taking into account the creep coefficient. For the purpose on validating the accuracy of TROPCS creep factors, the creep coefficient for Equation (7.17) is taken from TROPCS creep coefficient. For comparison to EC 2, the pre-camber is also predicted with reference to creep coefficient from EC 2. The average from measured PSB1 and PSB2 values, prediction computed from the simplified method and improved method incorporating TROPCS and EC 2 creep coefficient is presented in Table 7.12.

The difference between the measured results and the predictions is further illustrated through graph in Figure 7.10. Based on the graph, it is clearly seen that the simplified prediction value reflects the elastic deformation better even though this prediction refers to the ultimate pre-camber and is meant to be compared to pre-camber before loading. Generally the prediction of -0.87mm under predicts by approximately 31%.

For the improved predictions, a gradual curve after the instantaneous elastic strain is observed with the inclusion of creep coefficient. As shown in Figure 7.10, both the results with EC 2 and TROPCS creep coefficient reflect better prediction for the measured pre-camber and improvement is substantial. Mid-span deformation at 4

days after transfer, incorporating creep coefficient for EC 2 is at -1.26mm while the result by TROPCS is at -1.28mm. Unlike the theoretical prediction with a smooth increment curve, the laboratory measurement in Figure 7.10 does not show a gradual strain increment between the instantaneous strain and the time-dependent deformation at 1½ hours (0.05 days) after prestressing. This demarcates the difference between theoretical results which simulate an idealized model with gradual deformation and the actual condition when the prestressed beams were subjected to a jolted transfer in force along the short beam member.

Statistically, the coefficient of variation for pre-camber based on TROPCS and EC 2 creep coefficient is at 5.3% and 7.6%, respectively. The coefficient of variation for the simplified method is at 31.6%. Generally, the prediction by TROPCS factor under-estimates the pre-camber at an average of -2.9%. The prediction by EC 2 also under-estimates the pre-camber and the average percentage of error for EC 2 is at -5.6%. Based on the comparison, the prediction incorporating TROPCS creep provides a slightly better estimate. It is also interesting to note that the prediction with TROPCS creep exhibit higher strain than the EC 2 creep pre-camber. As it was explained earlier in the development of the modification, this is primarily due to the fact that the modified creep equation provides higher initial strain in the early age as compared to the EC 2 prediction. In addition to that, it is also worth noting that shrinkage estimation is not taken into account as the measurement datum was taken at 7 days after the specimens were exposed to drying.

Based on the study conducted here, it is concluded that the incorporation of creep into the calculation of pre-camber and deflection of prestressed beams is important even though the period between transfer and serviceability is short as compared to the designed structure life. The creep values recommended by TROPCS are also verified for its application for pre-camber of prestressed beams.

Table 7.12: Comparison of pre-camber of prestressed beams at mid-span from experiment results to TROPCS and EC 2 predictions

Time after prestressing (days)	Pre-camber (mm)			
	Average Experiment Measurement	Simplified Prediction	Improved Prediction (EC 2 ϕ)	Improved Prediction (TROPCS ϕ)
0.00	0.00	0.00	0.00	0.00
0.05	-1.17	-0.87	-0.97	-1.01
0.70	-1.21	-0.87	-1.10	-1.14
0.90	-1.21	-0.87	-1.12	-1.16
1.50	-1.22	-0.87	-1.16	-1.20
2.00	-1.26	-0.87	-1.19	-1.22
2.50	-1.27	-0.87	-1.21	-1.24
3.00	-1.26	-0.87	-1.23	-1.26
3.50	-1.26	-0.87	-1.24	-1.27
4.00	-1.26	-0.87	-1.26	-1.28

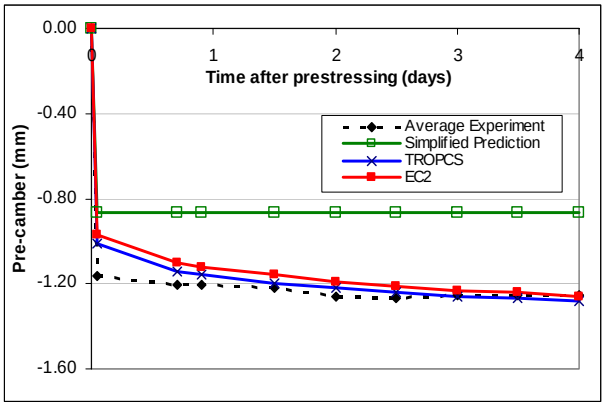

Figure 7.10: Comparison of pre-camber experimental results to improved prediction with TROPCS and EC 2 creep coefficient

7.3.3 Deflection of Pre-tensioned Prestressed Concrete Beams

Subsequent to the pre-camber measurement, the prestressed beams were loaded with concentrated load to assess the time-dependent deflection due to sustained load. Based on TROPCS prediction developed for local concrete, the

beams deflection is predicted and compared to the laboratory measurement. The deflection of prestressed beams due to two concentrated load points, δ_p is determined from Equation (7.18). The total downward deflection, $\delta_{d\text{-}short\text{-}term}$ as shown by Equation (7.19) is computed from superimposing δ_p with deflection due to self-weight, δ_o given by Equation (7.13). Direct application of Equation (7.18) and Equation (7.14) for deflection prediction is taken as a simplified calculation method. Similar to the prediction for pre-camber, these equations do not consider the effect of long-term deformation. Therefore, for a more accurate long-term prediction, the effect from creep has to be included. Beam deflection calculation incorporating creep coefficient is given in Equation (7.20).

$$\delta_p = \frac{P_L b}{24 E_c I_c}(3L^2 - 4b^2) \quad (7.18)$$

$$\delta_o = \frac{5wL^4}{384\, E_c I_c} \quad (7.13)$$

$$\delta_{d\text{-}short\text{-}term} = \delta_p + \delta_o \quad (7.19)$$

$$\delta_{def} = \delta_{d-short-term}(1+\phi) \quad (7.20)$$

where

δ_p = downward deflection of beam due to two-point load

δ_o = sagging of beam due to self-weight

$\delta_{d\text{-}short\text{-}term}$ = deflection from sagging effect

δ_{def} = deflection of beam incorporating creep coefficient

P_L = point load applied on the beam

L = beam span length

b = distance from the point load to the nearest beam support

E_c = elastic modulus of concrete

I_c = moment of inertia of section

w = dead load computed from the self weight of the beam.

Based on TROPCS creep values, accuracy of deflection prediction is assessed from the results of PSB1 and PSB2. The accuracy of three prediction methods are

analysed and compared to the average measured deflection as plotted in Figure 7.11. The first prediction is based on the simplified calculation method without incorporation of creep reduction as given by Equation (7.19). This results in deflection to the magnitude of 1.66mm consistently across the whole loading period. The TROPCS and EC2 prediction are calculated with inclusion of creep reduction factor, as provided by Equation (7.20). The difference between the two predictions is due to the creep prediction.

With reference to Figure 7.11, it is observed that the simplified prediction underestimated the deflection by almost half the experiment results. On an average, this simplified prediction is 45.0% lower than the laboratory measurements. As for the prediction incorporating creep reduction factors from TROPCS and EC 2, the calculated deflection for both are almost similar to the laboratory results. Statistically, the error percentage for TROPCS prediction is at 12.3% whereas the error percentage for EC2 is at 13.6%. The error percentage on the other hand is at 13.2% for TROPCS and 14.8% for EC 2. Smaller error percentage and coefficient of variation indicates that TROPCS calculation is a relatively better deflection prediction.

However it is noted that these two predictions underestimated the early-age deformation for the first 15 days. On an average, the underestimation for the first 15 days is at 14.1% for the modified prediction and at 16.0% for EC2. Even though differences are observed between the prediction and actual laboratory measurement during the early age of loading, the main concern for the case of beam deflection is the long term deflection. Therefore prediction for long term deflection is more critical and for this case, the long-term prediction is of satisfactory with a close magnitude to the experimental results.

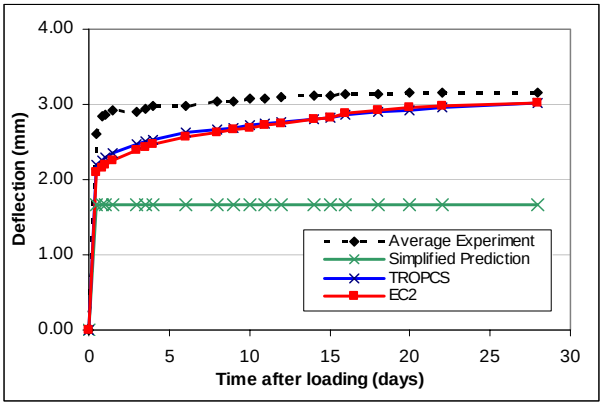

Figure 7.11: Comparison between the measured prestressed beams deflection and the prediction methods

7.3.4 Pre-camber of Post-tensioned Prestressed Beams on-Site

The post-tensioned prestressed beams tested on site are full sized beams with 36m length span and parabolic tendon profile. The calculation for pre-camber of post-tensioned beams is similar to the methods and equations given in sub-chapter 7.3.2.1. However, according to the equivalent weight method, the upward deflection, δ_{pi} at the mid-span of a simply supported beam with parabolic tendon profile is replaced by Equation (7.21). Subsequently all other calculation equations are similar to as presented in sub-chapter 7.3.2.1.

$$\delta_{pi} = -\frac{Pl^2}{8E_cI_c}\left[e_s + \frac{5}{8}(e_c - e_s)\right] \tag{7.21}$$

where

δ_{pi} = upward deflection of beam

δ_o = sagging of beam due to self-weight

$\delta_{c\text{-}short\text{-}term}$ = resultant deflection from hogging and sagging effect

L = beam length

E_c = elastic modulus of concrete

I_c = moment of inertia of section

P = prestressing force after initial losses

e = eccentricity of tendon

w = dead load computed from the self weight of the beam.

Figure 7.11 shows the profile of pre-camber of the four beams immediately after prestressing. The mid-span pre-camber of the four beams immediately after prestressing ranges from 37mm to 57mm and at 15 days after transfer, the pre-camber increased to a maximum of 75mm at the end of monitoring. With reference to Figure 7.11 and 7.12, it is observed that the pre-camber for the four beams are different even through the beams are designed using the same parameters. This difference in deformation may be due to the influence of various intrinsic such as concrete quality and properties as well as the extrinsic factors, consisting of the influence of the surrounding. Therefore information on properties and performance of concrete are important for prestressed concrete prediction. Method and sequence of placing concrete during production of beam can also affect the pattern and consistency of beam camber profile. During installation of post-tensioned cables, precaution has to be exercised as any changes in tendon's profile alignment will change the eccentricity of tendon from the neutral axis of beam and subsequently affect the cambering behaviour of the beam. Other site factors that may possibly influence beam camber are compaction of fresh concrete, curing process as well as the weather on concreting day. This result proves that an accurate estimation of beam pre-camber in bridge design is difficult to attain. Accurate estimation of camber cannot be obtained without a rational account of prestressed losses and an accurate prediction of the concrete properties (Tadros et al., 1975). Therefore time-dependent losses should be incorporated in the computation of pre-camber to avoid unnecessary error in prediction.

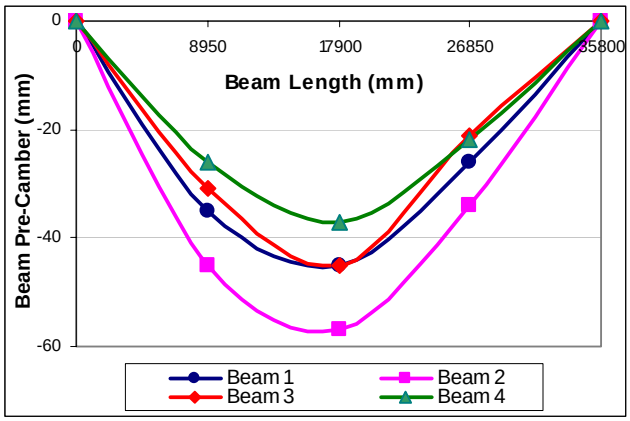

Figure 7.12: Beam pre-camber measured immediately after prestressing

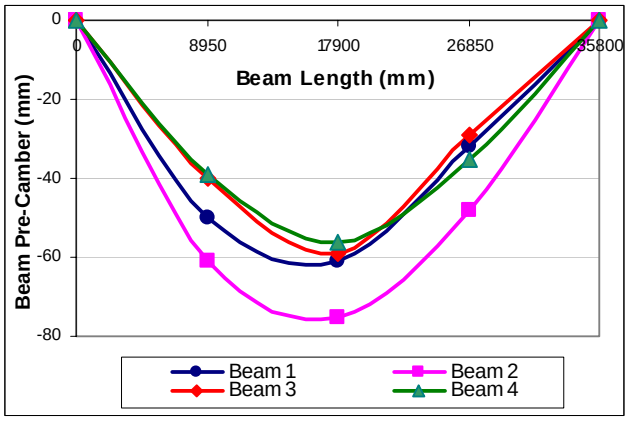

Figure 7.13: Beam pre-camber measured 15 days after prestressing

The ultimate pre-camber calculated based on the simplified and improved predictions are compared to the measured pre-camber in Table 7.13. Similar to pre-tensioned beam, the simplified prediction is calculated with only short-term deformation considered as in Equation (7.14) resulting in only one ultimate prediction value of -48.6mm. For comparison purpose, this simplified prediction is set constant from day 1 to day 15 without any demarcation. Based on the values shown in Table 7.13, the simplified prediction is closer to the actual measurement at the beginning stage, immediately after prestressing. This can be explained because only the short-term deformation is captured in the calculation computation, reflecting the scenario during initial deformation. However, an ingenuous comparison of the simplified prediction is to the instance when the pre-camber has almost stabilized, at

day 15. On average, the measured pre-camber is higher than the simplified estimation with difference between 8.0% and 48.0%.

Based on calculation with incorporation of long term losses with reference to Equation (7.21) and to sub-chapter 7.3.2.1, a comparison of the new prediction and the site measurement is plotted in Figure 7.14. The creep coefficient incorporated in the improved calculation of EC 2 and TROPCS is based on the recommended values of the respective predictions. It is observed that the magnitude of TROPCS pre-camber at 15 days after prestressing is 55.5mm, with 12.1% coefficient of variation as compared to the simplified prediction with coefficient of variation at 31.0%. With the inclusion of creep losses, the new prediction is closer to the average site measurement, resulting in a better pre-camber increment. The new prediction is within the range of ±10.0% than the measured pre-camber. This improvement compared to the initial prediction that stays at -48.6mm reveals the significant effect of time-dependent deformation on pre-camber.

Results from this study demonstrate a significant difference between the actual pre-camber on site and the simplified design estimation. This proves that the simplified calculation method currently being practiced is inaccurate and under predicts the actual camber.

Table 7.13: Comparison of measured and predicted pre-camber

Time after prestressing (days)	Beam Pre-Camber (mm)			
	Experimental Measured	**Simplified Prediction**	**Improved Prediction (EC 2 ϕ)**	**Improved Prediction (TROPCS ϕ)**
I**	-46.0	-48.6	-49.0	-48.4
3	-57.3	-48.6	-51.7	-50.8
6	-59.5	-48.6	-53.8	-52.6
9	-60.0	-48.6	-55.3	-53.8
12	-62.3	-48.6	-56.3	-54.8
15	-63.0	-48.6	-57.2	-55.5

** Between predicted value and average pre-camber measured on site*

*** Immediately after prestressing*

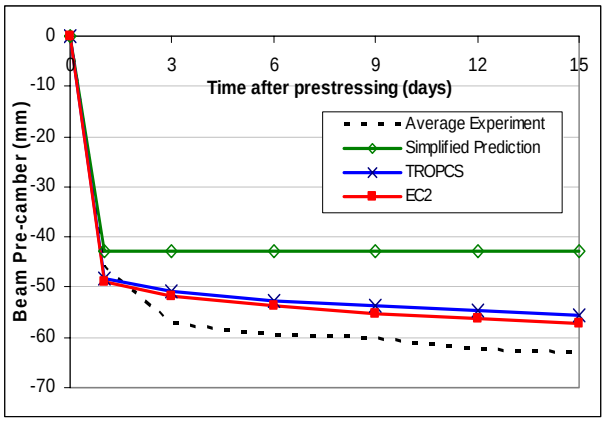

Figure 7.14: Comparison of average site measurement to the prediction values

7.4 Summary on the Proposed TROPCS Factors for Concrete in Tropical Climate

1. The increasing importance on time-dependent deformation on structures and the considerably vast difference between the experimental measurements to codes recommendations has lead to the introduction of TROPCS factors for creep and shrinkage of tropical concrete. The factors are designed to be incorporated to the best prediction model assessed, which is EC 2.

2. As a summary, the TROPCS modification factors are as follows:

Table 7.14: Summary of TROPCS correction factors for creep and shrinkage

Concrete Age at Loading (days)	***Creep Factors***		***Shrinkage Factors***	
	Power Coefficient, C_1	***RH Correction Factor, C_2***	***Power Coefficient, S_1***	***RH Correction Factor, S_2***
7	0.24	0.81	1.43	0.97
28	0.28	0.80	1.46	0.94

3. The TROPCS factors are empirical coefficients proposed based on the experimental results of time-dependent deformation of HSC in the tropical climate. For creep factor, C_1 basically corrected the early age deformation curve of EC 2 by introducing a higher initial surge in strain and subsequently,

C_2 lowers the long term creep. As for shrinkage, S_1 reduces the early age shrinkage strain while the factor S_2 lowers the final shrinkage strain.

4. It can be concluded that TROPCS results give a higher initial creep coefficient value and a slightly lower value beyond the age of approximately 50 days and subsequently lower magnitude for long term creep, as compared to the recommendation in EC 2.

5. The TROPCS predictions show good correlation with the experimental results. As a result, the coefficient of variation improved as compared to EC 2. The average coefficient of variation for the TROPCS prediction to the experimental data is between the ranges of 5.1% to 15.5% depending on the different concrete strength and age at loading. As for shrinkage, average the coefficient of variation is at 11.2% to 24.6%.

6. When the TROPCS is tested against the structural elements results, good correlation is observed as the coefficient of variation between the prediction and actual measurement is within the range of 20%, which is an acceptable range considering the effect of environment which is subjected to constant changes. It has been verified that the prediction calculation suits the concrete deformation for local concrete in the tropical condition.

7. Based on the study conducted here, it is concluded that the incorporation of creep into the calculation of pre-camber and deflection of prestressed beams is important for a better prediction values. The TROPCS creep and shrinkage values recommended in this research are also verified for its application for pre-camber of prestressed beams.

CHAPTER 8

CONCLUSIONS AND RECOMMENDATIONS

8.1 Conclusions

This research was conducted to critically examine the magnitude of time-dependent deformation of High Strength Concrete (HSC) exposed in the tropical climate condition. Subsequently, with detailed experimental testing, data recording and analysis on the time-dependent deformation, modification factors to EC 2 design code is proposed for better creep and shrinkage prediction of HSC in the tropical climate. The conclusions which follow are drawn from the results and observations presented in this thesis, acquired from the investigations carried out.

1. Complete set of creep and shrinkage data for HSC comprising of three strength classes - C40/50, C50/60 and C65/80 tested under controlled and natural tropical ambient were collected for a duration up to 320 days. As for the structural member testing, the deformation data was successfully gathered with the laboratory tested pre-camber measured for a total of 4 days, the pre-camber measurement on site monitored for 15 days, prestressed beams deflection tested for 28 days and a total of 120 days of testing for column testing.

2. In terms of accuracy and consistency in results, the average coefficient of variation is within an acceptable range for time-dependent deformation of concrete. The average coefficient of variation within a set of specimens for creep and shrinkage testing is at 13.9% and 16.3%. As for the structural members testing, the average coefficient of variation is at 7.4% for prestressed deflection testing, 13.8% for pre-camber monitoring on post-tensioned beams on site, 20.6% for pre-camber measurements on pretensioned beams tested in the laboratory and 22.4% for columns deformation.

3. It is concluded that the main environment influence in the tropical climate is the effect of relative humidity (RH) as variation between the ambient and controlled condition for RH is at 30% while the difference in temperature is only at 1.1^{o}C. Thus, it is concluded that variation in the test results between ambient and control specimens were primarily due to the difference in the RH.

4. Generally, the trend for concrete deformation measured from the experimental results shows that creep and shrinkage strain is lower as concrete strength increases for specimens tested in the controlled room. However under the influence of higher RH and temperature, concrete exhibit lower strain. The experiment results proved that a reduction in 10% to 30% strain is observed for the concrete stored under the tropical ambient as compared to the concrete of the same batch, tested under the controlled condition of 27^{o}C and 50% RH.

5. Both statistical results and graph comparison between experimental results and existing models recommendations show that creep for concrete tested in tropical condition is closer to the recommendation by EC 2, followed by the ACI-209, CEB 1990, B3 Model and AS 3600. As for shrinkage, existing model with the closest recommendation to concrete in the tropical condition is EC 2 prediction. The subsequent models that follow are the ACI-209, CEB 1990, AS 3600 and B3 Model. One of the obvious reasons for the accuracy for EC 2 model is because the model is contains the most up-to-date information on the influencing parameters and full coverage of concrete strength.

6. The average coefficient of variation for EC 2 to the experimental creep data obtained from this research is between the ranges of 12.2% to 27.13% for different set of concrete batch. As for shrinkage, average the coefficient of variation is at 9.88% to 38.9%. It is observed that the upper range has actually exceeded the accuracy stated in the code, which is at 20% for creep and 30% for shrinkage.

7. Due to the increasing importance on time-dependent deformation and the considerably vast difference between the experimental measurements to codes recommendations, modification factors are introduced for local concrete applications based on the best prediction model available, which is the EC 2.

8. The modification factors are empirical coefficients proposed based on the experimental results of time-dependent deformation of HSC in the tropical climate. For creep coefficient, the modification factor, C_1 basically corrected the early age deformation curve of EC 2 by introducing a higher initial surge in strain and subsequently, C_2 lowers the long term creep. As for shrinkage, the modification factor of S_1 reduces the early age shrinkage strain while the factor S_2 lowers the final shrinkage strain.

9. As a result of the modified model, the coefficient of variation improved as compared to EC 2. The average coefficient of variation for the Modified Model to the experimental creep data is between the ranges of 3.85% to 12.56% for different set of concrete batch. As for shrinkage, average the coefficient of variation is at 11.9% to 20.4%.

10. When the Modified Model is tested against the structural elements results, good correlation is observed as the coefficient of variation between the prediction and actual measurement is within the range of 20%, which is an acceptable range considering the effect of environment which is subjected to constant changes. This verifies that the prediction calculation suits the concrete deformation for local concrete in the tropical condition.

11. It is also concluded that incorporation of creep into the calculation of pre-camber and deflection of prestressed beams is vital for better accuracy.

These conclusions drawn are specific to the scope of work carried out, directly related to the specific concrete strength tested and the method of testing adopted. Consequently, caution should be exercised in attempts at generalizing from these specific conclusions drawn here. Nevertheless within the scope of this research, the results provided a significant contribution towards the understanding and knowledge of the time-dependent deformation of HSC in the tropical climate, which has not been critically researched and reviewed previously.

8.2 Recommendations

The work carried out and presented in this thesis has revealed areas where further research is necessary. It is therefore recommended that investigations could be made as follows:

1. Considering the significant magnitude of autogenous shrinkage reported for HSC, it is proposed for further study to be carried out on autogenous shrinkage for HSC in the tropical climate. Autogenous shrinkage occurs due to internal desiccation of the concrete material during the first 24 hours of concreting, not because of exchange in moisture to the surrounding ambient. Therefore theoretically, the influence of the surrounding is irrelevant. However in practical situations, all concreting works and concrete structures are exposed to the ambient and considering the fact that HSC has low w/c ratio, it is best to establish the knowledge on early age shrinkage for local concrete.

2. Further to the scope of this research work, it is also recommended to extend the testing to cover a wider range of parameters to TROPCS. Areas of studies may include other age of testing, a wider range of concrete strength tested under natural ambient and possibly to even monitor the time-dependent deformation of actual structures.

3. With the impending switch from British Standards to Eurocodes, one of the main apparent differences between the two codes is on the concrete strength specification. British Standards specifies concrete cube strength while the Eurocodes made reference to cylinder strength. In order to aid in a smoother transition, a verified conversion between cube and cylinder strength shall be established. Therefore a comprehensive study consisting of a wide range of concrete strength with proper consideration of mix proportions and materials properties is proposed to be conducted.

4. In the experimental work, it is necessary that every short-time shrinkage test to be accompanied by simultaneous measurements of the weight loss due to water evaporation. The idea is that the weight loss follows a similar curve as the shrinkage curve but, in contrast to shrinkage, the final water loss can be easily and reliably predicted — by heating the specimen in an oven at the end of the short-time shrinkage test. As shrinkage is small in magnitude, the linear measurement is sensitive to every slight deviation. As a result high instrumentation accuracy is required. The additional step in act as a reference data under the case when the linear measurement is inconsistent.

LAMPIRAN

WORKSHOP 1

Date : 2 July 2003

Venue : Pulai Spring Resort, Johor Bahru

List of Participants and

No.	Name	Organisation
1.	Assoc. Prof. Ir. Dr. Wahid Omar	Universiti Teknologi Malaysia
2.	Prof. Ir. Dr. Hj. Mohd Warid Hussin	
3.	Assoc. Prof. Dr. Ahmad Mahir Makhtar	
4.	Prof. Dr. Tam Chat Tim	National University of Singapore
5.	Ir. Dr. Norzan Yusuf	ACI KL Chapter
6.	Ir. Dr. Kribanandan G.N.	JTK Consult
7.	Ir. Hooi Wing Chuen	Cement and Concrete Association
8.	Ir. M.C. Hee	IEM
9.	Mr. Gary Wong	National Ready Mix Concrete Assoc.
10.	Mr. Jason Lee	
11.	Pn. Fazilah Mustafa	CIDB
12.	Mr. Roswadi Muhammad	
13.	Ms Tan Pui Lai	UTM
14.	Mr. Roslli Noor Mohamad	
15.	Mr. Zaizal Othman	

WORKSHOP 2

Date : 10 March 2005

Venue : ArmadaHotel, Petaling Jaya

List of Participants

No.	Name	Organisation
1	Ir. Dr. Kribanandan G.N.	JTK Consult Sdn. Bhd.
2	Mr. Lee Poh Huat	Zibina Jaya Sdn. Bhd.
3	Dr. Tam Chat Tim	National University of Singapore (NUS)
4	Ass. Prof. Ir. Kartini Amaruddin	Persatuan Konkrit Malaysia (PERKOM)
5	Dr. Hamidah Mohd. Saman	
6	Mr. Lee Meng Kee	National Ready Mix Concrete Association (NRMCA)
7	Mr. Teoh Boon Chiat	
8	Mr. Ting Hong Yew	
9	Ir. M.C. Hee	The Institution of Engineering, Malaysia (IEM)
10	Ir. Hooi Wing Chuen	American Concrete Institute (ACI) KL Chapter
11	Ms. Wong Koh Yin	Universiti Tenaga Malaysia (UNITEN)
12	Mr. Bryan Cheh	
13	Assoc. Prof. Dr. Mohammad Ismail	Universiti Teknologi Malaysia
14	Ms. Roslina Omar	
15	Ms. Tan Pui Lai	
16	Mr. Ng Ming Kwong	
17	Assoc. Prof. Ir. Dr. Wahid Omar (Research Leader)	
18	Ir. Mohamed bin Mohd. Nuruddin	Construction of Industry Development Board (CIDB)
19	Mr. Roswadi Muhammad	

FINAL REPORT CIDB

LIST OF PUBLICATIONS

1) Wahid Omar, Tan Pui Lai, Roslina Omar,'The Estimation of Time-Dependent Deformation in Concrete: How Relevant Are the Standard Codes Recommendations to Malaysian Environment?', CIDB Seminar on R&D Achievement (CIRAS) 2004, International Construction Week, September 22, 2004 Kuala Lumpur.

2) Roslina Omar, Tan Pui Lai, Wahid Omar,'The Study on Size Effect of Creep and Shrinkage Deformation of Normal Weight Concrete', Seminar Penyelidikan Kejuruteraan Awam 2004, Faculty of Civil Engineering, UTM, 1-2 September 2004.

3) Wahid Omar, Tan Pui Lai, Roslina Omar, ' Shifting to Eurocodes: Developing The Nationally Determined Parameters on Concrete Time-Dependent Deformation', Proceedings of The First International Conference of Asian Concrete Federation, Chiang Mai, Thailand, 28-29 October 2004.

4) Wahid Omar, Lee Poh Huat, Tan Pui Lai, Roslina Omar, 'Pre-camber in Post-Tensioned I-Beam: Comparison Between Site and Prediction Values', Proceedings Seminar Kebangsaan Penyelidikan Kejuruteraan Awam (SEPKA 2005), Faculty of Civil Engineering, UTM, 5-6 July 2005.

5) Wahid Omar, Tan Pui Lai, Roslina Omar, 'A Study on Creep and Shrinkage Deformation of Malaysian Concrete', International Concrete Convention, National Ready-Mixed Concrete Association, Malaysia, Awana Genting, 18-19 April 2006. (Invited paper)

6) Wahid Omar, Tan Pui Lai, Roslina Omar, 'Eurocode 2 vs BS 8110: Some Issues Concerning Concrete Properties and the Effect on Design, Proceedings, 9th International Conference on Concrete Engineering and Technology 2006 (CONCET 2006), 9-11 May 2006, Kuala Lumpur.

7) Wahid Omar, Tan Pui Lai, Khoo Hui Kiang, Roslina Omar,' Development of Creep and Shrinkage Prediction for Malaysian Concrete', 2nd Asian Concrete Federation Conference, 20-21 November 2006, Bali, Indonesia.

8) Wahid Omar, Shahrin Mohammad, Mohammad Ismail, Tan Pui Lai, 'Development of Local Design Values in Structural Concrete Design', Construction Industry Research Achievement International Conference (CIRAIC 2007), CIDB, 13-14 March 2007, Kuala Lumpur.

9) Wahid Omar, Tan Pui Lai, Lee Poh Huat, Roslina Omar, 'Improved Prediction of Precamber of Post-tensioned Prestressed I – Beam', Journal Institution of Engineers Malaysia, Vol. 69, No.1, March 2008.